UNIVERSITY OF CALIFORNIA,
IRVINE

Modeling the response of isoprene emissions from terrestrial ecosystems to drought and heatwaves

DISSERTATION

submitted in partial satisfaction of the requirements
for the degree of

DOCTOR OF PHILOSOPHY

in Earth System Science

by

Hui Wang

Dissertation Committee:
Professor Alex Guenther, Chair
Professor Claudia I. Czimczik
Associate Professor Saewung Kim

2024

TABLE OF CONTENTS

LIST OF FIGURES

LIST OF TABLES

Page

ACKNOWLEDGEMENTS

I would like to express my deepest gratitude to my advisor, Dr. Alex B. Guenther, for his unwavering support, guidance, and encouragement throughout my research journey. I am also sincerely thankful to my committee members, Dr. Claudia I. Czimczik and Dr. Saewung Kim, for their valuable insights and contributions to my work.

I am grateful to my collaborators from the University of Copenhagen, the Belgian Royal Institute for Space Aeronomy, and NCAR for their partnership and support, which have been integral to the success of this research.

A heartfelt thanks to my lab friends: Gracie, Bee, Sanjeevi, Jesus, Chris, Julie, Yinnan, Kat, Katie, Jared, Alvin, Yoel, Viri, Christina, Yolanda, Ashley, Eric, Sina, Shohbit, and many others who have made the lab a place of camaraderie and inspiration.

I also extend my thanks to my ESS cohort friends: Jin, Cindy, Hanning, Megan, Jaehun, Shayma, Marina, Adam, Tingting, Ashton, and Julianne. Your friendship and encouragement have made this journey much more enjoyable.

To my friends Yi, Yu, Hanchao, Yan Xia, Runze, Xuming, Yan Zhang, Lori, Lucia, Kaiwu, Shan, Yifei, Yulin, Shupeng, Allison, and all others in the ESS, EEB, CHEM, and Philosophy departments, thank you for your support and for being part of this academic journey.

Lastly, I would like to thank my beloved cats, Eco and Emo, for their constant companionship. To my family, my wife Jun, my son Chris, and my parents, thank you for your endless love, patience, and support. This achievement would not have been possible without you.

VITA

Hui Wang

Education

- **University of California, Irvine**, CA, USA 2019- 2024

  PhD in Earth System Science

- **Beijing Normal University**, Beijing, China 2015- 2018

  M.Sc. in Global Environment Change

- **He Fei University of Technology**, He Fei, China 2011- 2015

  B.Sc. in Geographic Information Science

Awards

- Outstanding Graduate Student Research Award in the Department of Earth System Science, UCI (2024)
- Future Investigators in NASA Earth and Space Science and Technology (2023)
- Diversity, Equity and Inclusion (DEI) Graduate Leaders Fellowship in University of California Irvine (2023)
- Tong-Ding Excellent Student Scholarship (2017)
- Best Paper Award in the Fourth Graduate Student Forum on Global Change in China (2017)

Community Involvement

- UCI-ESS Diverse Educational Community and Doctoral Experience (DECADE) representative
- Member of UCI-ESS Professional Development and Seminar Committee
- UCI-ESS Graduate/Undergrade Student mentor
- Mentees: Trinity S. McGinnis, Christopher A. Leong, Jared Novelly, Sunwoo Kim, Yu Ye

(undergraduate researchers), Han-chao Cheng, Ting-Wei Hsieh (graduate students)

- Reviewer for *Geophysical Research Letters, Geoscientific Model Development, Atmospheric Chemistry and Physics, Atmosphere Environment, Journal of Geophysical Research: Biogeoscience, and Urban Greening & Urban Forestry*

Peer-reviewed Publications

- **Wang, H.**, Welch, A. M., Nagalingam, S., Leong, C., Czimczik, C. I., Tang, J., Seco, R., Rinnan, R., Vettikkat, L., Schobesberger, S., Holst, T., Brijesh, S., Sheesley, R. J., Barsanti, K. C., and Guenther, A. B.: High temperature sensitivity of Arctic isoprene emissions explained by sedges, *Nature Communications*, 15, 6144, 10.1038/s41467-024-49960-0, 2024.
- **Wang, H.**, Welch, A., Nagalingam, S., Leong, C., Kittitananuvong, P., Barsanti, K. C., et al. (2024). Arctic heatwaves could significantly influence the isoprene emissions from shrubs. *Geophysical Research Letters*, 51, e2023GL107599. https://doi.org/10.1029/2023GL107599, 2024.
- Wong, G., **Wang, H.,** Park, M., Park, J., Ahn, J.-Y., Sung, M., Choi, J., Park, T., Ban, J., Kang, S., Lee, T., Kim, J., Seo, B.-K., Yu, J.-H., Kim, J., Woo, J.-H., and Kim, S.: Optimizing an airborne mass-balance methodology for accurate emission rate quantification of industrial facilities: A case study of industrial facilities in South Korea, *Science of The Total Environment*, 912, 169204, https://doi.org/10.1016/j.scitotenv.2023.169204, 2024.
- **Wang, H.**, Lu, X., Seco, R., Stavrakou, T., Karl, T., Jiang, X., Gu, L., and Guenther, A.: Modeling isoprene emission response to drought and heatwaves within MEGAN using evapotranspiration data and by coupling with the Community Land Model. *Journal of Advances in Modeling Earth Systems*, 14, e2022MS003174. https://doi.org/10.1029/2022MS003174, 2022.

- **Wang, H.**, Wu, Q., Guenther, A. B., Yang, X., Wang, L., Xiao, T., Li, J., Feng, J., Xu, Q., and Cheng, H.: A long-term estimation of biogenic volatile organic compound (BVOC) emission in China from 2001–2016: the roles of land cover change and climate variability, *Atmos. Chem. Phys.*, 21, 4825-4848, https://doi.org/10.5194/acp-21-4825-2021, 2021.
- **Wang, H.**, Lin, J., Wu, Q., Chen, H., Tang, X., Wang, Z., Chen, X., Cheng, H., and Wang, L.: MP CBM-Z V1.0: design for a new Carbon Bond Mechanism Z (CBM-Z) gas-phase chemical mechanism architecture for next-generation processors, *Geosci. Model Dev.*, 12, 749–764, https://doi.org/10.5194/gmd-12-749-2019, 2019.
- **Wang, H.**, Wu, Q., Liu, H., Wang, Y., Cheng, H., Wang, R., Wang, L., Xiao, H., and Yang, X.: Sensitivity of biogenic volatile organic compound emissions to leaf area index and land cover in Beijing, *Atmos. Chem. Phys.*, 18, 9583-9596, https://doi.org/10.5194/acp-18-9583-2018, 2018.
- Wang, Y., Chen, H., Wu, Q., Chen, X., **Wang, H.**, Gbaguidi, A., Wang, W., and Wang, Z.: Three-year, 5 km resolution China PM2.5 simulation: Model performance evaluation, *Atmospheric Research*, 207, 1-13, https://doi.org/10.1016/j.atmosres.2018.02.016, 2018.
- **Wang, H.**, Chen, H., Wu, Q., Lin, J., Chen, X., Xie, X., Wang, R., Tang, X., and Wang, Z.: GNAQPMS v1.1: accelerating the Global Nested Air Quality Prediction Modeling System (GNAQPMS) on Intel Xeon Phi processors, *Geosci. Model Dev.*, 10, 2891-2904, https://doi.org/10.5194/gmd-10-2891-2017, 2017.

Conference Presentations

- Biogenic Hydrocarbons and the Atmosphere (GRS) and Biogenic Hydrocarbons and the Atm osphere, Gordon Conference, June 11-17, 2022, Oxnard, California, US (Talk).
- Model Inter-Comparison Study for Asia Phase III (MICS-Asia III) workshop, March 8-10 20

17, IIASA, Vienna, Austria (Talk).

- American Geophysical Union (AGU) Annual Fall Meeting, December 11-15, 2023, San Francisco, California, US (Poster).
- American Geophysical Union (AGU) Annual Fall Meeting, December 11-15, 2021, New Orleans, Louisiana, US (Poster).
- American Geophysical Union (AGU) Annual Fall Meeting, December 11-15, 2017, New Orleans, Louisiana, US (Poster).

ABSTRACT OF THE DISSERTATION

Modeling the response of isoprene emissions from terrestrial ecosystems to drought and heatwaves

by

Hui Wang

Doctor of Philosophy in Earth System Science

University of California, Irvine, 2024

Professor Alex B. Guenther, Chair

The heatwave and drought stresses induced by rapid climate change can alter the emission of isoprene from terrestrial ecosystems. This, in turn, affects climate and air quality by modifying photochemistry and forming secondary organic aerosols. Understanding the complex interactions and feedback loops between climate and isoprene emissions is a challenging yet urgent task. This study integrates laboratory experiments and in-situ measurements to investigate and model these impacts within the Model of Emissions of Gases and Aerosols from Nature (MEGAN).

In the first chapter, an empirical algorithm was developed to simulate drought effects on isoprene emissions, revealing an 11% global decrease in isoprene in 2012 due to drought. This algorithm improved the agreement between model simulations and satellite formaldehyde observations during droughts, as formaldehyde is widely used as a proxy for isoprene. However, its performance was limited by the model's ability to accurately capture drought severity.

The second and third chapters focus on Arctic ecosystems, where rapid warming is accelerating isoprene emissions. The second chapter characterizes the temperature response of Arctic willows, finding that their hourly temperature response curve is similar to that of temperate plants. Isoprene emissions increase with rising temperature, reaching an optimal level before

declining due to enzyme denaturation. Additionally, the isoprene capacity of willows could increase rapidly with rising ambient temperatures from the previous day. During heatwaves, Arctic willows exhibited a 66% higher isoprene emission when using a modified algorithm based on my measurements.

The third chapter investigates sedges, another major Arctic isoprene emitter, and finds that their temperature response is notably stronger compared to other isoprene emitters. Integrating these findings into MEGAN improved the capacity of model to reproduce observations. The omission of these strong temperature responses from both willows and sedges led to a 20% underestimation of isoprene emissions in high-latitude regions between 2000 and 2009, and a 55% underestimation of long-term trends from 1960 to 2009. Therefore, rapid warming in the Arctic could significantly increase isoprene emissions, altering local chemistry and impacting the climate.

CHAPTER 1

INTRODUCTION

1.1 The importance of isoprene

Isoprene from terrestrial ecosystems plays a significant role in tropospheric atmospheric chemistry due to its large emission volume and chemical properties. The estimated annual isoprene emission from land vegetation ranges from 412 to 682 Tg yr^{-1} (Guenther et al., 2012; Opacka et al., 2021), which is considerably higher than the global anthropogenic non-methane volatile organic compounds (VOCs) emission of 169 Tg yr^{-1} (Huang et al., 2017). Additionally, the high chemical reactivity of isoprene has profound effects on air quality and the climate system. Isoprene is a crucial precursor of ozone and secondary organic aerosol (SOA) (Sillman, 1999; Claeys et al., 2004). Tropospheric ozone is a significant air pollutant and a greenhouse gas, with studies highlighting the importance of isoprene in local ozone pollution. For example, Duane et al. (2002) inferred that isoprene contributes to 50-75% of local ozone formation in Insubria, Italy, based on observations of VOCs and NOx. Another study by Geng et al. (2011), combining model simulations and observations, demonstrated that the interaction between isoprene and anthropogenic NOx leads to a 6-8 ppb h^{-1} ozone increase in the city region of Shanghai, China. In addition, isoprene is also a significant source of SOA, which can markedly influence both air quality and the climate system. SOA affects air quality through its composition of particulate matter and impacts the climate system directly by reflecting solar radiation and indirectly by acting as cloud condensation nuclei (Kulmala et al., 2004). Carlton et al. (2009) concluded that isoprene is a major contributor to SOA due to its large emission volume, with isoprene-derived SOA constituting 30%-80% of the total global SOA. Therefore, accurately estimating isoprene

emissions is crucial for understanding its contribution to local air quality issues as well as climate change.

1.2 The influence of drought and heatwave stress on isoprene emission

Droughts and high temperatures often coincide, and both affect the isoprene emission. Isoprene can help plants defend against thermal stress (Sharkey et al., 2008) and may also act as a signaling substance that stimulates chemical defense during stress periods (Monson et al., 2021). The optimal temperature for isoprene synthase (ISPS) can reach 40°C (Monson et al., 1992; Guenther et al., 1993), which is much higher than the optimal temperature for photosynthesis. In addition, leaves growing at high temperatures have a relatively higher isoprene emission capacity, with increased ISPS protein accumulation (Fortunati et al., 2008) under the influence of high temperatures (Monson et al., 1994; Sharkey et al., 2008). Additionally, short-term high-temperature events can also trigger a burst of isoprene emission (Singsaas and Sharkey, 2000; Sharkey and Loreto, 1993). Therefore, heatwaves are favorable for the emission of isoprene.

Regarding drought stress, isoprene biosynthesis and emission exhibit relatively higher tolerance compared to photosynthesis (Sharkey and Loreto, 1993; Brüggemann and Schnitzler, 2002; Fortunati et al., 2008; Brilli et al., 2007). Isoprene emissions only decrease significantly due to the inhibition of substrate supply under severe drought conditions (Fang et al., 1996; Pegoraro et al., 2004; Brilli et al., 2007). However, some experiments have provided evidence of alternative carbon sources for isoprene synthase during drought, besides current photosynthates (Brilli et al., 2007). A recent study (Bamberger et al., 2017) concluded that the effects of heatwave-drought events on isoprene emission are likely dominated by the response of trees to high temperatures. However, Geron et al. (2016) revealed that the behavior of different tree species regarding isoprene

emission during drought could vary depending on their drought resistance capacities. In addition to the direct impact of temperature and drought on isoprene emission, Potosnak et al. (2014a) hypothesized that isoprene emission could increase at the mild stage of drought, indirectly influenced by the rise in leaf temperature caused by reduced stomatal conductance. In conclusion, the response of isoprene emissions to drought is complicated and depends on the severity of the drought stress.

1.3 High temperature sensitivity of isoprene in the Arctic

Isoprene is the most abundant reactive biogenic volatile organic compound (BVOC) emitted globally and in the Arctic (Guenther et al., 2012; Rinnan et al., 2020; Tang et al., 2023), and a rapidly warming climate in the Arctic is favorable for increasing the emission of isoprene (Lindwall et al., 2016; Kramshøj et al., 2016; Faubert et al., 2010; Tiiva et al., 2009). Quantifying the temperature control of isoprene emission from plants has been a fundamental research effort since plant isoprene emissions were first identified (Rasmussen and Jones, 1973). Based on emission measurements of a wide range of tree species, an average isoprene Q10 coefficient of about 3 is currently used in atmospheric chemistry models (Sharkey and Monson, 2014). However, some recent whole-ecosystem measurements suggest that the temperature response of isoprene emissions in high-latitude tundra ecosystems has a Q10 of over 8 (Figure 1.1), which is also much higher than that predicted by the widely used BVOC emission model, the Model of Emissions of Gases and Aerosols from Nature (MEGAN) (Seco et al., 2022; Seco et al., 2020; Vettikkat et al., 2022; Li et al., 2023). In contrast, leaf/branch-level studies showed that the Arctic willow species (*Salix pulchra* CHAM., *S. glauca* L., and *S. myrsinites* L.), which are one of main isoprene emitters in high-latitude tundra ecosystems, have a short-term temperature response that is similar to that of temperate plants (Potosnak et al., 2013; Li et al., 2023). Therefore, species-specific

investigations are necessary to further explore the strong temperature responses observed at the ecosystem level.

1.4 The framework of the MEGAN model

MEGAN (Guenther et al., 2012; Guenther et al., 2006) is a widely used model for calculating BVOC emission from regional to global scales (Sindelarova et al., 2014; Wang et al., 2011; Wang et al., 2021; Wang et al., 2018). MEGAN calculates canopy scale flux for 19 major VOC compound categories using the fundamental algorithm [Eq. 1.1]:

$$F = \varepsilon\gamma \quad [1.1]$$

where F (nmol m^{-2} s^{-1}), ε (nmol m^{-2} s^{-1}) and γ represent the emission amount, standard emission factor and emission activity factor. The emission activity factor γ accounts for the impact of multiple environmental factors. The emission activity factor for isoprene is expressed as:

$$\gamma_{iso} = C_{\mathrm{CE}} LAI \gamma_{\mathrm{P}} \gamma_{\mathrm{T}} \gamma_{\mathrm{A}} \gamma_{\mathrm{SM}} \gamma_{\mathrm{C}} \quad [1.2]$$

where γ_p, γ_T, γ_A, γ_{SM} and γ_C represent the activity factors for light, temperature, leaf age, soil moisture and CO_2 inhibition impact. The C_{ce} (=0.57) is a factor to set the γ_{iso} equal to 1 at the standard conditions. The LAI is the leaf area index and defines the amount of foliage and changes in LAI determine leaf age in MEGAN.

The effects of high temperature and drought stresses will be reflected on the factors γ_T and γ_{SM}. MEGAN considers the impacts of the long-term temperature and the current temperature on isoprene emission. The γ_T for isoprene in MEGAN is written as:

$$\gamma_{\mathrm{T}} = E_{\mathrm{opt}} \frac{C_{\mathrm{T2}} \exp(C_{\mathrm{T1}} \cdot x)}{\mathrm{C_{T2}} - C_{\mathrm{T1}}(1 - \exp(C_{\mathrm{T2}} \cdot x))} \quad [1.3]$$

, where *x* is as:

$$x = \frac{1}{0.00831} \cdot \left(\frac{1}{T_{\mathrm{opt}}} - \frac{1}{T} \right) \quad [1.4]$$

. T is the leaf temperature. C_{T1} and C_{T2} are both empirical coefficients. E_{opt} and T_{opt} are as:

$$T_{opt} = 313 + 0.6 \cdot (T_{240} - 297) \quad [1.5]$$

$$E_{opt} = 2.034 \cdot \exp\big(0.05 \cdot (T_{24} - 297)\big) \cdot \exp(0.05 \cdot (T_{240} - 297)) \quad [1.6]$$

, where T_{24} and T_{240} denote the averaged leaf temperature during the previous 24 hours and 240 hours, respectively. T_{opt} and E_{opt} represent the impact of long-term temperatures on the optimal temperature and the shape of the temperature response curve. As shown in Figure 1.2, the responses of γ_T to temperature are affected by the temperatures in previous 24 hours.

Drought stress is represented by γ_{SM} in the MEGAN model. Generally, the severity of drought determines the response of isoprene emission (Niinemets, 2010). During mild or moderate drought, plants can continue to emit isoprene even when photosynthesis is affected by drought (Niinemets, 2010; Seco et al., 2015). In some cases, the isoprene emission rate may even increase under mild drought conditions (Potosnak et al., 2014b; Otu-Larbi et al., 2020). However, during severe drought events, isoprene emissions will decline over time (Pegoraro et al., 2004). In MEGAN 2.1, the impact of drought on isoprene emission is described using a simple empirical algorithm based on Pegoraro et al. (2004). The activity factor response to drought, γ_{SM}, is:

$$\begin{cases} \gamma_{SM} = 1 (\theta > \theta_1) \\ \gamma_{SM} = (\theta - \theta_w)/\Delta\theta_1 \ (\theta_w < \theta < \theta_1) \\ \gamma_{SM} = 0 (\theta < \theta_w) \end{cases} \quad [1.7]$$

where θ is soil moisture, and θw is the wilting point. $\Delta\theta 1$ is an empirical parameter of 0.06 m^{-3} m^{-3} and θ_1 is defined as $\theta w + \Delta\theta_1$. The wilting point is the soil moisture level at which a plant cannot extract water from the soil. The wilting points in MEGAN are from Chen and Dudhia (2001), but some recent studies have pointed out that using the wilting point algorithm cannot capture the impact of drought on isoprene emission if representative wilting point values are not available (Seco et al., 2015; Huang et al., 2015). In addition, this algorithm does not account for the increase

in isoprene induced by changes in leaf temperature. Therefore, a better algorithm is needed in MEGAN to represent the impact of drought on isoprene emissions.

1.5 Objectives and structure of the dissertation

My dissertation focuses on investigating and establishing modeling frameworks to simulate the impact of drought and heat stress on isoprene emissions in the MEGAN model. In the first chapter, I used whole-canopy flux measurements of isoprene and established a simple parameterization scheme for simulating the impact of drought on isoprene emissions. The new mode can better capture the impact of drought from the mild to severe stages. Model simulations also indicate that drought can lead to an 11% decrease in global isoprene emissions. In the second and third chapters, I investigated the high-temperature sensitivity of isoprene emissions in the Arctic. I evaluated the impact of temperature on isoprene emissions from Arctic willows and sedges, two major isoprene emitters in the Arctic, in the second and third chapters, respectively. I investigated the short-term and long-term temperature responses of the willows and sedges in the Arctic. I used the results from plant chamber experiments to establish new modeling frameworks for both sedges and willows. The updated model revealed an underestimation of isoprene and its changing trends in high-latitude regions. My research highlights the impact of changes in isoprene emissions caused by more frequent drought and heatwave events due to ongoing global warming and climate change.

Reference

Bamberger, I., Ruehr, N. K., Schmitt, M., Gast, A., Wohlfahrt, G., and Arneth, A.: Isoprene emission and photosynthesis during heatwaves and drought in black locust, Biogeosciences, 14, 3649-3667, 10.5194/bg-14-3649-2017, 2017.

Brilli, F., Barta, C., Fortunati, A., Lerdau, M., Loreto, F., and Centritto, M.: Response of isoprene emission and carbon metabolism to drought in white poplar (Populus alba) saplings, New Phytologist, 175, 244-254, https://doi.org/10.1111/j.1469-8137.2007.02094.x, 2007.

Brüggemann, N., and Schnitzler, J. P.: Comparison of Isoprene Emission, Intercellular Isoprene Concentration and Photosynthetic Performance in Water-Limited Oak (Quercus pubescens Willd. and Quercus robur L.) Saplings, Plant Biology, 4, 456-463, https://doi.org/10.1055/s-2002-34128, 2002.

Carlton, A. G., Wiedinmyer, C., and Kroll, J. H.: A review of Secondary Organic Aerosol (SOA) formation from isoprene, Atmos. Chem. Phys., 9, 4987-5005, 10.5194/acp-9-4987-2009, 2009.

Chen, F., and Dudhia, J.: Coupling an Advanced Land Surface–Hydrology Model with the Penn State–NCAR MM5 Modeling System. Part I: Model Implementation and Sensitivity, Monthly Weather Review, 129, 569-585, 10.1175/1520-0493(2001)129<0569:CAALSH>2.0.CO;2, 2001.

Claeys, M., Graham, B., Vas, G., Wang, W., Vermeylen, R., Pashynska, V., Cafmeyer, J., Guyon, P., Andreae, M. O., and Artaxo, P.: Formation of secondary organic aerosols through photooxidation of isoprene, Science, 303, 1173-1176, 2004.

Clapp, R. B., and Hornberger, G. M.: Empirical equations for some soil hydraulic properties, Water Resources Research, 14, 601-604, 10.1029/WR014i004p00601, 1978.

Duane, M., Poma, B., Rembges, D., Astorga, C., and Larsen, B. R.: Isoprene and its degradation products as strong ozone precursors in Insubria, Northern Italy, Atmospheric Environment, 36, 3867-3879, https://doi.org/10.1016/S1352-2310(02)00359-X, 2002.

Fang, C., Monson, R. K., and Cowling, E. B.: Isoprene emission, photosynthesis, and growth in sweetgum (Liquidambar styraciflua) seedlings exposed to short- and long-term drying cycles, Tree Physiology, 16, 441-446, 10.1093/treephys/16.4.441, 1996.

Faubert, P., Tiiva, P., Rinnan, Å., Michelsen, A., Holopainen, J. K., and Rinnan, R.: Doubled volatile organic compound emissions from subarctic tundra under simulated climate warming, New Phytologist, 187, 199-208, https://doi.org/10.1111/j.1469-8137.2010.03270.x, 2010.

Fortunati, A., Barta, C., Brilli, F., Centritto, M., Zimmer, I., Schnitzler, J.-P., and Loreto, F.: Isoprene emission is not temperature-dependent during and after severe drought-stress: a physiological and biochemical analysis, The Plant Journal, 55, 687-697, https://doi.org/10.1111/j.1365-313X.2008.03538.x, 2008.

Geng, F., Tie, X., Guenther, A., Li, G., Cao, J., and Harley, P.: Effect of isoprene emissions from major forests on ozone formation in the city of Shanghai, China, Atmospheric Chemistry and Physics, 11, 10449-10459, 10.5194/acp-11-10449-2011, 2011.

Geron, C., Daly, R., Harley, P., Rasmussen, R., Seco, R., Guenther, A., Karl, T., and Gu, L.: Large drought-induced variations in oak leaf volatile organic compound emissions during PINOT NOIR 2012, Chemosphere, 146, 8-21, https://doi.org/10.1016/j.chemosphere.2015.11.086, 2016.

Guenther, A., Karl, T., Harley, P., Wiedinmyer, C., Palmer, P., and Geron, C.: Estimates of global terrestrial isoprene emissions using MEGAN (Model of Emissions of Gases and Aerosols from Nature), Atmos. Chem. Phys, 6, 3181-3210, 2006.

Guenther, A. B., Zimmerman, P. R., Harley, P. C., Monson, R. K., and Fall, R.: Isoprene and monoterpene emission rate variability: Model evaluations and sensitivity analyses, Journal of Geophysical Research: Atmospheres, 98, 12609-12617, doi:10.1029/93JD00527, 1993.

Guenther, A. B., Jiang, X., Heald, C. L., Sakulyanontvittaya, T., Duhl, T., Emmons, L. K., and Wang, X.: The Model of Emissions of Gases and Aerosols from Nature version 2.1 (MEGAN2.1): an extended and updated framework for modeling biogenic emissions, Geoscientific Model Development, 5, 1471-1492, 10.5194/gmd-5-1471-2012, 2012.

Huang, G., Brook, R., Crippa, M., Janssens-Maenhout, G., Schieberle, C., Dore, C., Guizzardi, D., Muntean, M., Schaaf, E., and Friedrich, R.: Speciation of anthropogenic emissions of non-methane volatile organic compounds: a global gridded data set for 1970–2012, Atmos. Chem. Phys., 17, 7683-7701, 10.5194/acp-17-7683-2017, 2017.

Jiang, X., Guenther, A., Potosnak, M., Geron, C., Seco, R., Karl, T., Kim, S., Gu, L., and Pallardy, S.: Isoprene emission response to drought and the impact on global atmospheric chemistry, Atmospheric Environment, 183, 69-83, https://doi.org/10.1016/j.atmosenv.2018.01.026, 2018.

Kramshøj, M., Vedel-Petersen, I., Schollert, M., Rinnan, Å., Nymand, J., Ro-Poulsen, H., and Rinnan, R.: Large increases in Arctic biogenic volatile emissions are a direct effect of warming, Nature Geoscience, 9, 349-352, 10.1038/ngeo2692, 2016.

Kulmala, M., Suni, T., Lehtinen, K. E. J., Dal Maso, M., Boy, M., Reissell, A., Rannik, Ü., Aalto, P., Keronen, P., Hakola, H., Bäck, J., Hoffmann, T., Vesala, T., and Hari, P.: A new feedback mechanism linking forests, aerosols, and climate, Atmos. Chem. Phys., 4, 557-562, 10.5194/acp-4-557-2004, 2004.

Li, T., Baggesen, N., Seco, R., and Rinnan, R.: Seasonal and diel patterns of biogenic volatile organic compound fluxes in a subarctic tundra, Atmospheric Environment, 292, 119430, https://doi.org/10.1016/j.atmosenv.2022.119430, 2023.

Lindwall, F., Svendsen, S. S., Nielsen, C. S., Michelsen, A., and Rinnan, R.: Warming increases isoprene emissions from an arctic fen, Science of The Total Environment, 553, 297-304, https://doi.org/10.1016/j.scitotenv.2016.02.111, 2016.

Monson, R. K., Jaeger, C. H., Adams, W. W., Driggers, E. M., Silver, G. M., and Fall, R.: Relationships among Isoprene Emission Rate, Photosynthesis, and Isoprene Synthase Activity as Influenced by Temperature, Plant Physiology, 98, 1175, 10.1104/pp.98.3.1175, 1992.

Monson, R. K., Harley, P. C., Litvak, M. E., Wildermuth, M., Guenther, A. B., Zimmerman, P. R., and Fall, R.: Environmental and developmental controls over the seasonal pattern of isoprene emission from aspen leaves, Oecologia, 99, 260-270, 10.1007/BF00627738, 1994.

Monson, R. K., Weraduwage, S. M., Rosenkranz, M., Schnitzler, J.-P., and Sharkey, T. D.: Leaf isoprene emission as a trait that mediates the growth-defense tradeoff in the face of climate stress, Oecologia, 10.1007/s00442-020-04813-7, 2021.

Niinemets, U.: Mild versus severe stress and BVOCs: thresholds, priming and consequences, Trends Plant Sci, 15, 145-153, 10.1016/j.tplants.2009.11.008, 2010.

Opacka, B., Müller, J. F., Stavrakou, T., Bauwens, M., Sindelarova, K., Markova, J., and Guenther, A. B.: Global and regional impacts of land cover changes on isoprene emissions derived from spaceborne data and the MEGAN model, Atmos. Chem. Phys., 21, 8413-8436, 10.5194/acp-21-8413-2021, 2021.

Otu-Larbi, F., Bolas, C. G., Ferracci, V., Staniaszek, Z., Jones, R. L., Malhi, Y., Harris, N. R. P., Wild, O., and Ashworth, K.: Modelling the effect of the 2018 summer heatwave and drought on isoprene emissions in a UK woodland, Global Change Biology, 26, 2320-2335, 10.1111/gcb.14963, 2020.

Pegoraro, E., Rey, A., Greenberg, J., Harley, P., Grace, J., Malhi, Y., and Guenther, A.: Effect of drought on isoprene emission rates from leaves of Quercus virginiana Mill, Atmospheric Environment, 38, 6149-6156, https://doi.org/10.1016/j.atmosenv.2004.07.028, 2004.

Potosnak, M. J., Baker, B. M., LeStourgeon, L., Disher, S. M., Griffin, K. L., Bret-Harte, M. S., and Starr, G.: Isoprene emissions from a tundra ecosystem, Biogeosciences, 10, 871-889, 10.5194/bg-10-871-2013, 2013.

Potosnak, M. J., LeStourgeon, L., and Nunez, O.: Increasing leaf temperature reduces the suppression of isoprene emission by elevated CO2 concentration, Science of The Total Environment, 481, 352-359, https://doi.org/10.1016/j.scitotenv.2014.02.065, 2014a.

Potosnak, M. J., LeStourgeon, L., Pallardy, S. G., Hosman, K. P., Gu, L., Karl, T., Geron, C., and Guenther, A. B.: Observed and modeled ecosystem isoprene fluxes from an oak-dominated temperate forest and the influence of drought stress, Atmospheric Environment, 84, 314-322, https://doi.org/10.1016/j.atmosenv.2013.11.055, 2014b.

Rinnan, R., Iversen, L. L., Tang, J., Vedel-Petersen, I., Schollert, M., and Schurgers, G.: Separating direct and indirect effects of rising temperatures on biogenic volatile

emissions in the Arctic, Proceedings of the National Academy of Sciences, 117, 32476, 10.1073/pnas.2008901117, 2020.

Rasmussen, R. A., and Jones, C. A. Emission isoprene from leaf discs of Hamamelis. Phytochemistry, 12(1), 15-19, 1973.

Seco, R., Karl, T., Guenther, A., Hosman, K. P., Pallardy, S. G., Gu, L., Geron, C., Harley, P., and Kim, S.: Ecosystem-scale volatile organic compound fluxes during an extreme drought in a broadleaf temperate forest of the Missouri Ozarks (central USA), Global Change Biology, 21, 3657-3674, doi:10.1111/gcb.12980, 2015.

Seco, R., Holst, T., Matzen, M. S., Westergaard-Nielsen, A., Li, T., Simin, T., Jansen, J., Crill, P., Friborg, T., Rinne, J., and Rinnan, R.: Volatile organic compound fluxes in a subarctic peatland and lake, Atmos. Chem. Phys., 20, 13399-13416, 10.5194/acp-20-13399-2020, 2020.

Seco, R., Holst, T., Davie-Martin, C. L., Simin, T., Guenther, A., Pirk, N., Rinne, J., and Rinnan, R.: Strong isoprene emission response to temperature in tundra vegetation, Proceedings of the National Academy of Sciences, 119, e2118014119, 10.1073/pnas.2118014119, 2022.

Sharkey, T. D., and Loreto, F.: Water stress, temperature, and light effects on the capacity for isoprene emission and photosynthesis of kudzu leaves, Oecologia, 95, 328-333, 1993.

Sharkey, T. D., Wiberley, A. E., and Donohue, A. R.: Isoprene Emission from Plants: Why and How, Annals of Botany, 101, 5-18, 10.1093/aob/mcm240, 2008.

Sharkey, T. D., and Monson, R. K.: The future of isoprene emission from leaves, canopies and landscapes, Plant, Cell & Environment, 37, 1727-1740, https://doi.org/10.1111/pce.12289, 2014.

Sillman, S.: The relation between ozone, NOx and hydrocarbons in urban and polluted rural environments, Atmospheric Environment, 33, 1821-1845, http://dx.doi.org/10.1016/S1352-2310(98)00345-8, 1999.

Sindelarova, K., Granier, C., Bouarar, I., Guenther, A., Tilmes, S., Stavrakou, T., Müller, J. F., Kuhn, U., Stefani, P., and Knorr, W.: Global data set of biogenic VOC emissions calculated by the MEGAN model over the last 30 years, Atmos. Chem. Phys., 14, 9317-9341, 10.5194/acp-14-9317-2014, 2014.

Singsaas, E. L., and Sharkey, T. D.: The effects of high temperature on isoprene synthesis in oak leaves, Plant, Cell & Environment, 23, 751-757, https://doi.org/10.1046/j.1365-3040.2000.00582.x, 2000.

Tang, J., Zhou, P., Miller, P. A., Schurgers, G., Gustafson, A., Makkonen, R., Fu, Y. H., and Rinnan, R.: High-latitude vegetation changes will determine future plant volatile impacts on atmospheric organic aerosols, npj Climate and Atmospheric Science, 6, 147, 10.1038/s41612-023-00463-7, 2023.

Tiiva, P., Faubert, P., Räty, S., Holopainen, J. K., Holopainen, T., and Rinnan, R.: Contribution of vegetation and water table on isoprene emission from boreal peatland microcosms, Atmospheric Environment, 43, 5469-5475, https://doi.org/10.1016/j.atmosenv.2009.07.026, 2009.

Vettikkat, L., Miettinen, P., Buchholz, A., Rantala, P., Yu, H., Schallhart, S., Seco, R., Männistö, E., Tuittila, E. S., Guenther, A. B., and Schobesberger, S.: High emission rates and strong temperature response make boreal wetlands a large source of terpenes, Atmos. Chem. Phys. Discuss., 2022, 1-21, 10.5194/acp-2022-588, 2022.

Wang, H., Wu, Q., Liu, H., Wang, Y., Cheng, H., Wang, R., Wang, L., Xiao, H., and Yang, X.: Sensitivity of biogenic volatile organic compound emissions to leaf area index and land cover in Beijing, Atmos. Chem. Phys., 18, 9583-9596, 10.5194/acp-18-9583-2018, 2018.

Wang, H., Wu, Q., Guenther, A. B., Yang, X., Wang, L., Xiao, T., Li, J., Feng, J., Xu, Q., and Cheng, H.: A long-term estimation of biogenic volatile organic compound (BVOC) emission in China from 2001–2016: the roles of land cover change and climate variability, Atmos. Chem. Phys., 21, 4825-4848, 10.5194/acp-21-4825-2021, 2021.

Wang, X., Situ, S., Guenther, A., Chen, F. E. I., Wu, Z., Xia, B., and Wang, T.: Spatiotemporal variability of biogenic terpenoid emissions in Pearl River Delta, China, with high-resolution land-cover and meteorological data, Tellus B, 63, 241-254, 10.1111/j.1600-0889.2010.00523.x, 2011.

Figures

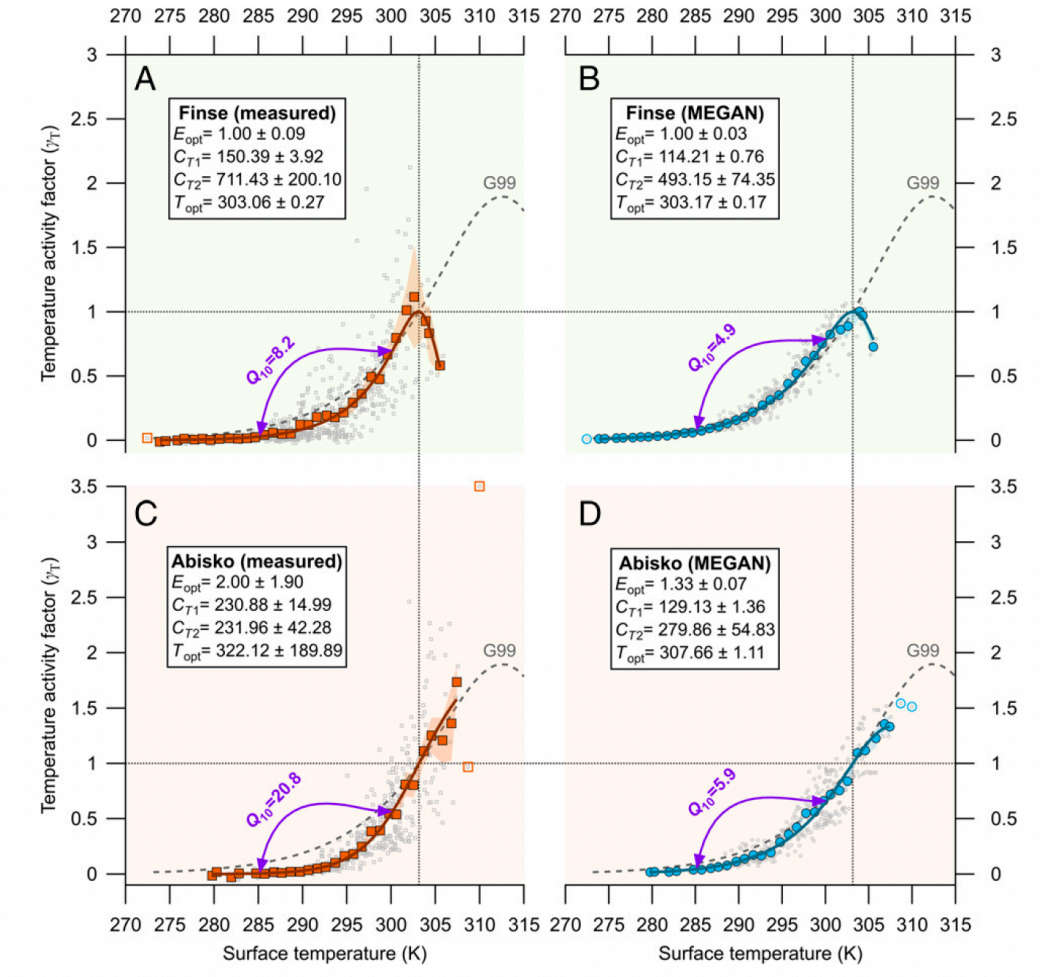

Figure 1.1. (A and C) Measured (square symbols) and (B and D) modeled (circle symbols) isoprene temperature activity factors (γ_T) plotted against the measured vegetation surface temperature for Finse, Norway (A and B), and Abisko, Sweden (C and D). The temperature emission activity factors here are essentially measured and modeled fluxes normalized to 1 at 30 °C (=303.15 K), as indicated by the dotted horizontal lines at γ_T = 1 and dotted vertical lines at T = 303.15 K. The small gray open symbols depict the individual temperature activity factors derived from the individual 30-min fluxes (n = 599 for Finse and n = 432 for Abisko) that passed the eddy covariance quality criteria and were not limited by available sunlight (PPFD ≥ 1,000 μmol m^{-2} s^{-1}). (Seco et al., 2022).

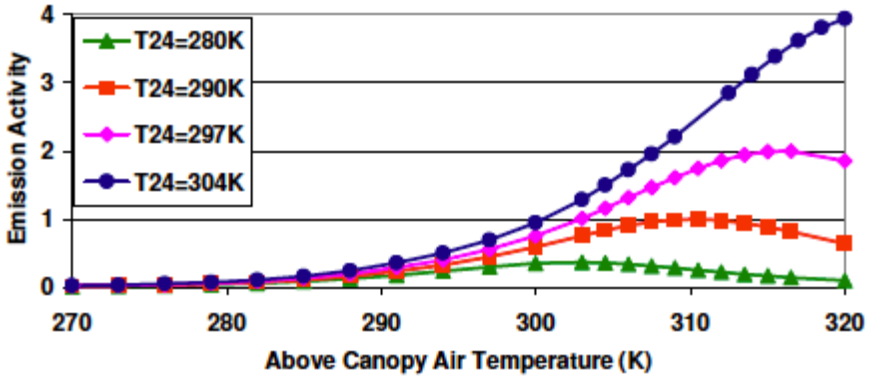

Figure 1.2. The temperature response curves under the different long-term temperatures (Guenther et al., 2006).

CHAPTER 2

MODELING ISOPRENE EMISSION RESPONSE TO DROUGHT AND HEATWAVES WITHIN MEGAN USING EVAPOTRANSPIRATION DATA AND BY COUPLING WITH THE COMMUNITY LAND MODEL

The material presented in this chapter is reproduced from:
Wang, H., Lu, X., Seco, R., Stavrakou, T., Karl, T., Jiang, X., Gu, L., and Guenther, A. B.: Modeling Isoprene Emission Response to Drought and Heatwaves Within MEGAN Using Evapotranspiration Data and by Coupling With the Community Land Model, Journal of Advances in Modeling Earth Systems, 14, e2022MS003174, https://doi.org/10.1029/2022MS003174, 2022.

Abstract:

We introduce two new drought stress algorithms designed to simulate isoprene emission with the Model of Emissions of Gases and Aerosols from Nature (MEGAN) model. The two approaches include the representation of the impact of drought on isoprene emission with a simple empirical approach for offline MEGAN applications and a more process-based approach for online MEGAN in Community Land Model (CLM) simulations. The two versions differ in their implementation of leaf-temperature impacts of mild drought. For the online version of MEGAN that is coupled to CLM, the impact of drought on leaf temperature is simulated directly and the calculated leaf temperature is considered for the estimation of isoprene emission. For the offline version, we apply an empirical algorithm derived from whole-canopy flux measurements for simulating the impact of drought ranging from mild to severe stage. In addition, the offline approach adopts the ratio (f_{PET}) of actual evapotranspiration to potential evapotranspiration to quantify the severity of drought instead of using soil moisture. We applied the two algorithms in the CLM-CAM-chem (the Community Atmosphere Model with Chemistry) model to simulate the impact of drought on isoprene emission and found that drought can decrease isoprene emission globally by 11% in 2012. We further compared the formaldehyde (HCHO) vertical column density simulated by CAM-chem to satellite HCHO observations. We found that the proposed drought algorithm can improve the match with the HCHO

observations during droughts, but the performance of the drought algorithm is limited by the capacity of the model to capture the severity of drought.

2.1 Introduction

Isoprene plays a significant role in tropospheric chemistry due to the large amount of emission and its high chemical reactivity. It is the major species of Biogenic Volatile Organic Compounds (BVOCs) emitted from terrestrial vegetation and accounts for half of global BVOC emission (Guenther et al., 2012). Isoprene is an important precursor of ozone and secondary organic aerosol (SOA) (Sillman, 1999; Claeys et al., 2004), so accurately estimating isoprene emission is required to understand the ozone and SOA relevant chemical and physical processes for improving air quality and managing their climatic impact.

The emission of isoprene is affected by multiple environmental factors like light condition and temperature (Guenther et al., 1993; Guenther et al., 2006; Arneth et al., 2007; Seco et al., 2020). Extreme weather events such as drought and heat waves can also play a role in determining isoprene emission (Potosnak et al., 2014; Seco et al., 2015; Ferracci et al., 2020). The isoprene biosynthesis and emission present a relatively higher drought tolerance than photosynthesis (Tingey et al., 1981; Sharkey and Loreto, 1993; Brüggemann and Schnitzler, 2002; Brilli et al., 2007; Fortunati et al., 2008), and isoprene emission decreases only under a severe drought situation because of the inhibition of substrate supply (Fang et al., 1996; Pegoraro et al., 2004; Brilli et al., 2007). Potosnak et al. (2014) hypothesized that isoprene emission could also be increased at the mild stage of drought indirectly by the increase of leaf temperature induced by reducing stomatal conductance. Supporting evidence of increased isoprene emissions under the mild stage of drought or heat stress has come from a number of studies in different environments (Seco et al. 2015; Otu-Larbi et al., 2020; Kaser et al., 2022). Some of these studies (Jiang et al., 2018; Emmerson et al., 2019; Otu-Larbi et al., 2020; Wang et al., 2021) have proposed algorithms to represent the

influence of drought and heat stress on isoprene emission in earth system models. Niinemets (2010) established a conceptual model for describing the impact of drought and heatwave stress based on the severities of drought and heatwave. In this study, we adopt the model framework of Potosnak et al. (2014) to conceptualize the integrated impact of drought and heatwave. This approach simulates an isoprene emission rate that does not change with mild drought but is increased under moderate drought conditions as leaf temperature increases due to changes in stomatal conductance (Potosnak et al., 2014; Otu-Larbi et al., 2020), which is considered as an indirect impact of drought on isoprene emission through changing leaf temperature. In severe drought events, isoprene emission drops because the substrate supply is eventually affected by the drought (Pegoraro et al., 2004; Fortunati et al., 2008; Niinemets, 2010; Potosnak et al., 2014), and we define this process as the direct impact of drought.

We introduce two drought stress algorithms in the MEGAN v3.2 model in this study. We based our algorithm parameter coefficients on canopy scale flux measurements and scaled up the algorithms in regional and global models. The two drought stress algorithms adopted different ways to represent the impact of mild and moderate droughts on isoprene by stimulating leaf temperature. One major improvement of our drought algorithms is that we considered the two mechanisms of drought impact mentioned above on isoprene emission. Another major improvement of the offline algorithm is the use of a new drought indicator based on the ratio of actual evapotranspiration (ET) to potential evapotranspiration (PET) to evaluate the impact of water stress on isoprene emission. For model validation, we used satellite formaldehyde (HCHO) vertical column density to determine if the drought algorithms could improve the performance of HCHO simulation. In Section 2, we introduce the datasets, including in-situ and satellite-based datasets, that were used in this study. In Section 3, we introduce the emission model and the

drought algorithms. In Section 4, the results of in-situ and global simulations are presented and discussed.

2.2 Datasets

2.2.1 Field measurements

The isoprene flux measurements (Seco et al., 2015) used to parameterize the drought response algorithm were made at the Missouri Ozarks Forest AmeriFlux site (MOFLUX, 38.74° N, -92.2° W) (Gu et al., 2016) in 2012. The site is in the Baskett Wildlife Research and Education (BWREA) Center of the University of Missouri. The isoprene flux and meteorological variables were measured on a 32-m scaffold tower, which is about 10m above the canopy. The site is covered by deciduous broadleaf forest with dominant tree species including white oak and black oak, shagbark hickory, sugar maple and eastern red cedar, and the dominant soils at the site are Weller silt loam and Clinkenbeard very flaggy clay loam (Gu et al., 2016). The campaign started on May 2 and ended on October 22 in 2012, during which a severe drought occurred. The campaign covered the whole growing season and the entire drought event and the associated variability of isoprene flux under the impact of drought, which enabled the development of a canopy scale drought stress algorithm for isoprene emission. More details about the campaign and measurements can be found in Seco et al. (2015).

2.2.2 Satellite observations

Satellite HCHO observations were used to assess the drought algorithm for isoprene emission. Isoprene is the major source of HCHO in most rural regions (Palmer et al., 2003; Wolfe et al., 2016), and the satellite-derived HCHO vertical column density has been widely used to investigate the variability of isoprene emission (Duncan et al., 2009; Zhu et al., 2017; Zheng et al., 2017; Stavrakou et al., 2018) and to constrain isoprene emission (Palmer et al., 2003; Stavrakou et al.,

2009; Stavrakou et al., 2015; Kaiser et al., 2018). We used the monthly HCHO vertical column density derived from the Ozone Monitoring Instrument (OMI) sensor (De Smedt et al., 2015) to investigate the impact of drought on isoprene emission and determine if updating the drought algorithm could improve the simulation of HCHO concentration distributions. The monthly Level-3 HCHO vertical column density with 0.25° spatial resolution used in this study is from the website of the Royal Belgian Institute for Space Aeronomy (BIRA-IASB, https://h2co.aeronomie.be) (De Smedt et al., 2012; De Smedt et al., 2015).

The satellite-derived soil moisture from the ESA-CCI dataset (Dorigo et al., 2017; Gruber et al., 2019) was also used in this study. The ESA-CCI soil moisture (SM) dataset v5.2 used here is a combined product that merged the soil moisture derived from the passive and active microwave-based sensors (Gruber et al., 2019). The ESA-CCI SM dataset v5.2 has a 0.25° spatial resolution with daily temporal frequency, and it was interpolated to the Community Land Model (CLM) model grids and compared to the surface soil moisture simulated by CLM to evaluate the performance of the model.

In addition, a satellite-based drought index, the evaporative stress index (ESI) (Anderson et al., 2011; Anderson et al., 2013), was also used to upscale the offline drought algorithm. ESI is based on the ratio of actual evapotranspiration (ET) to potential evapotranspiration (PET). ESI is derived from the remote sensing Atmosphere-Land Exchange Inverse (ALEXI) model and satellite imagery of the thermal infrared (TIR) band collected by the Geostationary Environmental Satellites (GOES). We downloaded the ESI index over 4-week and 12-week periods from the website of SERVIR GLOBAL (http://catalogue.servirglobal.net/Product?product_id=198).

2.3 Description of the models

MEGAN (Guenther et al., 2006; Guenther et al., 2012) is a widely used flexible model framework for estimating BVOC emissions from individual sites (e.g., Seco et al. (2015) and Seco et al. (2017)) to the global scale (e.g., Müller et al. (2008); Chen et al. (2018); Opacka et al. (2021)). MEGAN v3.2 calculates canopy scale flux of isoprene is estimated as:

$$F = \varepsilon LAI\gamma_{\mathrm{P}}\gamma_{\mathrm{T}}\gamma_{\mathrm{A}}\gamma_{\mathrm{SM}}\gamma_{\mathrm{C}} \quad [2.1]$$

where F (mg m-2 h-1), ε (mg m-2 h-1), and LAI (m2 m-2) represent the isoprene flux amount, the standardized emission factor, and the leaf area index, respectively. γP, γT, γA, γSM, and γC represent the activity factors for light, temperature, leaf age, drought, and CO2 inhibition, respectively.

The applications of MEGAN to estimate BVOC emission for chemistry transport models and earth system models use two approaches: an online version that couples MEGAN into a land ecosystem model (e.g., CLM) that can simulate the stomatal and leaf temperature change implicitly and an offline version that uses an independent MEGAN code. Therefore, we provide two different schemes for models with different complexity: an online isoprene response to drought scheme was directly implemented into a land ecosystem model using CLM as an example with an explicit temperature stimulation algorithm, and an empirical algorithm with a parameterized temperature stimulation algorithm was designed for the independent MEGAN code (Table 2.1).

In this study, we simulated the isoprene flux at the MOFLUX site using both the online and the offline single-point models. The online single-point MEGAN was integrated into the single point version of CLM 5, SP-CLM 5. The offline single-point MEGAN is designed for site-scale simulation and is written in Python. The single-point simulations are driven by the meteorological measurements at the MOFLUX site. The SP-CLM 5 adopted the framework of MEGAN v2.1 (Guenther et al., 2012) and used the canopy scale emission factor of 10 mg m-2 h-1 that represents

the averaged emission potential of the whole canopy. The offline version MEGAN v3.2 used the leaf scale emission factor of 2.45 mg m-2 h-1, which represents the emission capacity of the unit leaf area.

We also conducted global scale simulations using the Community Atmosphere Model with Chemistry (CAM-chem) model and used the results to evaluate the impact of drought on isoprene emission regionally and globally. The simulations were conducted on the NCAR Cheyenne HPE/SGI ICE XA System (CISL 2019). The impact of the drought induced isoprene change on atmospheric chemistry was simulated by CAM-chem. The gas-chemistry and aerosol processes in CAM-chem have been updated recently to better capture biogenic terpenoid (BVOC) relevant reactions and SOA formation (Tilmes et al., 2019; Schwantes et al., 2020; Emmons et al., 2020). In addition, since isoprene is the main contributor to formaldehyde in regions dominated by biogenic emissions (Palmer et al., 2003; Wolfe et al., 2016), we compared the model outputs of the HCHO vertical column density with the satellite product from OMI to study whether the model can capture the change of HCHO during the drought year.

2.3.1 Drought indicators

Accurate estimation of drought severity is important for modeling the drought response of isoprene emission. Previous versions of MEGAN used soil moisture as the indicator of drought (Guenther et al., 2012; Potosnak et al., 2014; Seco et al., 2015; Bonn et al., 2019; Emmerson et al., 2019; Otu-Larbi et al., 2020), and a soil moisture driven algorithm that required soil characteristics (wilting point) information as inputs. However, there are significant limitations with using soil moisture as the drought indicator. First, it is challenging to assign the thresholds for defining drought severity for isoprene emission modeling. For instance, the wilting point, the soil moisture at which a plant cannot extract water from soil, is used to define the severity of drought in MEGAN

v2.1. However, some previous studies (Potosnak et al., 2014; Huang et al., 2015; Seco et al., 2015; Opacka et al., 2022) have shown that the wilting point estimates are a major source of uncertainty for isoprene emission estimation during the drought. Second, the soil moisture driven drought algorithm is sensitive to the accuracy of the soil moisture inputs, and the systematic errors of the soil moisture datasets from land surface models or satellites will directly affect the estimation of isoprene emission (Emmerson et al., 2019; Opacka et al., 2022). In addition, different soil moisture datasets will also affect the performance of algorithms. For instance, soil moisture estimated by various models or observational systems (e.g., satellite or in-situ measurements) could represent different soil depths, so different empirical thresholds are required to simulate the same impact on isoprene emission (Opacka et al., 2022). Third, the hydrologic stress of an ecosystem is affected not only by soil water availability but also the atmospheric vapor pressure deficit (VPD), which represents the atmospheric demand for water (Novick et al., 2016; Park Williams et al., 2013; Porporato et al., 2001; Schulze, 1986).

In this study, we introduce direct vegetation water stress indicators for evaluating the impact of drought on isoprene emission. In the online version of MEGAN in CLM 5, we adopted the water stress function (β_t) to drive the isoprene response to water stress. The β_t is a water stress indicator, ranging between 0 and 1 in CLM, and is calculated as:

$$\beta_t = \sum_{i=1}^{n} w_i r_i \qquad [2.2]$$

where w_i and r_i represent the wilting factor and the fraction of root distribution for different plant functional types (PFT) in soil layer i with n layers in total. The wilting factor in CLM 4.5/5 is as (Oleson et al., 2013):

$$w = \frac{\psi_c - \psi}{\psi_c - \psi_o} \cdot \left(\frac{\theta_s - \theta_{ice}}{\theta_s}\right) \quad [2.3]$$

, where ψ is the soil matric potential (mm), ψ_c and ψ_o are the soil water potential (mm) when stomata are fully closed and fully open, respectively. ψ_c and ψ_o are PFT-dependent parameters, and θ_{ice} is the volumetric soil ice content ($m^3\ m^{-3}$). More details about the calculation of β_t can be found in Oleson et al. (2013). The wilting factor is different from the wilting point. The wilting point is an absolute value based on the soil texture only (Chen and Dudhia, 2001), while the wilting factor is a relative variable to describe the severity of ecosystem water stress based on soil wetness and PFT types. The wilting factor considers the openness of the stomata, which connects plant water stress with soil wetness.

For the offline version model, we used the ratio (f_{PET}) of actual evapotranspiration (ET) to potential evapotranspiration (PET) to indicate drought. Compared to previous studies using soil moisture as the proxy of drought severity (Bonn et al., 2019; Otu-Larbi et al., 2020; Wang et al., 2021), the ET-based drought indicator is expected to provide a more direct measure of water stress on vegetation (Yan et al., 2015).

The half-hour ET (mm day^{-1}) is calculated as:

$$ET = \frac{LE}{\lambda} \quad [2.4]$$

where LE is the latent heat flux (MJ m^{-2} day^{-1}) and λ (MJ kg^{-1}) is the latent heat of vaporization calculated as (Stull, 1988):

$$\lambda = 2.501 - 0.00237 \cdot T \quad [2.5]$$

where T is the air temperature (°C). We treated the reference evapotranspiration as PET, and calculated it using the Penman–Monteith equation as:

$$PET = \frac{0.408\Delta(R_n - G) + \gamma \frac{37}{T + 273.15} u_2(e_s - e_a)}{\Delta + \gamma(1 + 0.34u_2)} \quad [2.6]$$

In equation [2.6], R_n is the net radiation (MJ m^{-2} day^{-1}), G is the soil heat flux density (MJ m^{-2} day^{-1}), Δ (kPa $°C^{-1}$) is the slope of the saturation water vapor pressure at air temperature T (°C), γ is the psychrometric constant (kPa $°C^{-1}$) and u_2 is the wind speed at 2m height (m s^{-1}). e_s and e_a denote the saturation vapor pressure (kPa) at air temperature T and the actual vapor pressure (kPa), respectively. To develop the algorithm, we only take the values of f_{PET} on relatively sunny days when the incoming shortwave radiation is above 500 W m^{-2}. We filled the missing values with the mean of the remaining data points in that day, then we conducted a seven-day smoothing to the f_{PET}. We also adopted a f_{PET} based satellite drought index, ESI (Anderson et al., 2011; Anderson et al., 2013), to spatially upscale the algorithm.

2.3.2 Online Explicit Drought Stress (EDS) algorithm

The online drought stress algorithm introduced here is coupled to the CLM model and is referred to here as the Explicit Drought Stress (EDS) algorithm. As we mentioned above, there are two main mechanisms driving the drought impact on isoprene emission: 1) the indirect impact of drought through changing leaf temperature which drives enzymatic activity, and 2) the direct impact of drought by affecting substrate supply. CLM is a process-based model with comprehensive considerations of the plant physiology, therefore, it can provide inputs for directly simulating the drought impact of leaf temperature and substrate availability. Currently, there are two stomatal conductance models available in CLM 5. Our work is based on the Ball-Berry conductance model described in Collatz et al. (1991) and Sellers et al. (1996), and the leaf stomatal conductance (g_s, μmol s^{-1} m^{-2}) as described by Collatz et al. (1991):

$$g_s = m\frac{A_n}{C_s/P_{atm}}h_s + b\beta_t \quad [2.7]$$

where m is a PFT-dependent parameter, A_n is the leaf net photosynthesis (μmol m^{-2} s^{-1}), C_s is the partial pressure of CO_2 at the leaf surface (Pa), P_{atm} is the atmospheric pressure (Pa), and h_s is the leaf surface humidity at the leaf surface, b is the minimum stomatal conductance (μmol s^{-1} m^{-2}) and β_t is the water stress function described in the previous section. β_t can decrease g_s in response to drought leading to an increase in leaf temperature.

The drought stress is represented by γ_{SM} in the MEGAN model as shown in equation [2.1]. The impact of the severe drought on isoprene emission is presented in Jiang et al. (2018). The drought algorithm in Jiang et al. (2018) is calculated as:

$$\begin{cases} \gamma_{SM} = 1 \ (\beta_t \geq 0.6) \\ \gamma_{SM} = V_{cmax}/\alpha \ (0 < \beta_t < 0.6) \\ \gamma_{SM} = 0 (\beta_t = 0) \end{cases} \quad [2.8]$$

where γ_{SM} is the isoprene emission activity factor response to drought, β_t is the water stress function, V_{cmax} is the maximum rate of carboxylation by the photosynthesis enzyme Rubisco, and α (=37) is an empirical parameter derived from the observations at the MOFLUX site in 2012 (Seco et al., 2015). With this algorithm, the isoprene emission will not be affected when drought is in the mild and moderate stage ($\beta_t \geq 0.6$). In the severe drought condition ($\beta_t < 0.6$), when photosynthesis and the supply of carbon substrates is limited, the emission of isoprene will be decreased. Since the impact of drought on leaf temperature can be simulated by CLM, the MEGAN model integrated within CLM uses CLM parameters to drive the two mechanisms that control how drought influences isoprene emission. However, since this online version of MEGAN relies on CLM to calculate parameters based on detailed biogeochemistry and plant physiology processes,

it cannot be directly applied in simpler model frameworks. Therefore, we developed a parameterized drought algorithm for offline simulations as described in section 3.3.

2.3.3 Offline Parameterized Drought Stress (PDS) algorithm

In MEGAN v2 (Guenther et al. 2006), the drought (soil moisture) impact on isoprene emission is described by a simple empirical algorithm that represents the isoprene emission activity factor response to drought, γ_{SM}, as:

$$\begin{cases} \gamma_{\mathrm{SM}} = 1(\theta > \theta_1) \\ \gamma_{\mathrm{SM}} = (\theta - \theta_w)/\Delta\theta_1 \ (\theta_w < \theta < \theta_1) \\ \gamma_{\mathrm{SM}} = 0(\theta < \theta_w) \end{cases} \quad [2.9]$$

where θ is soil moisture, θ_w is wilting point. $\Delta\theta_1$ is an empirical parameter and θ_1 is defined as $\theta_w+\Delta\theta_1$. The initial version, MEGAN v2 (Guenther et al. 2006), assigned $\Delta\theta_1$ a value of 0.06 m^{-3} m^{-3} based on the potted plant enclosure measurements of Pegoraro et al. (2004). The subsequent version, MEGAN v2.1 (Guenther et al. 2012), assigned a value of 0.04 m^{-3} m^{-3}. As mentioned in Sec. 3.1, there are three main limitations of using soil moisture to evaluate drought severity: uncertainty of thresholds, inconsistences of wilting point and soil moisture values among different datasets and neglecting the impact of atmospheric vapor pressure deficit. In addition, the algorithm in MEGAN v2.1 cannot represent the indirect impact of drought on isoprene through increased leaf temperature induced by lower stomatal conductance.

Two aspects were considered for the new offline algorithm: 1) a reliable way to quantify the severity of drought impacts on inhibiting vegetation biochemical substrates and 2) consideration of the indirect impact of the drought on enhancing isoprene emission through elevated leaf temperature. We refer to this new offline drought algorithm as the Parameterized Drought Stress (PDS) algorithm with empirical coefficients derived from canopy scale observations of isoprene

flux during 2012 at the MOFLUX site. The PDS approach calculates isoprene drought response as:

$$\gamma_{\mathrm{sm}} = \gamma_{\mathrm{sm\_max}} \cdot \gamma_{\mathrm{sub}} \cdot \gamma_{\mathrm{lt}} \quad [2.10]$$

$$\gamma_{\mathrm{sub}} = \frac{1}{1 + b_1 \cdot e^{a_1 \cdot (f_{pet} - 0.2)}} \quad [2.11]$$

$$\gamma_{\mathrm{lt}} = \frac{1}{\gamma_{\mathrm{sm\_max}}} + \frac{\left(1 - \frac{1}{\gamma_{sm\_max}}\right)}{1 + b_2 \cdot e^{a_2 \cdot (1.3 - f_{pet})}} \quad [2.12]$$

In this algorithm, γ_{sm_max} (=1.4) represents the maximum value of γ_{sm}. γ_{sub} and γ_{lt} account for the impacts of the substrate supply (sub) and the leaf temperature (lt) stimulation, respectively. The parameters a_1 (=-7.45), a_2 (=-28.76), b_1 (=3.26) and b_2 (=2.35 × 10^6) control the shape of the curve. We propose f_{PET} as a suitable drought indicator because the transpiration of plants would decrease with stomata closure when plants feel the water stress (Hanson, 1991). We normalized the seven-day running averaged f_{PET} for the 2012 MOFLUX study to span the range of 0 to 1 by using the minimum value of 0 and the maximum value of 0.82 (95% percentile of the seven-day running averaged f_{PET} between 2006-2017). Other vegetation water stress indexes or indicators (e.g., ESI drought index in this study) can alternatively be used as inputs after being normalized the maximum to 1 and the minimum to 0, and this feature is important for using the PDS algorithm in other model framework with other drought indexes or inputs. The PDS algorithm responses of γ_{sm}, γ_{sub} and γ_{lt} to the normalized drought index are shown in Figure 2.1. The estimates of γ_{sm} derived from the ratios between the flux observations (F_{obs}) and the offline model outputs (F_{mod}) are calculated as:

$$\gamma_{\text{sm\_obs}} = \frac{F_{obs}}{F_{mod}} \quad [2.13]$$

The normalized drought indexes were divided into bins with an interval of 0.05, and the averaged values of γ_{sm_obs} in each bin of normalized f_{PET} were used to fit the model. All averaged ratios were divided by the first value of the array to set γ_{sm_obs} to unity when there is no drought. γ_{lt} increases when drought gets into the moderate stage (index < 0.9) and stays stable, while the γ_{sub} decreases when drought is severe enough (index < 0.7) to affect the supply of substrate for isoprene synthase (Figure 2.1).

2.4 Results and discussion

2.4.1 Comparison of drought indicators

We compared the different drought indicators for the 2012 MOFLUX study as shown in Figure 2.2. We also calculated the residuals between the isoprene flux observed at the MOFLUX site and the isoprene flux modeled by the independent MEGAN v3.2 without the drought algorithm. The independent MEGANv3.2 was driven by the meteorological inputs observed at the site. The residuals (green dots) of the model increase at the beginning of the drought and decrease near the end of the drought (Figure 2.2). The soil moisture datasets from the in-situ measurements (green solid line) at 10 cm depth and the ESA-CCI SM (Gruber et al., 2019) satellite product (pink triangles) show a similar pattern of soil moisture that is not fully consistent with the changes of the model residual. The soil moisture decreases before the drought starts to affect the emission of isoprene from May 3 to June 2. We also presented the time-series of other drought indicators for the MOFLUX site in 2012. The variabilities of f_{PET} and β_t are more consistent with the change of the model residuals (Figure 2.2). Using soil moisture as a drought indicator is an indirect way to reflect the water stress of vegetation. The f_{PET} and β_t used in the offline and online drought

algorithms in this study are a more direct representation of water stress for vegetation. More importantly, using f_{PET} and β_t could relatively decrease the need to set wilting point threshold values, which are a major contributor to the uncertainties described in Sec. 3.1. We used the 2012 observations from the MOFLUX site as the benchmark to choose the suitable inputs for scaling up the model. We tested different normalized drought indexes using the PDS algorithm in this study, and the results are shown in Figure S2.1. The satellite-based ESI drought index over a 12-week period shows a good consistency with the f_{PET} behavior (Figure 2.2) and can therefore be used to scale up the PDS offline algorithm for regional to global scale modeling. Compared with the approach using soil moisture as the drought indicator, the approaches using the direct plant water stress indexes is a more suitable way to simulate the impact of drought on isoprene emission by connecting plant physiology with the soil and atmosphere wetness. However, these indexes are also limited by the models and parameters used for estimating the severity of water stress. For instance, there are still some discrepancies among f_{PET}, βt and ESI (e.g., start date of the water stress) even though their general patterns are the same for the MOFLUX site in 2012.

2.4.2 Site scale simulations

We ran site scale simulations to investigate the impact of the drought on isoprene emission at the MOFLUX site. The online model results came from SP-CLM 5 model, and the offline model results from the independent version MEGAN v3.2. Both models were driven by the meteorology variables measured at the MOFLUX site in 2012. The input of the PDS algorithm for the offline model is the normalized seven-day running average f_{PET} as shown in Figure 2.2. The comparisons between the model results and observations are shown in Figure 2.3 and Figure 2.4. The online and offline models both overestimated the isoprene flux during the drought period when drought was neglected (Figure 2.3). When the drought algorithm was adopted, both the online and offline

versions of the model captured the drought impact on isoprene emission (Figure 2.3). We also presented the results of the offline model embedded in the original drought algorithm (equation [2.9]) with θ_w of 0.194 (orange line in Figure 2.3). The original algorithm can have a comparable performance with the new one in this study with a suitable wilting point, however, the difficulty still exists for determining the wilting point. The difference between the drought algorithms developed in this study and the previous algorithms is discussed in Section 4.4.

The performance of the SP-CLM model with embedded MEGAN and that of the offline MEGAN v3.2 model differed in the simulation of isoprene flux at MOFLUX in 2012 (Figure 2.4). This is at least partly because they have different canopy models for simulating the environmental conditions including leaf temperature and light conditions. Furthermore, both the online and offline models captured the variabilities of isoprene flux when the drought algorithms were adopted ((c) and (d) in Figure 2.4). For the SP-CLM-MEGAN model, the R^2 increased from 0.39 to 0.59, and the mean bias (MB), the mean error (ME) and the root mean square error (RMSE) decreased from -3.82, 5.13 and 7.32 mg m^{-2} h^{-1} to -0.19, 2.49 and 3.76 mg m^{-2} h^{-1}, respectively. For the offline version MEGAN v3.2, the R^2 increased from 0.53 to 0.78. The MB, the ME and the RMSE decreased from -4.6, 5.08 and 5.53 mg m^{-2} h^{-1} to -1.61, 2.31 and 2.68 mg m^{-2} h^{-1}, respectively.

We used the results of SP-CLM-MEGAN model to present 1) the indirect impact of drought through changing leaf temperature and 2) the direct impact of drought by affecting substrate supply on isoprene emissions at the MOFLUX site in 2012. As shown in Figure 2.5, the impact of drought on leaf temperature appears with the onset of water stress ($\beta_t < 1$). By decreasing the stomatal conductance following equation [2.7], the leaf temperature could increase up to 0.83°C at the MOFLUX site during the 2012 drought ((a) in Figure 2.5). Correspondingly, the change of leaf

temperature could lead to an increase of isoprene emission up to 14.5% ((b) in Figure 2.5). Meanwhile, the direct impact of drought on substrate supply started to affect the simulated isoprene emission when β_t is lower than 0.6 according to equation [2.8]. The direct impact of drought is related to the severity of drought in CLM, and the change of isoprene emission could be near 100% when the drought is very severe (Figure 2.5). The final impact of drought is the combination of these two mechanisms.

In the offline model, the two mechanisms are represented by γ_{sub} and γ_{lt}. As shown in Figure 2.6, the onset of drought causes γ_{lt}, which represents the indirect impact of drought, to increase and then stay stable. Meanwhile, the direct impact is controlled by the severity of drought with γ_{sub} decreasing with normalized drought index. Based on observations at the MOFLUX site, we assign a maximum of a 40% increase of isoprene emission (γ_{sm_max} = 1.4) due to the increase in leaf temperature. After combining with the direct impact of drought (γ_{sub}), the maximum value of γ_{sm} is about 1.27, which results in an up to 27% increase in isoprene emission due to drought. Therefore, with the development of drought, the simulated γ_{sm} will initially increase and then decrease due to severe drought (Figure 2.6).

2.4.3 Global scale simulations

The drought algorithms were scaled up with global simulations using the FCSD component set (https://www.cesm.ucar.edu/models/cesm2/config/compsets.html) in the Community Earth System Model Version 2.1.3 (CESM2) (Danabasoglu et al., 2020). This was accomplished by integrating the drought response into the MEGAN component of the CLM-CAM-chem model and using this to simulate the impact of drought on isoprene emission and atmospheric chemistry in 2012 as an example. The model system was driven by the Modern-Era Retrospective analysis for

Research and Applications Version 2 (MERRA 2) reanalysis dataset with about 1-degree spatial resolution. The BVOC emissions were calculated by MEGAN embedded in the CLM 5 model with the prescribed satellite vegetation phenology. Anthropogenic and biomass burning emissions are obtained from the standard Coupled Model Intercomparison Project round 6 (CMIP6) (Eyring et al., 2016). Three model experiments were performed to test the drought algorithms: 1) without any drought algorithm, 2) with the online EDS drought algorithm and 3) with the offline PDS drought algorithm. When we applied the offline PDS algorithm to the CLM, we modified equation [2.7] and removed the impact of drought on stomatal conductance by deleting β_t from equation [2.7], which means that the stomatal conductance could not be changed by the water stress function β_t. The input for the offline model is the water stress function β_t, which is also a normalized drought indicator in the range of 0-1 and is close to the normalized f_{PET} (Figure S2.1) at the MOFLUX site. Both the online and offline models show a decrease of isoprene emission (Figure S2.2), with the EDS and PDS algorithms decreasing the global isoprene emission by 11.0% and 10.4%, respectively.

The offline PDS drought algorithm can also employ other drought indexes besides using β_t from the CLM model. This feature is useful for developing BVOC emission estimates for regional air quality simulations using readily available model inputs. This includes calculating the offline γ_{sm} using the ESI drought index. The 12-week ESI index was normalized by the values of -3.5 and -0.5 to the range of 0-1. We compared the γ_{sm} calculated by the different combinations of algorithms and inputs for the CONtiguous United States (CONUS) region during the summer of 2012 as shown in Figure 2.7, and the inputs, β_t and the normalized ESI, are shown in Figure S2.3. The propagation of γ_{sm} from the satellite input is shown in Figure S2.4, and γ_{sm} from the satellite input reflects the impact of drought among the regions around Missouri, Illinois and Indiana states,

but the spatial distribution of γ_{sm} derived from the CLM model shows a horizontally wider impact of drought. The γ_{sm} derived from the CLM model also shows the impact of drought in arid or semi-arid regions like Texas and Arizona. One potential reason is that the CLM model overestimates the severity of drought. As shown in Figure 2.8, we compared the surface moisture simulated by CLM 5 with the ESA-CCI satellite soil moisture datasets, and the CLM model shows an underestimation of the surface soil moisture with a negative mean bias during the summer of 2012 in the regions where the drought occurred. This indicates that the impact of drought might be exaggerated by the CLM model. Therefore, the skill of the land model to capture the drought behavior directly affects the simulated drought influence on isoprene emission.

We compared the monthly OMI HCHO vertical column densities with the modeled HCHO vertical column densities. The horizontal distribution of the HCHO vertical column densities for CONUS from the models and the satellite are compared in Figure 2.9 and show that the drought algorithms decrease the MB of simulated HCHO vertical column densities in the regions including the Missouri, Illinois, Arkansas, and Indiana states where the drought occurred in 2012 (Figure 2.9). However, the drought algorithms also increased the simulation errors in Oklahoma and Texas because the land model exaggerated the severity of drought in these two regions as shown in Figure 2.7 and Figure 2.8. We also assessed the grids where tree cover fraction is greater than 30% and β_t is less than 0.85 in CONUS during May to September in 2012. As shown in Figure 2.10, the drought algorithms had a negative impact on the R^2 and decreased the slope. The models assuming no drought affects shows an overestimation of HCHO vertical column density in CONUS in the high concentration regime, and the implementation of drought algorithms results in a better agreement with the observations as shown in Figure 2.10. The MB, ME and RMSE in CONUS decreased from 1.28, 2.39 and 2.72×10^{15} molecules cm^{-2} to 0.31, 1.92 and 2.41×10^{15} molecules

cm^{-2}, respectively, with the online EDS drought algorithm and to 0.36, 1.92 and 2.41 × 10^{15} molecules cm^{-2}, respectively, with the offline PDS drought algorithm. The results show that the drought algorithms could decrease the model biases in simulating the HCHO in drought regions. However, our assessment could also be affected by uncertainties from other sources besides the drought algorithms and the biogenic emission model. Therefore, more in-situ observations, especially long-term isoprene flux measurements, are required to fully validate the isoprene drought response algorithms for future predictions.

2.4.4 Comparison with previous studies

As shown in Table 2.2, previous drought algorithms for isoprene emission have mostly been based on volumetric soil water content (θ or SWC) or other soil moisture-relevant parameters like soil water availability because of the relatively easy access to the data (Bonn et al., 2019). Two threshold values of soil water content, the wilting point (θ_w) and the critical soil moisture (θ_c), play a key role in these algorithms to define the severity of drought and the calculation of γ_{sm} (Guenther et al., 2012; Bonn et al., 2019; Otu-Larbi et al., 2020). The assumption among these algorithms is that isoprene emission would not be affected when $\theta \geq \theta_c$. When the soil moisture is in the range of $\theta_w < \theta < \theta_c$, γ_{sm} would decrease with the soil moisture and reach 0 when the soil moisture reaches the wilting point. The value of γ_{sm} is always in the range of 0-1, with lower values accounting for the negative impact of drought on isoprene emission by cutting off the supply of the carbon substrate for isoprene synthase. Bonn et al. (2019) uses the soil water availability (SWA) index to replace SWC as input for the algorithm, but the SWA is also based on soil moisture and the wilting point. SWA can be normalized to SWC with the range of 0-1 and is calculated as:

$$SWA = \frac{\theta - \theta_w}{\theta_{max} - \theta_w} \quad (14)$$

where θ_{max} and θ_w denote the maximum value of SWC and the wilting point, respectively. We compared the soil moisture-based algorithms as shown in Figure 2.11. The wilting point at the MOFLUX site is about 0.23 m^3 m^{-3} according to Seco et al. (2015), and the maximum measured SWC was 0.47 m^3 m^{-3} at the MOFLUX site during 2012. As shown in Figure 2.11 and Table 2.2, the previous soil moisture algorithms follow the assumptions that we mentioned above, and the differences are the shape of the curve and the values of $\Delta\theta_1$, which is the difference between θ_w and θ_c. Therefore, these algorithms are sensitive to the threshold values, as noted in previous studies (Seco et al., 2015; Huang et al., 2015; Potosnak et al., 2014; Müller et al., 2008; Bonn et al., 2019). We also presented these algorithms with the normalized inputs of SWA in Figure 2.11. These algorithms simulate lower isoprene when the SWA is below 0.4 because the isoprene emission is affected when the soil moisture is near or below the wilting point. In addition, the thresholds of the algorithms differ because of different $\Delta\theta_1$. In this study, we adopted the normalized f_{PET} as the model input for the offline algorithms. Because f_{PET} is a relatively more direct reflection of the water stress on the ecosystem, the impact of drought on isoprene emission during different stages may be better represented by f_{PET}. That is, at the early stage of drought, the isoprene emission will not be affected by drought, and from the moderate stage to the severe stage of drought ($f_{PET} < 0.9$), the drought will initially increase isoprene emission due to an increase in leaf temperature and then decrease the isoprene emission due to the limited supply of the substrate as photosynthesis rates decline.

We applied each of the soil moisture-based algorithms listed in Table 2.2 for the MOFLUX site during 2012. The default wilting point dataset used for MEGANv2 and v2.1 comes from the global database of Chen and Dudhia (2001) and has a wilting point of 0.084 m^3 m^{-3} for the MOFLUX site. The models listed in Table 2.2 will never have any drought impacts with a wilting

point of 0.084 m^3 m^{-3} because the θ_w and θ_c are always below the observed soil moisture levels. Therefore, we used the value of 0.23 m^3 m^{-3} recommended by Seco et al. (2015) and based on site characteristics. However, the previous soil moisture-based algorithms did not capture the variability of isoprene flux (Figure S2.5 in the supplement). We also tested the case of using the minimum value of soil moisture (0.196 m^3 m^{-3}) as the wilting point at the MOFLUX site (Figure 2.12), and the results showed better agreement with the observations than the results with the wilting point of 0.23 m^3 m^{-3} (Figure S2.5). The choice of θ_w, or the thresholds, overwhelmingly determines the performance of these algorithms. The soil moisture input data, which is difficult to simulate in global models, will also affect the performance of these algorithms. In our experiments, we used the in-situ soil moisture measurements at 10 cm depth as the model input. There is a strong vertical gradient in soil moisture so the soil depth where measurements are made, or modeled values predicted, could also affect model performance. If the input is changed to other soil moisture datasets for different depths, such as the surface soil moisture datasets from satellite or root zone soil moisture datasets, the current threshold values would not be appropriate (Opacka et al., 2022).

2.4.5 Future Direction

Heatwaves and drought often happen simultaneously, and both can influence isoprene emission. Ferracci et al. (2020) and Potosnak et al. (2014) both observed a higher-than-expected increase of isoprene concentration and flux during mild drought and heatwave events. Recent evidence from the satellite HCHO observation also shows an increase of isoprene during the drought and heatwave events (Morfopoulos et al., 2022). It is difficult to distinguish any individual impacts of these two processes directly from the in-situ observations. Besides the γ_{sm}, Otu-Larbi et al. (2020) introduced another independent correction factor to explain the impact of high temperature. In the framework of MEGAN, the impact of heatwaves on isoprene emission is

currently not considered independently, and the impact of high temperature is described by the temperature response algorithm. In addition to the impact of the current temperature, MEGAN also considers the influence of past temperature. This includes the average temperature of the past twenty-four hours and the average temperature of the past ten days. As shown in Figure 2.4 of Guenther et al. (2006), elevated temperature for the preceding days would also increase isoprene emission in the temperature response algorithm. Otu-Larbi et al. (2020) used the original temperature algorithm of Guenther et al. (1993) that only accounts for the current temperature that represents the instantaneous isoprene synthase enzyme activity. Besides the impact of the past high temperature during a heat wave, another factor that could increase the isoprene emission is the drought impact on the leaf temperature, which has been considered in this study and was estimated to reach an increase of 27% in the offline PDS drought algorithm and reach a maximum increase of 14.5% caused by a ~0.84 °C temperature change in the online EDS algorithm. However, this is based on the leaf temperature results simulated by the CLM model, which is subject to model uncertainties, including the stomatal conductance algorithm. Field and laboratory experiments have shown that water stress could increase the leaf temperature to a much higher level of about 3-4°C under high photosynthetically active radiation (Reynolds-Henne et al., 2010; Gerhards et al., 2016). Therefore, there is a need for further investigation of the connections among drought, stomatal conductance, leaf temperature, ET, and isoprene emission using observations and modeling.

In addition, isoprene emission drought response studies are still limited by having canopy scale flux observations only from a single site and there is an urgent need for more observations. For example, at the same MOFLUX site, Geron et al. (2016) found that the tree species with diverse tolerance of water stress show different reactions of isoprene emission to drought. The

purpose of this study is to establish new model frameworks for simulating the impact of drought, and the further validation and improvements require more observations. This include more observations at deciduous broadleaf forests as well as observations of the responses of other ecosystem, and it could be important to include isohydric as well as anisohydric plant species. The flux measurements are currently rare due to the expense and the measurements that focus on drought and heatwave are difficult to obtain. Relaxed eddy accumulation (REA) technique (Ciccioli et al., 2003; Sarkar et al., 2020) combined with a gas chromatograph with photoionization detection (GC-PID) (Bolas et al., 2020) is an example of a lower-cost alternative for isoprene flux measurements and create more data for model validation and improvement. Besides having more in-situ ground observations, the existing and future airborne observations and satellite products could also provide an opportunity to further investigate and understand the impact of environmental stress on BVOC emission. The high resolution (30m-70m) ET and ESI index products from the ECOsystem Spaceborne Thermal Radiometer Experiment on Space Station (ECOSTRESS) could be a good tool for monitoring water stress and providing model inputs. In addition, the high resolution HCHO observations from the TROPOspheric Monitoring Instrument (TROPOMI) instrument (Veefkind et al., 2012) and recent direct observations of isoprene from the Cross-track Infrared Sounder (CrIS) instrument (Fu et al., 2019; Wells et al., 2020) may also provide information on atmospheric chemistry processes and improve assessments of the impact of drought.

Reference

Anderson, M. C., Hain, C., Wardlow, B., Pimstein, A., Mecikalski, J. R., and Kustas, W. P.: Evaluation of drought indices based on thermal remote sensing of evapotranspiration over the continental United States, Journal of Climate, 24, 2025-2044, 2011.

Anderson, M. C., Hain, C., Otkin, J., Zhan, X., Mo, K., Svoboda, M., Wardlow, B., and Pimstein, A.: An intercomparison of drought indicators based on thermal remote sensing and NLDAS-2 simulations with US Drought Monitor classifications, Journal of Hydrometeorology, 14, 1035-1056, 2013.

Arneth, A., Niinemets, Ü., Pressley, S., Bäck, J., Hari, P., Karl, T., Noe, S., Prentice, I., Serça, D., and Hickler, T.: Process-based estimates of terrestrial ecosystem isoprene emissions: incorporating the effects of a direct CO 2-isoprene interaction, Atmospheric Chemistry and Physics, 7, 31-53, 2007.

Bolas, C. G., V. Ferracci, A. D. Robinson, M. I. Mead, M. S. M. Nadzir, J. A. Pyle, R. L. Jones, and N. R. P. Harris (2020), iDirac: a field-portable instrument for long-term autonomous measurements of isoprene and selected VOCs, Atmos. Meas. Tech., 13(2), 821-838, doi:10.5194/amt-13-821-2020.

Bonn, B., Magh, R. K., Rombach, J., and Kreuzwieser, J.: Biogenic isoprenoid emissions under drought stress: different responses for isoprene and terpenes, Biogeosciences, 16, 4627-4645, 10.5194/bg-16-4627-2019, 2019.

Brilli, F., Barta, C., Fortunati, A., Lerdau, M., Loreto, F., and Centritto, M.: Response of isoprene emission and carbon metabolism to drought in white poplar (Populus alba) saplings, New Phytologist, 175, 244-254, https://doi.org/10.1111/j.1469-8137.2007.02094.x, 2007.

Brüggemann, N., and Schnitzler, J. P.: Comparison of Isoprene Emission, Intercellular Isoprene Concentration and Photosynthetic Performance in Water-Limited Oak (Quercus pubescens Willd. and Quercus robur L.) Saplings, Plant Biology, 4, 456-463, https://doi.org/10.1055/s-2002-34128, 2002.

Chen, F., and Dudhia, J.: Coupling an Advanced Land Surface–Hydrology Model with the Penn State–NCAR MM5 Modeling System. Part I: Model Implementation and Sensitivity, Monthly Weather Review, 129, 569-585, 10.1175/1520-0493(2001)129<0569:CAALSH>2.0.CO;2, 2001.

Chen, W. H., Guenther, A. B., Wang, X. M., Chen, Y. H., Gu, D. S., Chang, M., Zhou, S. Z., Wu, L. L., and Zhang, Y. Q.: Regional to Global Biogenic Isoprene Emission Responses to Changes in Vegetation From 2000 to 2015, Journal of Geophysical Research: Atmospheres, 123, 3757-3771, 10.1002/2017JD027934, 2018.

Ciccioli, P., E. Brancaleoni, M. Frattoni, S. Marta, A. Brachetti, M. Vitullo, G. Tirone, and R. Valentini (2003), Relaxed eddy accumulation, a new technique for measuring emission and deposition fluxes of volatile organic compounds by capillary gas chromatography and mass spectrometry, Journal of Chromatography A, 985(1), 283-296, doi:https://doi.org/10.1016/S0021-9673(02)01731-4.

Computational and Information Systems Laboratory. 2019. Cheyenne: HPE/SGI ICE XA System (University Community Computing). Boulder, CO: National Center for Atmospheric Research. doi:10.5065/D6RX99HX.

Claeys, M., Graham, B., Vas, G., Wang, W., Vermeylen, R., Pashynska, V., Cafmeyer, J., Guyon, P., Andreae, M. O., and Artaxo, P.: Formation of secondary organic aerosols through photooxidation of isoprene, Science, 303, 1173-1176, 2004.

Collatz, G. J., Ball, J. T., Grivet, C., and Berry, J. A.: Physiological and environmental regulation of stomatal conductance, photosynthesis and transpiration: a model that includes a laminar boundary layer, Agricultural and Forest meteorology, 54, 107-136, 1991.

Danabasoglu, G., Lamarque, J. F., Bacmeister, J., Bailey, D. A., DuVivier, A. K., Edwards, J., Emmons, L. K., Fasullo, J., Garcia, R., Gettelman, A., Hannay, C., Holland, M. M., Large, W. G., Lauritzen, P. H., Lawrence, D. M., Lenaerts, J. T. M., Lindsay, K., Lipscomb, W. H., Mills, M. J., Neale, R., Oleson, K. W., Otto-Bliesner, B., Phillips, A. S., Sacks, W., Tilmes, S., van Kampenhout, L., Vertenstein, M., Bertini, A., Dennis, J., Deser, C., Fischer, C., Fox-Kemper, B., Kay, J. E., Kinnison, D., Kushner, P. J., Larson, V. E., Long, M. C., Mickelson, S., Moore, J. K., Nienhouse, E., Polvani, L., Rasch, P. J., and Strand, W. G.: The Community Earth System Model Version 2 (CESM2), Journal of Advances in Modeling Earth Systems, 12, e2019MS001916, https://doi.org/10.1029/2019MS001916, 2020.

De Smedt, I., Van Roozendael, M., Stavrakou, T., Müller, J. F., Lerot, C., Theys, N., Valks, P., Hao, N., and van der A, R.: Improved retrieval of global tropospheric formaldehyde columns from GOME-2/MetOp-A addressing noise reduction and instrumental degradation issues, Atmos. Meas. Tech., 5, 2933-2949, 10.5194/amt-5-2933-2012, 2012.

De Smedt, I., Stavrakou, T., Hendrick, F., Danckaert, T., Vlemmix, T., Pinardi, G., Theys, N., Lerot, C., Gielen, C., Vigouroux, C., Hermans, C., Fayt, C., Veefkind, P., Müller, J. F., and Van Roozendael, M.: Diurnal, seasonal and long-term variations of global formaldehyde columns inferred from combined OMI and GOME-2 observations, Atmos. Chem. Phys., 15, 12519-12545, 10.5194/acp-15-12519-2015, 2015.

De Smedt, I., Pinardi, G., Vigouroux, C., Compernolle, S., Bais, A., Benavent, N., Boersma, F., Chan, K. L., Donner, S., Eichmann, K. U., Hedelt, P., Hendrick, F., Irie, H., Kumar, V., Lambert, J. C., Langerock, B., Lerot, C., Liu, C., Loyola, D., Piters, A., Richter, A., Rivera Cárdenas, C. I., Romahn, F., Ryan, R. G., Sinha, V., Theys, N., Vlietinck, J., Wagner, T., Wang, T., Yu, H., and Van Roozendael, M.: Comparative assessment of TROPOMI and OMI formaldehyde observations against MAX-DOAS network column measurements, Atmos. Chem. Phys. Discuss., 2021, 1-51, 10.5194/acp-2021-378, 2021.

Dorigo, W., Wagner, W., Albergel, C., Albrecht, F., Balsamo, G., Brocca, L., Chung, D., Ertl, M., Forkel, M., Gruber, A., Haas, E., Hamer, P. D., Hirschi, M., Ikonen, J., de Jeu, R., Kidd, R., Lahoz, W., Liu, Y. Y., Miralles, D., Mistelbauer, T., Nicolai-Shaw, N., Parinussa, R., Pratola, C., Reimer, C., van der Schalie, R., Seneviratne, S. I., Smolander, T., and Lecomte, P.: ESA CCI Soil Moisture for improved Earth system understanding: State-of-the art and future directions, Remote Sensing of Environment, 203, 185-215, https://doi.org/10.1016/j.rse.2017.07.001, 2017.

Duncan, B. N., Yoshida, Y., Damon, M. R., Douglass, A. R., and Witte, J. C.: Temperature dependence of factors controlling isoprene emissions, Geophysical Research Letters, 36, n/a-n/a, 10.1029/2008GL037090, 2009.

Emmerson, K. M., Palmer, P. I., Thatcher, M., Haverd, V., and Guenther, A. B.: Sensitivity of isoprene emissions to drought over south-eastern Australia: Integrating models and satellite observations of soil moisture, Atmospheric Environment, 209, 112-124, https://doi.org/10.1016/j.atmosenv.2019.04.038, 2019.

Emmons, L. K., Schwantes, R. H., Orlando, J. J., Tyndall, G., Kinnison, D., Lamarque, J.-F., Marsh, D., Mills, M. J., Tilmes, S., Bardeen, C., Buchholz, R. R., Conley, A., Gettelman,

A., Garcia, R., Simpson, I., Blake, D. R., Meinardi, S., and Pétron, G.: The Chemistry Mechanism in the Community Earth System Model Version 2 (CESM2), Journal of Advances in Modeling Earth Systems, 12, e2019MS001882, https://doi.org/10.1029/2019MS001882, 2020.

Eyring, V., Bony, S., Meehl, G. A., Senior, C. A., Stevens, B., Stouffer, R. J., and Taylor, K. E.: Overview of the Coupled Model Intercomparison Project Phase 6 (CMIP6) experimental design and organization, Geosci. Model Dev., 9, 1937-1958, 10.5194/gmd-9-1937-2016, 2016.

Fang, C., Monson, R. K., and Cowling, E. B.: Isoprene emission, photosynthesis, and growth in sweetgum (Liquidambar styraciflua) seedlings exposed to short- and long-term drying cycles, Tree Physiology, 16, 441-446, 10.1093/treephys/16.4.441, 1996.

Ferracci, V., Bolas, C. G., Freshwater, R. A., Staniaszek, Z., King, T., Jaars, K., Otu-Larbi, F., Beale, J., Malhi, Y., Waine, T. W., Jones, R. L., Ashworth, K., and Harris, N. R. P.: Continuous Isoprene Measurements in a UK Temperate Forest for a Whole Growing Season: Effects of Drought Stress During the 2018 Heatwave, Geophysical Research Letters, 47, e2020GL088885, 10.1029/2020GL088885, 2020.

Fortunati, A., Barta, C., Brilli, F., Centritto, M., Zimmer, I., Schnitzler, J.-P., and Loreto, F.: Isoprene emission is not temperature-dependent during and after severe drought-stress: a physiological and biochemical analysis, The Plant Journal, 55, 687-697, https://doi.org/10.1111/j.1365-313X.2008.03538.x, 2008.

Fu, D., Millet, D. B., Wells, K. C., Payne, V. H., Yu, S., Guenther, A., and Eldering, A.: Direct retrieval of isoprene from satellite-based infrared measurements, Nature Communications, 10, 3811, 10.1038/s41467-019-11835-0, 2019.

Gerhards, M., Rock, G., Schlerf, M., and Udelhoven, T.: Water stress detection in potato plants using leaf temperature, emissivity, and reflectance, International Journal of Applied Earth Observation and Geoinformation, 53, 27-39, https://doi.org/10.1016/j.jag.2016.08.004, 2016.

Geron, C., R. Daly, P. Harley, R. Rasmussen, R. Seco, A. Guenther, T. Karl, and L. Gu (2016), Large drought-induced variations in oak leaf volatile organic compound emissions during PINOT NOIR 2012, Chemosphere, 146, 8-21, doi:https://doi.org/10.1016/j.chemosphere.2015.11.086.

Gruber, A., Scanlon, T., van der Schalie, R., Wagner, W., and Dorigo, W.: Evolution of the ESA CCI Soil Moisture climate data records and their underlying merging methodology, Earth Syst. Sci. Data, 11, 717-739, 10.5194/essd-11-717-2019, 2019.

Gu, D., Guenther, A. B., Shilling, J. E., Yu, H., Huang, M., Zhao, C., Yang, Q., Martin, S. T., Artaxo, P., Kim, S., Seco, R., Stavrakou, T., Longo, K. M., Tóta, J., de Souza, R. A. F., Vega, O., Liu, Y., Shrivastava, M., Alves, E. G., Santos, F. C., Leng, G., and Hu, Z.: Airborne observations reveal elevational gradient in tropical forest isoprene emissions, Nature Communications, 8, 15541, 10.1038/ncomms15541 https://www.nature.com/articles/ncomms15541#supplementary-information, 2017.

Gu, L., Pallardy, S. G., Yang, B., Hosman, K. P., Mao, J., Ricciuto, D., Shi, X., and Sun, Y.: Testing a land model in ecosystem functional space via a comparison of observed and modeled ecosystem flux responses to precipitation regimes and associated stresses in a Central U.S. forest, Journal of Geophysical Research: Biogeosciences, 121, 1884-1902, https://doi.org/10.1002/2015JG003302, 2016.

Guenther, A., Karl, T., Harley, P., Wiedinmyer, C., Palmer, P., and Geron, C.: Estimates of global terrestrial isoprene emissions using MEGAN (Model of Emissions of Gases and Aerosols from Nature), Atmos. Chem. Phys, 6, 3181-3210, 2006.

Guenther, A. B., Zimmerman, P. R., Harley, P. C., Monson, R. K., and Fall, R.: Isoprene and monoterpene emission rate variability: Model evaluations and sensitivity analyses, Journal of Geophysical Research: Atmospheres, 98, 12609-12617, doi:10.1029/93JD00527, 1993.

Guenther, A. B., Jiang, X., Heald, C. L., Sakulyanontvittaya, T., Duhl, T., Emmons, L. K., and Wang, X.: The Model of Emissions of Gases and Aerosols from Nature version 2.1 (MEGAN2.1): an extended and updated framework for modeling biogenic emissions, Geoscientific Model Development, 5, 1471-1492, 10.5194/gmd-5-1471-2012, 2012.

Hanson, R. L.: Evapotranspiration and droughts, National Water Summary 1988–89: Hydrologic Events and Floods and Droughts (US Geological Survey Water-Supply Paper 2375), 99-104, 1991.

Huang, L., McGaughey, G., McDonald-Buller, E., Kimura, Y., and Allen, D. T.: Quantifying regional, seasonal and interannual contributions of environmental factors on isoprene and monoterpene emissions estimates over eastern Texas, Atmospheric Environment, 106, 120-128, https://doi.org/10.1016/j.atmosenv.2015.01.072, 2015.

Jiang, X., Guenther, A., Potosnak, M., Geron, C., Seco, R., Karl, T., Kim, S., Gu, L., and Pallardy, S.: Isoprene emission response to drought and the impact on global atmospheric chemistry, Atmospheric Environment, 183, 69-83, https://doi.org/10.1016/j.atmosenv.2018.01.026, 2018.

Kaser, L., Peron, A., Graus, M., Striednig, M., Wohlfahrt, G., Juráň, S., and Karl, T.: Interannual variability of terpenoid emissions in an alpine city, Atmos. Chem. Phys., 22, 5603-5618, 10.5194/acp-22-5603-2022, 2022.

Kaiser, J., Jacob, D. J., Zhu, L., Travis, K. R., Fisher, J. A., González Abad, G., Zhang, L., Zhang, X., Fried, A., Crounse, J. D., St. Clair, J. M., and Wisthaler, A.: High-resolution inversion of OMI formaldehyde columns to quantify isoprene emission on ecosystem-relevant scales: application to the southeast US, Atmos. Chem. Phys., 18, 5483-5497, 10.5194/acp-18-5483-2018, 2018.

Morfopoulos, C., Müller, J.-F., Stavrakou, T., Bauwens, M., De Smedt, I., Friedlingstein, P., Prentice, I. C., and Regnier, P.: Vegetation responses to climate extremes recorded by remotely sensed atmospheric formaldehyde, Global Change Biology, 28, 1809-1822, https://doi.org/10.1111/gcb.15880, 2022.

Müller, J. F., Stavrakou, T., Wallens, S., De Smedt, I., Van Roozendael, M., Potosnak, M. J., Rinne, J., Munger, B., Goldstein, A., and Guenther, A. B.: Global isoprene emissions estimated using MEGAN, ECMWF analyses and a detailed canopy environment model, Atmos. Chem. Phys., 8, 1329-1341, 10.5194/acp-8-1329-2008, 2008.

Niinemets, U.: Mild versus severe stress and BVOCs: thresholds, priming and consequences, Trends Plant Sci, 15, 145-153, 10.1016/j.tplants.2009.11.008, 2010.

Novick, K. A., Ficklin, D. L., Stoy, P. C., Williams, C. A., Bohrer, G., Oishi, A. C., Papuga, S. A., Blanken, P. D., Noormets, A., Sulman, B. N., Scott, R. L., Wang, L., and Phillips, R. P.: The increasing importance of atmospheric demand for ecosystem water and carbon fluxes, Nature Climate Change, 6, 1023-1027, 10.1038/nclimate3114, 2016.

Oleson, K., Lawrence, D., Bonan, G., Drewniak, B., Huang, M., Koven, C., Levis, S., Li, F., Riley, W., and Subin, Z.: Technical description of version 4.5 of the community land model (CLM), NCAR Tech. Note, NCAR/TN-503+ STR, 420 pp., https://doi. org/10.5065/D6RR1W7M, 2013.

Opacka, B., Müller, J. F., Stavrakou, T., Bauwens, M., Sindelarova, K., Markova, J., and Guenther, A. B.: Global and regional impacts of land cover changes on isoprene emissions derived from spaceborne data and the MEGAN model, Atmos. Chem. Phys., 21, 8413-8436, 10.5194/acp-21-8413-2021, 2021.

Opacka, B., Müller, J.-F., Stavrakou, T., Miralles, D. G., Koppa, A., Pagán, B. R., Potosnak, M. J., Seco, R., De Smedt, I., and Guenther, A. B.: Impact of Drought on Isoprene Fluxes Assessed Using Field Data, Satellite-Based GLEAM Soil Moisture and HCHO Observations from OMI, Remote Sensing, 14, 2021, 2022.

Otu-Larbi, F., Bolas, C. G., Ferracci, V., Staniaszek, Z., Jones, R. L., Malhi, Y., Harris, N. R. P., Wild, O., and Ashworth, K.: Modelling the effect of the 2018 summer heatwave and drought on isoprene emissions in a UK woodland, Global Change Biology, 26, 2320-2335, 10.1111/gcb.14963, 2020.

Palmer, P. I., Jacob, D. J., Fiore, A. M., Martin, R. V., Chance, K., and Kurosu, T. P.: Mapping isoprene emissions over North America using formaldehyde column observations from space, Journal of Geophysical Research: Atmospheres, 108, n/a-n/a, 10.1029/2002JD002153, 2003.

Park Williams, A., Allen, C. D., Macalady, A. K., Griffin, D., Woodhouse, C. A., Meko, D. M., Swetnam, T. W., Rauscher, S. A., Seager, R., Grissino-Mayer, H. D., Dean, J. S., Cook, E. R., Gangodagamage, C., Cai, M., and McDowell, N. G.: Temperature as a potent

driver of regional forest drought stress and tree mortality, Nature Climate Change, 3, 292-297, 10.1038/nclimate1693, 2013.

Pegoraro, E., Rey, A., Greenberg, J., Harley, P., Grace, J., Malhi, Y., and Guenther, A.: Effect of drought on isoprene emission rates from leaves of Quercus virginiana Mill, Atmospheric Environment, 38, 6149-6156, https://doi.org/10.1016/j.atmosenv.2004.07.028, 2004.

Porporato, A., Laio, F., Ridolfi, L., and Rodriguez-Iturbe, I.: Plants in water-controlled ecosystems: active role in hydrologic processes and response to water stress: III. Vegetation water stress, Advances in Water Resources, 24, 725-744, https://doi.org/10.1016/S0309-1708(01)00006-9, 2001.

Potosnak, M. J., LeStourgeon, L., Pallardy, S. G., Hosman, K. P., Gu, L., Karl, T., Geron, C., and Guenther, A. B.: Observed and modeled ecosystem isoprene fluxes from an oak-dominated temperate forest and the influence of drought stress, Atmospheric Environment, 84, 314-322, https://doi.org/10.1016/j.atmosenv.2013.11.055, 2014.

Reynolds-Henne, C. E., Langenegger, A., Mani, J., Schenk, N., Zumsteg, A., and Feller, U.: Interactions between temperature, drought and stomatal opening in legumes, Environmental and Experimental Botany, 68, 37-43, https://doi.org/10.1016/j.envexpbot.2009.11.002, 2010.

Sarkar, C., et al. (2020), A portable, low-cost relaxed eddy accumulation (REA) system for quantifying ecosystem-level fluxes of volatile organics, Atmospheric Environment, 242, 117764, doi:https://doi.org/10.1016/j.atmosenv.2020.117764.

Schulze, E. D.: Carbon dioxide and water vapor exchange in response to drought in the atmosphere and in the soil, Annual Review of Plant Physiology, 37, 247-274, 1986.

Schwantes, R. H., Emmons, L. K., Orlando, J. J., Barth, M. C., Tyndall, G. S., Hall, S. R., Ullmann, K., St. Clair, J. M., Blake, D. R., Wisthaler, A., and Bui, T. P. V.: Comprehensive isoprene and terpene gas-phase chemistry improves simulated surface ozone in the southeastern US, Atmos. Chem. Phys., 20, 3739-3776, 10.5194/acp-20-3739-2020, 2020.

Seco, R., Karl, T., Guenther, A., Hosman, K. P., Pallardy, S. G., Gu, L., Geron, C., Harley, P., and Kim, S.: Ecosystem-scale volatile organic compound fluxes during an extreme drought in a broadleaf temperate forest of the Missouri Ozarks (central USA), Global Change Biology, 21, 3657-3674, doi:10.1111/gcb.12980, 2015.

Seco, R., Karl, T., Turnipseed, A., Greenberg, J., Guenther, A., Llusia, J., Peñuelas, J., Dicken, U., Rotenberg, E., Kim, S., and Yakir, D.: Springtime ecosystem-scale monoterpene fluxes from Mediterranean pine forests across a precipitation gradient, Agricultural and Forest Meteorology, 237-238, 150-159, https://doi.org/10.1016/j.agrformet.2017.02.007, 2017.

Seco, R., Holst, T., Matzen, M. S., Westergaard-Nielsen, A., Li, T., Simin, T., Jansen, J., Crill, P., Friborg, T., Rinne, J., and Rinnan, R.: Volatile organic compound fluxes in a subarctic peatland and lake, Atmos. Chem. Phys., 20, 13399-13416, 10.5194/acp-20-13399-2020, 2020.

Sellers, P. J., Randall, D. A., Collatz, G. J., Berry, J. A., Field, C. B., Dazlich, D. A., Zhang, C., Collelo, G. D., and Bounoua, L.: A Revised Land Surface Parameterization (SiB2) for Atmospheric GCMS. Part I: Model Formulation, Journal of Climate, 9, 676-705, 10.1175/1520-0442(1996)009<0676:ARLSPF>2.0.CO;2, 1996.

Sharkey, T. D., and Loreto, F.: Water stress, temperature, and light effects on the capacity for isoprene emission and photosynthesis of kudzu leaves, Oecologia, 95, 328-333, 1993.

Sillman, S.: The relation between ozone, NOx and hydrocarbons in urban and polluted rural environments, Atmospheric Environment, 33, 1821-1845, http://dx.doi.org/10.1016/S1352-2310(98)00345-8, 1999.

Stavrakou, T., Müller, J.-F., Smedt, I. D., Roozendael, M. V., Van der Werf, G., Giglio, L., and Guenther, A.: Evaluating the performance of pyrogenic and biogenic emission inventories against one decade of space-based formaldehyde columns, Atmospheric Chemistry and Physics, 9, 1037-1060, 2009.

Stavrakou, T., Müller, J. F., Bauwens, M., De Smedt, I., Van Roozendael, M., De Mazière, M., Vigouroux, C., Hendrick, F., George, M., Clerbaux, C., Coheur, P. F., and Guenther, A.: How consistent are top-down hydrocarbon emissions based on formaldehyde observations from GOME-2 and OMI?, Atmos. Chem. Phys., 15, 11861-11884, 10.5194/acp-15-11861-2015, 2015.

Stavrakou, T., Müller, J. F., Bauwens, M., Smedt, I., Roozendael, M., and Guenther, A.: Impact of Short-term Climate Variability on Volatile Organic Compounds Emissions Assessed Using OMI Satellite Formaldehyde Observations, Geophysical Research Letters, 0, 10.1029/2018GL078676, 2018.

Stull, R. B.: An introduction to boundary layer meteorology, Springer Science & Business Media, 1988.

Tilmes, S., Hodzic, A., Emmons, L. K., Mills, M. J., Gettelman, A., Kinnison, D. E., Park, M., Lamarque, J. F., Vitt, F., Shrivastava, M., Campuzano-Jost, P., Jimenez, J. L., and Liu, X.: Climate Forcing and Trends of Organic Aerosols in the Community Earth System

Model (CESM2), Journal of Advances in Modeling Earth Systems, 11, 4323-4351, https://doi.org/10.1029/2019MS001827, 2019.

Tingey, D. T., Evans, R., and Gumpertz, M.: Effects of environmental conditions on isoprene emission from live oak, Planta, 152, 565-570, 10.1007/BF00380829, 1981.

Veefkind, J. P., Aben, I., McMullan, K., Förster, H., de Vries, J., Otter, G., Claas, J., Eskes, H. J., de Haan, J. F., Kleipool, Q., van Weele, M., Hasekamp, O., Hoogeveen, R., Landgraf, J., Snel, R., Tol, P., Ingmann, P., Voors, R., Kruizinga, B., Vink, R., Visser, H., and Levelt, P. F.: TROPOMI on the ESA Sentinel-5 Precursor: A GMES mission for global observations of the atmospheric composition for climate, air quality and ozone layer applications, Remote Sensing of Environment, 120, 70-83, https://doi.org/10.1016/j.rse.2011.09.027, 2012.

Wang, P., Liu, Y., Dai, J., Fu, X., Wang, X., Guenther, A., and Wang, T.: Isoprene Emissions Response to Drought and the Impacts on Ozone and SOA in China, Journal of Geophysical Research: Atmospheres, 126, e2020JD033263, https://doi.org/10.1029/2020JD033263, 2021.

Wells, K. C., Millet, D. B., Payne, V. H., Deventer, M. J., Bates, K. H., de Gouw, J. A., Graus, M., Warneke, C., Wisthaler, A., and Fuentes, J. D.: Satellite isoprene retrievals constrain emissions and atmospheric oxidation, Nature, 585, 225-233, 10.1038/s41586-020-2664-3, 2020.

Wolfe, G. M., Kaiser, J., Hanisco, T. F., Keutsch, F. N., de Gouw, J. A., Gilman, J. B., Graus, M., Hatch, C. D., Holloway, J., Horowitz, L. W., Lee, B. H., Lerner, B. M., Lopez-Hilifiker, F., Mao, J., Marvin, M. R., Peischl, J., Pollack, I. B., Roberts, J. M., Ryerson, T. B., Thornton, J. A., Veres, P. R., and Warneke, C.: Formaldehyde production from

isoprene oxidation across NOx regimes, Atmos. Chem. Phys., 16, 2597-2610, 10.5194/acp-16-2597-2016, 2016.

Yan, H., Wang, S.-q., Billesbach, D., Oechel, W., Bohrer, G., Meyers, T., Martin, T. A., Matamala, R., Phillips, R. P., Rahman, F., Yu, Q., and Shugart, H. H.: Improved global simulations of gross primary product based on a new definition of water stress factor and a separate treatment of C3 and C4 plants, Ecological Modelling, 297, 42-59, https://doi.org/10.1016/j.ecolmodel.2014.11.002, 2015.

Zheng, Y., Unger, N., Tadić, J. M., Seco, R., Guenther, A. B., Barkley, M. P., Potosnak, M. J., Murray, L. T., Michalak, A. M., Qiu, X., Kim, S., Karl, T., Gu, L., and Pallardy, S. G.: Drought impacts on photosynthesis, isoprene emission and atmospheric formaldehyde in a mid-latitude forest, Atmospheric Environment, 167, 190-201, https://doi.org/10.1016/j.atmosenv.2017.08.017, 2017.

Zhu, L., Mickley, L. J., Jacob, D. J., Marais, E. A., Sheng, J., Hu, L., Abad, G. G., and Chance, K.: Long-term (2005–2014) trends in formaldehyde (HCHO) columns across North America as seen by the OMI satellite instrument: Evidence of changing emissions of volatile organic compounds, Geophysical Research Letters, 44, 7079-7086, 10.1002/2017GL073859, 2017.

Figures and Tables

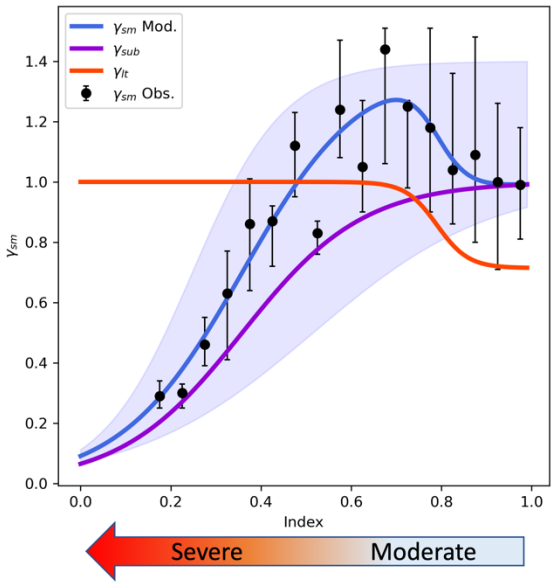

Figure 2.1. The parameterized drought stress (PDS) algorithm for offline MEGAN simulations. γ_{sm} represents the response of isoprene emission to drought. The index, 7-day running averaged f_{PET}, represents the severity of drought. The observed values were grouped into 0.05 index intervals, and the upper (lower) cap of error bars represents the upper (lower) quartile. The blue, red and purple solid lines represent the fitting model of γ_{sm}, γ_{lt} and γ_{sub}, respectively, and the blue shadow represents 95% confident intervals of the fitting model of γ_{sm}.

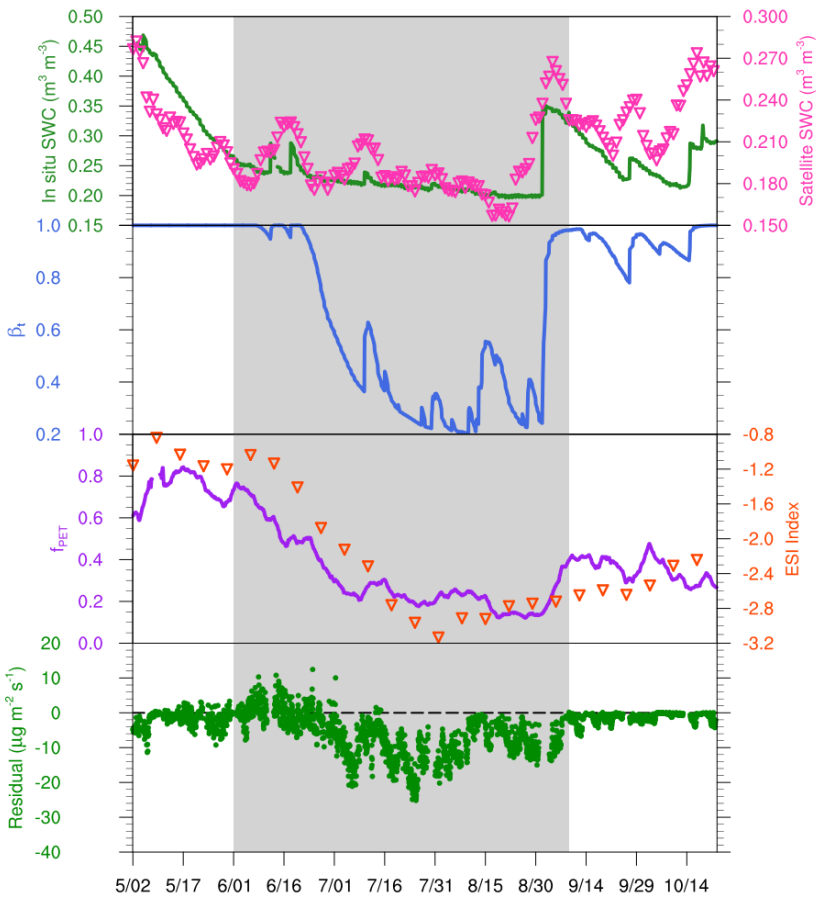

Figure 2.2. Comparison of drought indicators at the MOFLUX site in 2012. The drought period is indicated with a grey background. The first panel represents the 10cm soil water content (SWC) from the in-situ observations at the MOFLUX site (green solid line) and the surface soil water content (SWC) from the ESA-CCI satellite product (pink triangles). The second panel represents the β_t simulated by the Community Land Model (blue solid line), and the third panel represents the drought indexes (f_{PET}) based on the ratio of the real evapotranspiration (ET) and the potential evapotranspiration (PET) from the in-situ observations (purple solid line) and the satellite 12-week ESI drought index (orange triangles). The last panel represents the residuals of MEGAN v3.2 without the drought algorithm (green dots).

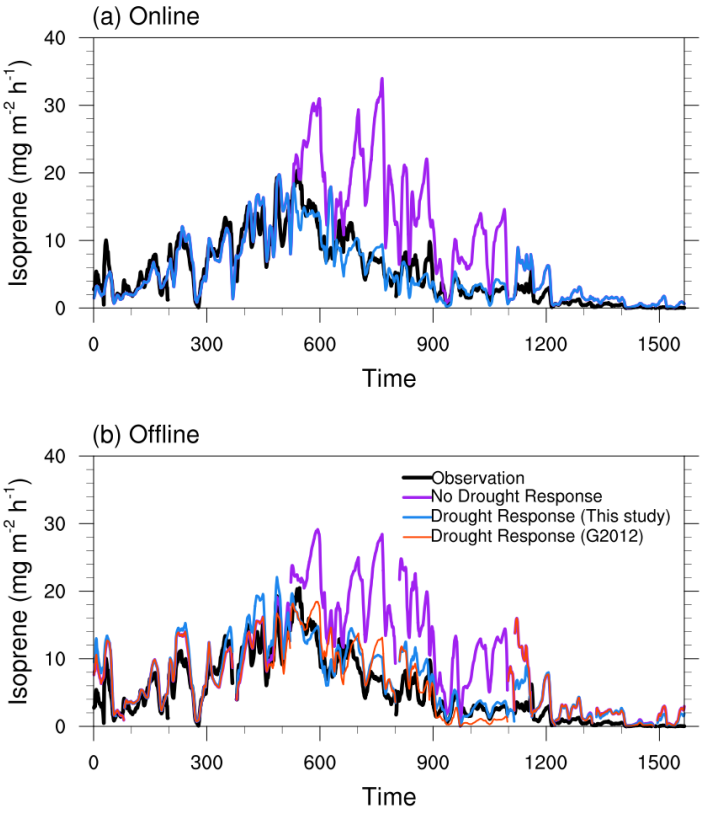

Figure 2.3. The 9-hour running averaged time series of the hourly isoprene flux during the daytime observed and simulated by (a) SP-CLM-MEGAN and (b) the offline version MEGAN v3.2 at the MOFLUX site in 2012. The observations, model results with and without the drought algorithm in this study are presented by the black, blue and purple solid lines, respectively. The offline model results by the original drought algorithm are presented by the orange line in (b).

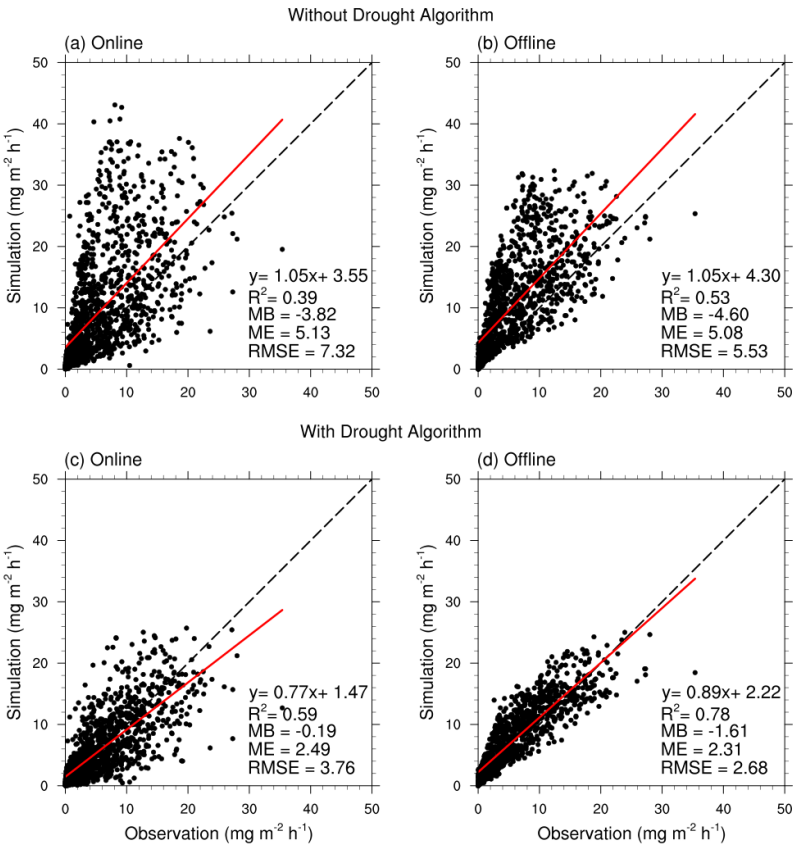

Figure 2.4. Scatter plots of measured and modelled hourly isoprene fluxes during the daytime. The results of SP-CLM-MEGAN with and without the EDS drought algorithm are presented in (a) and (c). The results of the offline version MEGAN v3.2 model with and without the PDS drought algorithm are presented in (b) and (d). MB, ME and RMSE are abbreviations of the mean bias, the mean error and the root mean square error with the unit of mg m^{-2} h^{-1}, respectively.

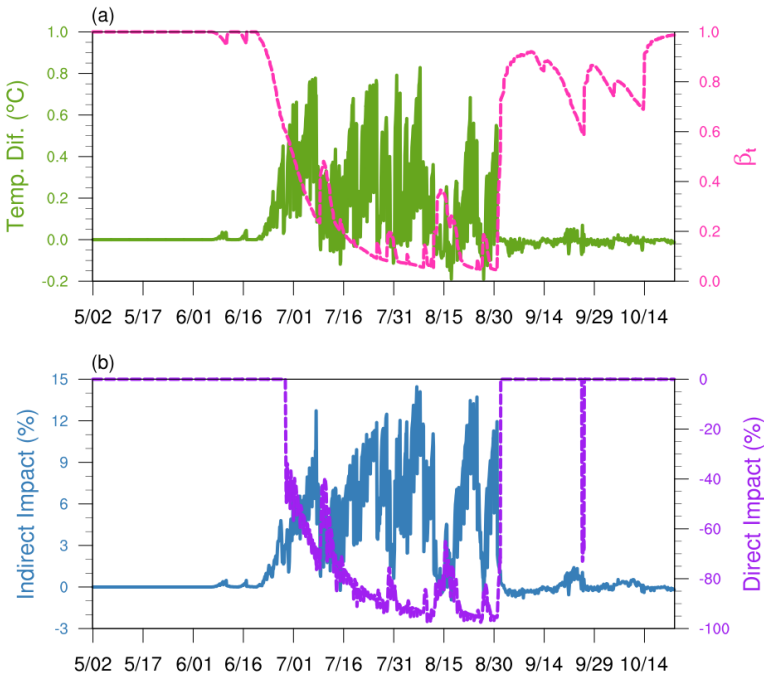

Figure 2.5. The change of leaf temperature and isoprene emission change simulated by SP-CLM-MEGAN during the drought at the MOFLUX site in 2012. The leaf temperature change induced by drought (green solid line) and βt simulated by SP-CLM (pink dashed line) are presented in (a), and the indirect impact of drought caused by stimulating temperature (blue solid line) and the direct impacts of drought caused by affecting substrate availability on isoprene emission (purple dashed line) are presented in (b).

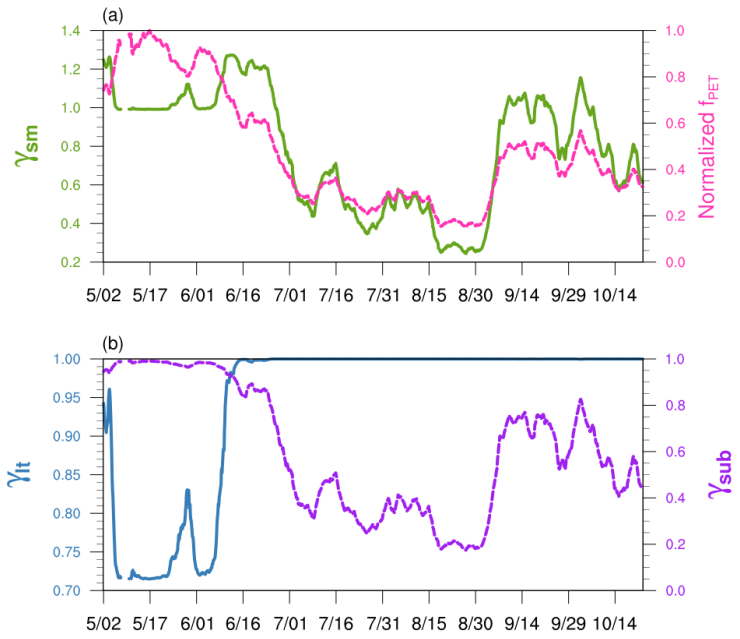

Figure 2.6. The impact of drought simulated by the offline PDS algorithm at the MOFLUX site in 2012. The total impact of drought (γ_{sm}) on isoprene emission (green solid line) and the the normalized seven-day running averaged f_{PET} (pink dashed line) are presented in (a). The indirect impact of drought caused by stimulating temperature (γ_{lt}, blue solid line) and the direct impact of drought caused by affecting substrate availability on isoprene emission (γ_{sub}, purple dashed line) are presented in (b).

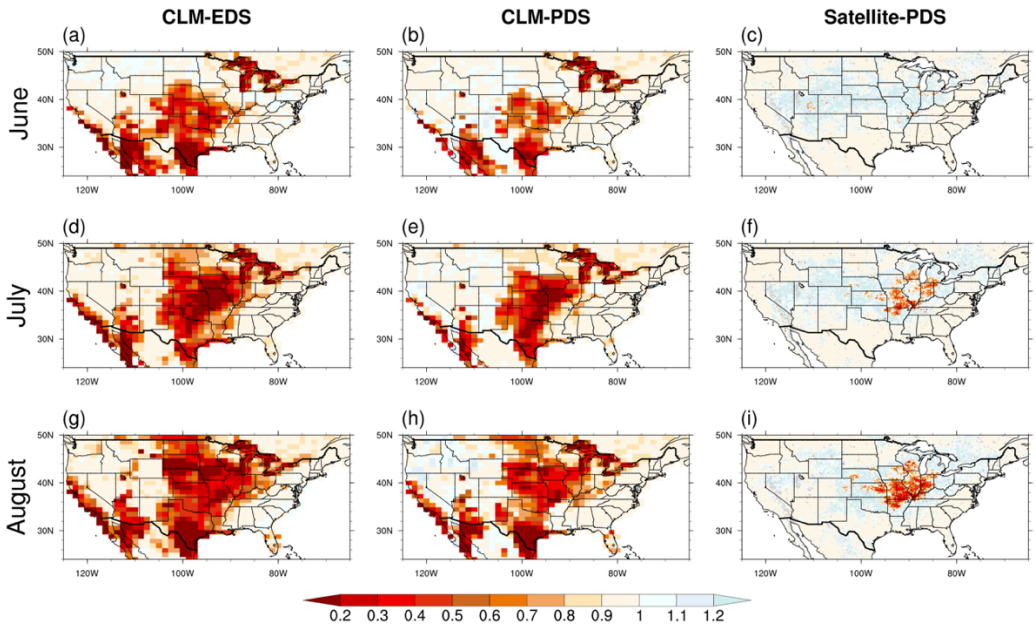

Figure 2.7. The spatial distributions of γ_{sm} calculated by the online Explicit Drought Stress (EDS) (first columns), the offline Parameterized Drought Stress (PDS) algorithms with β_t as inputs (second column) and with the satellite evaporative stress index (ESI) as inputs (third column). The three rows represent different months from June to August.

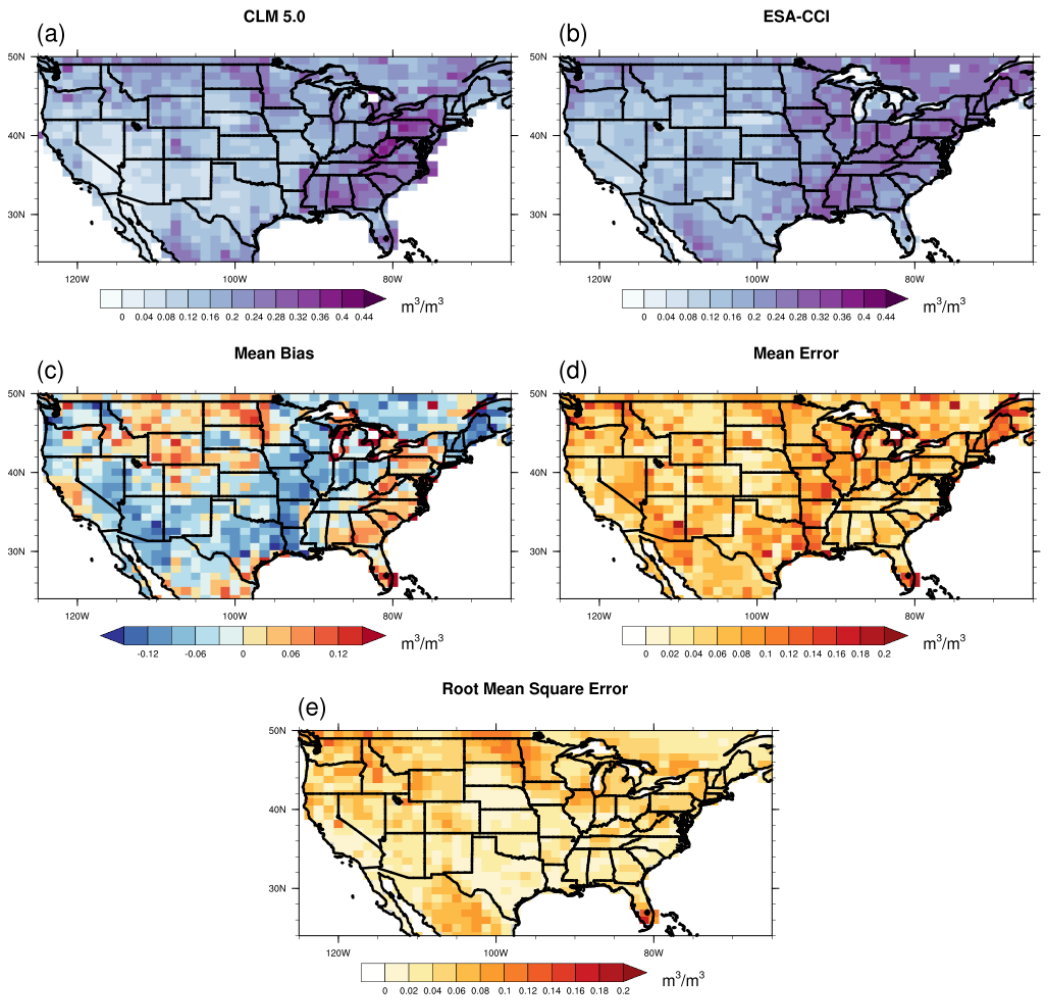

Figure 2.8. Comparison of the monthly surface soil moisture from the CLM model (a) and the ESA-CCI dataset (b) during July to August in 2012. The spatial distributions of the Mean Bias (c), the Mean Error (d) and the Root Mean Square Error (e) are also shown expressed in $m^3\ m^{-3}$.

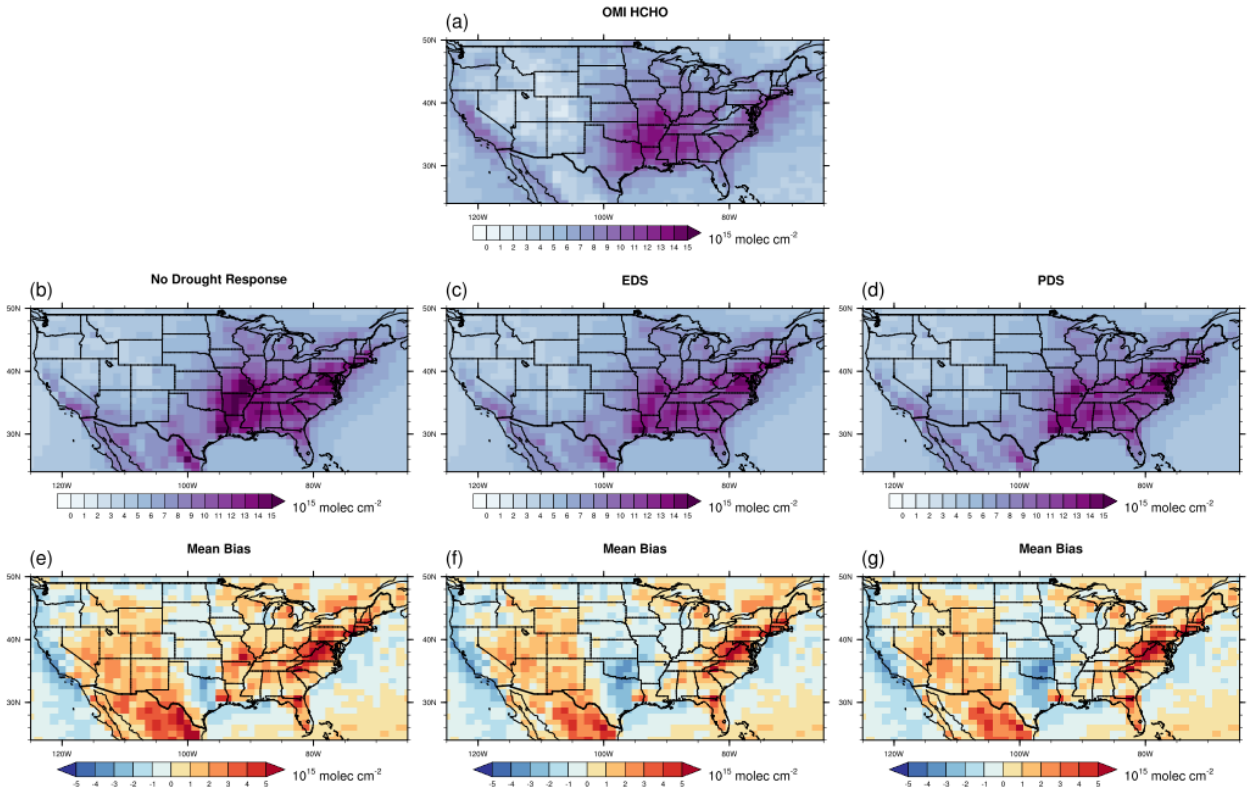

Figure 2.9. Comparison of the monthly OMI formaldehyde vertical column densities and the simulated formaldehyde vertical column densities by CAM-chem in the CONUS region during May-September 2012. The results by the no drought response experiment, the online Explicit Drought Stress (EDS) and the offline Parameterized Drought Stress (PDS) algorithm experiments are presented in the first, second and third columns, respectively. (a)-(d) shows the spatial distribution of the averaged formaldehyde vertical column densities by OMI and CAM-chem model with different drought treatment. The spatial distributions of the Mean Bias are also presented with the unit of 10^{15} molecules cm^{-2}.

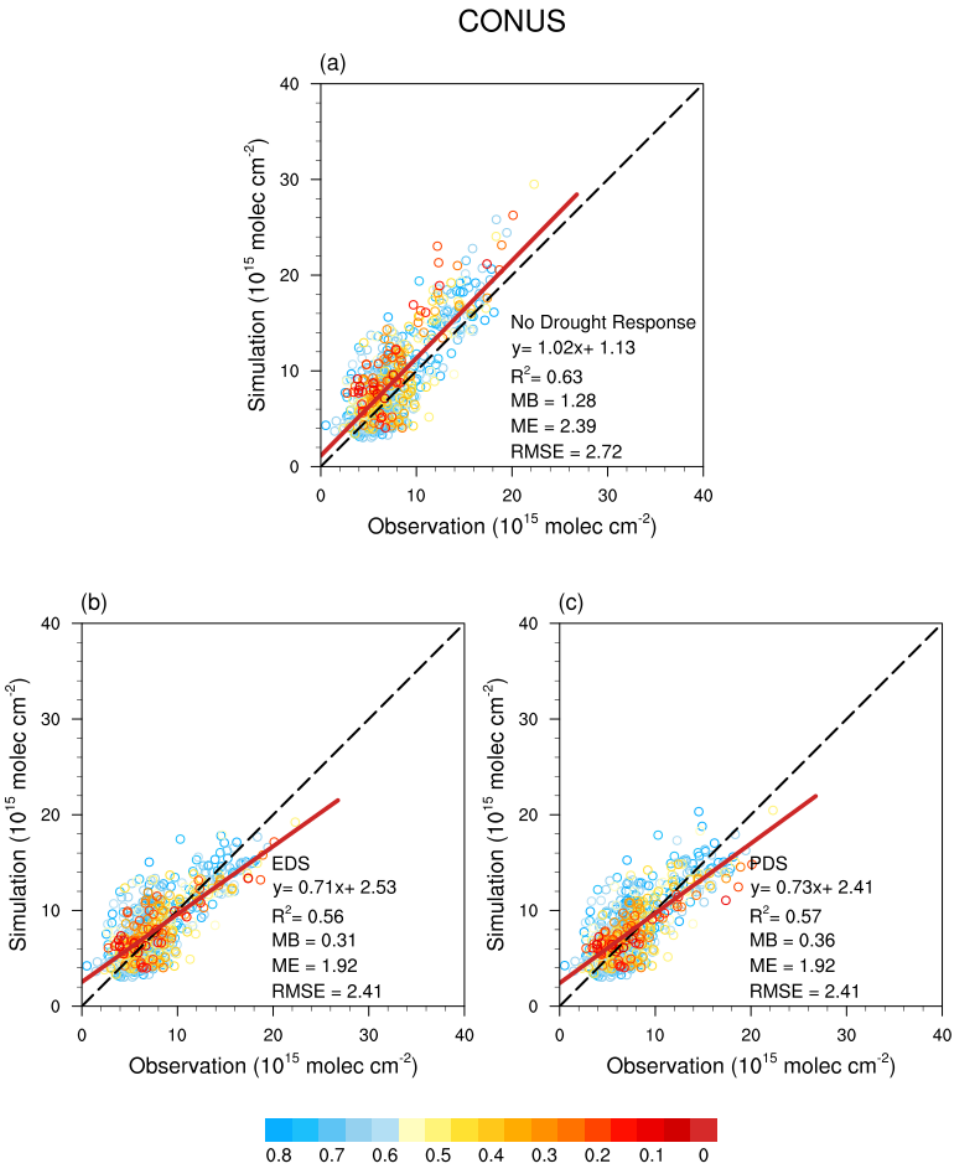

Figure 2.10. Comparisons between the monthly OMI formaldehyde vertical column densities and the simulated formaldehyde vertical column densities by CAM-chem in the CONtiguous United States (CONUS). The results by the online Explicit Drought Stress (EDS) and the offline Parameterized Drought Stress (PDS) algorithms are presented in (b) and (c), respectively. The color of the points represents the value of the monthly β_t. The mean bias (MB), the mean error (ME) and the root mean square error (RMSE) are presented with the unit of 10^{15} molecules cm^{-2}.

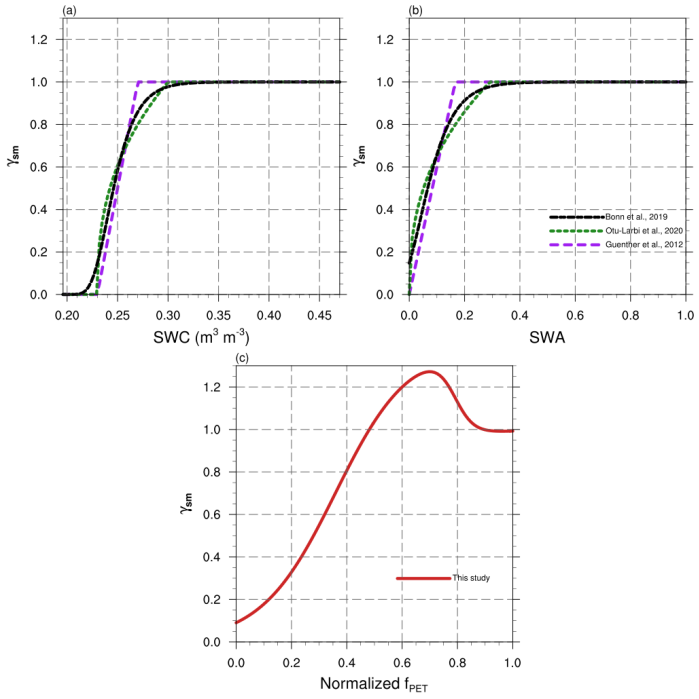

Figure 2.11. Comparison of drought algorithms with soil water content (SWC) as inputs (a) and with the normalized soil water availability (SWA) as inputs (b). (c) presents the model proposed in this study with the normalized f_{PET} as inputs.

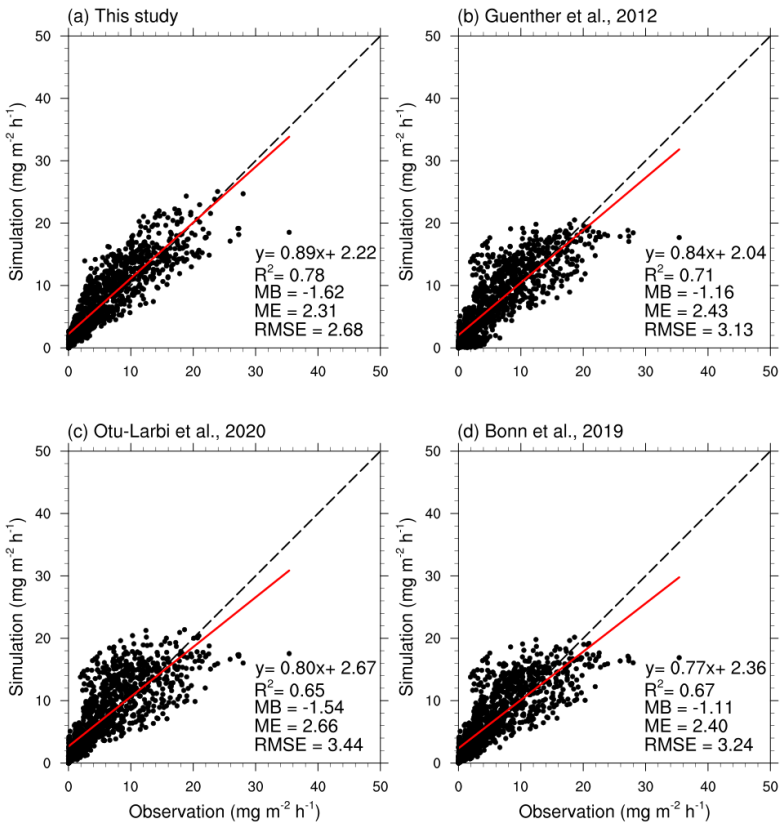

Figure 2.12. Scatter plots of measured diurnal isoprene fluxes and modelled daily isoprene fluxes with different drought algorithms and a wilting point of 0.196 m^3 m^{-3}.

Table 2.1. Descriptions of the online Explicit Drought Stress (EDS) algorithm and the offline Parameterized Drought Stress (PDS) algorithm.

	The Explicit Drought Stress (EDS) algorithm	The Parameterized Drought Stress (PDS) algorithm
Drought Indicator	The water stress function (β_t) in CLM 5	The ratio (f_{PET}) of evapotranspiration (ET) to potential evapotranspiration (PET)
Mild or moderate drought impact induced by the leaf temperature change	The leaf temperature change induced by drought can be simulated directly by CLM. The change of leaf temperature could increase the isoprene emission following the temperature response curve in MEGAN (Guenther et al., 2012).	The impact of the leaf temperature change induced by drought is parameterized based on the canopy level flux measurements. The isoprene emission is increased during the drought following equation [2.11].
Severe drought impact induced by the biochemical substrate supply	When droughts get severe ($\beta_t < 0.6$), the drought impact would be modelled by using the maximum rate of carboxylation by the photosynthesis enzyme Rubisco (Vcmax) in CLM 5 following equation [2.8] in this study.	The limitation of the biochemical substrate supply induced by severe drought is parameterized based on the canopy level flux measurements, and it could decrease the isoprene emission when the drought gets severe following equation [2.12].

Table 2.2. Drought algorithms used for simulating isoprene emission in the previous and these studies.

Equation	Parameters	Inputs	Reference
$\begin{cases} \gamma_{SM} = 1(\theta \geq \theta_c) \\ \gamma_{SM} = (\theta - \theta_w)/\Delta\theta_1 \ (\theta_w < \theta < \theta_c) \\ \gamma_{SM} = 0(\theta \leq \theta_w) \end{cases}$	• θ_w: Wilting point; • θ_1: Threshold (=θ_w + $\Delta\theta_1$); • $\Delta\theta_1$: 0.04 m^3 m^{-3} (Guenther et al., 2012); 0.06 m^3 m^{-3} (Guenther et al. 2006)	• θ: Volumetric soil water content;	Guenther et al. (2012)
$\begin{cases} \gamma_{SM} = 1 \ (\beta_t \geq 0.6) \\ \gamma_{SM} = V_{cmax}/\alpha \ (0 < \beta_t < 0.6) \\ \gamma_{SM} = 0(\beta_t = 0) \end{cases}$	• α:37.	• β_t: Water stress function; • Vcmax: the maximum rate of carboxylation by the photosynthesis enzyme Rubisco.	Jiang et al. (2018)
$\begin{cases} \gamma_{SM} = 1(\theta \geq \theta_c) \\ \gamma_{SM} = [(\theta - \theta_w)/(\theta_c - \theta_w)]^{0.4} \ (\theta_w < \theta < \theta_c) \\ \gamma_{SM} = 0(\theta \leq \theta_w) \end{cases}$	• θ_w: Wilting point; • θ_c: Threshold (=θ_w + $\Delta\theta_1$); • $\Delta\theta_1$: 0.07 m^3 m^{-3}.	• θ: Volumetric soil water content;	Otu-Larbi et al. (2020)
$\gamma_{SM} = exp\ (-exp\big((0.056) * exp(1) * (-2.3 - SWA) + 1\big))$	-	• SWA: Soil water availability;	Bonn et al. (2019)
$\gamma_{SM} = \gamma_{sm\_max}\left(\frac{1}{1 + b_1 \cdot e^{\alpha_1 \cdot (K_c - 0.2)}}\right)\left(\frac{1}{\gamma_{sm\_max}} + \frac{\left(1 - \frac{1}{\gamma_{sm\_max}}\right)}{1 + b_2 \cdot e^{\alpha_2 \cdot (1.3 - K_c)}}\right)$	• γ_{sm_max}: 1.4;	• f_{PET}: Normalized drought indicator;	This study

Supplementary figures

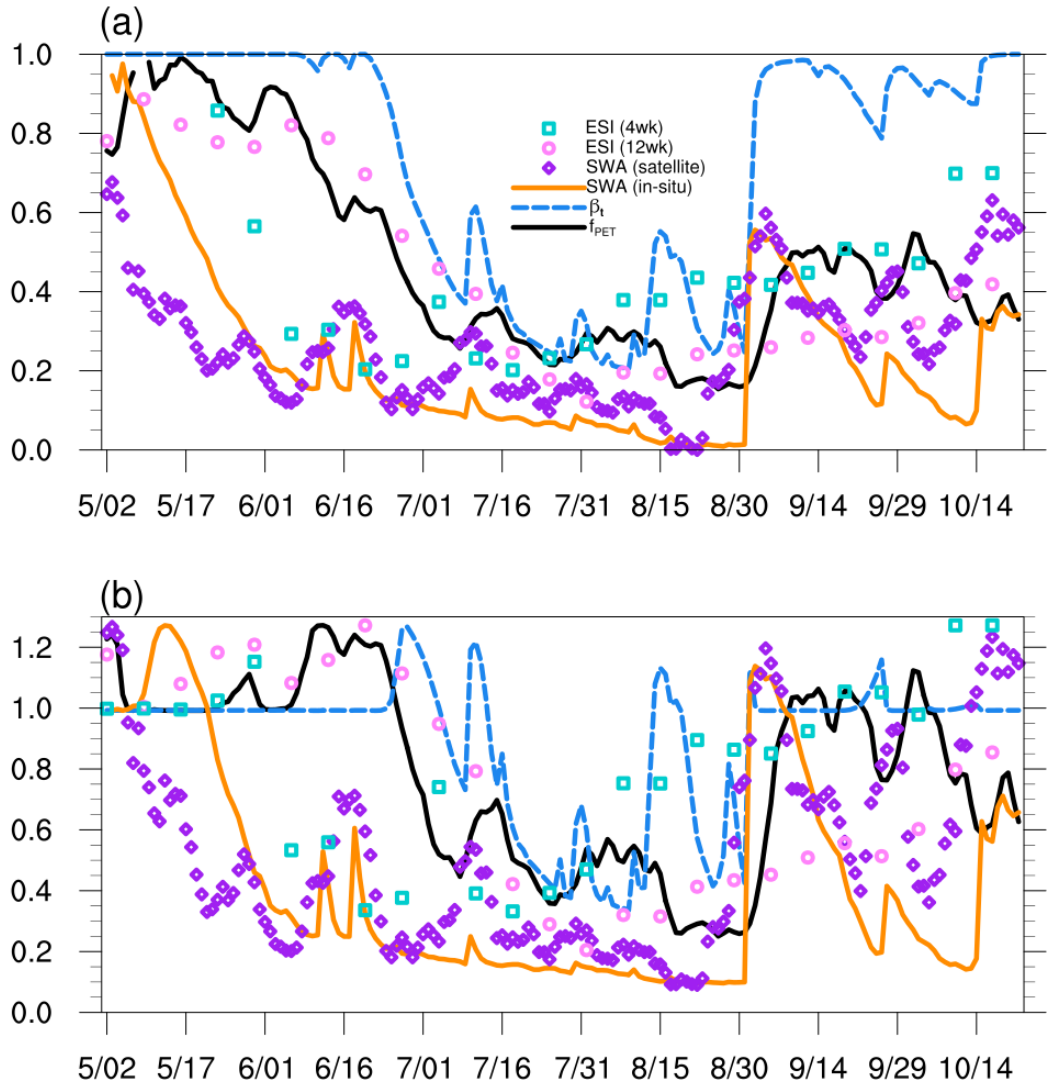

Figure S2.1. Comparison of the different normalized drought indexes including ESI drought indexes over 4-week (cyan square) and 12-week (pink circle) periods, the Soil Water Availability (SWA) from the in-situ (purple diamond) and satellite (orange solid line) observations, βt (blue dashed line) from the CLM model and the 7 day running averaged normalized f_{PET} (black solid line) in this study. The outputs of the Parameterized Drought Stress (PDS) offline algorithm with above inputs are presented in (b).

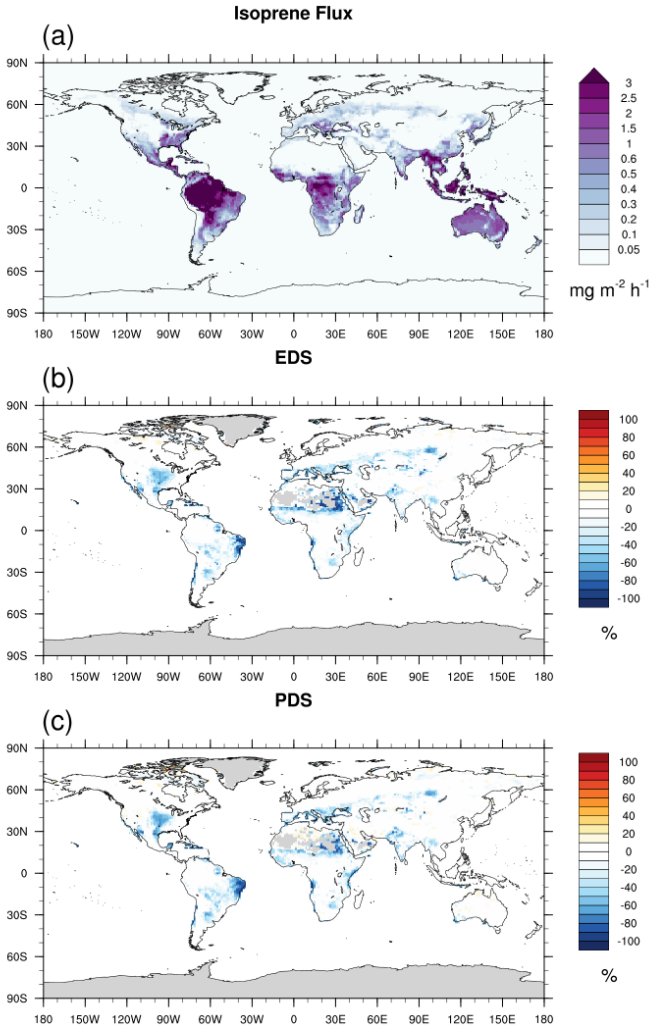

Figure S2.2. The spatial distribution of the isoprene flux estimated by CLM in 2012 (b) and the impact of drought estimated by the EDS algorithm (b) and the PDS algorithm (c).

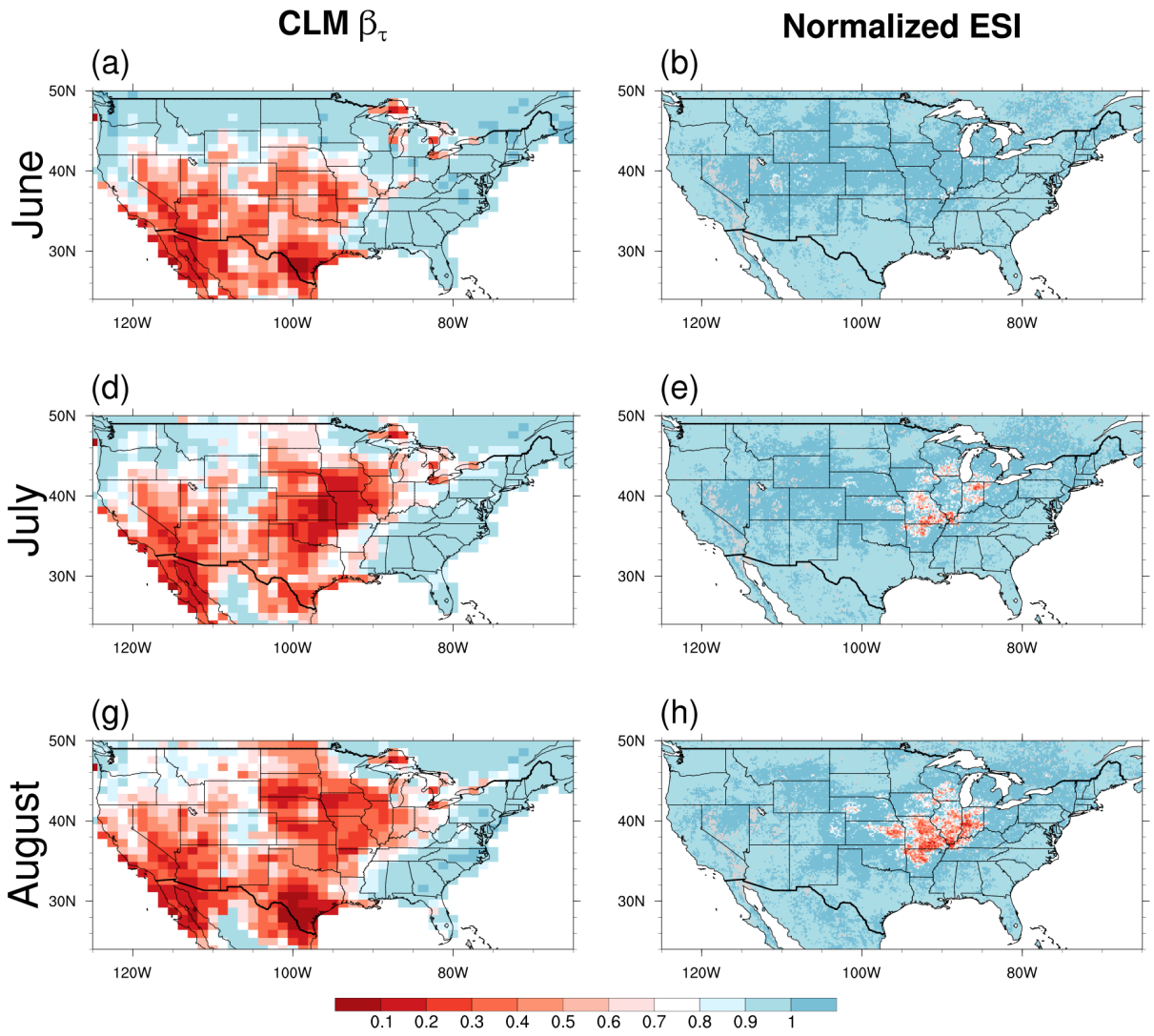

Figure S2.3. The spatial distributions of β_t simulated by CLM5 and the normalized satellite evaporative stress index (ESI) during the summer. The three rows represent different months from June to August.

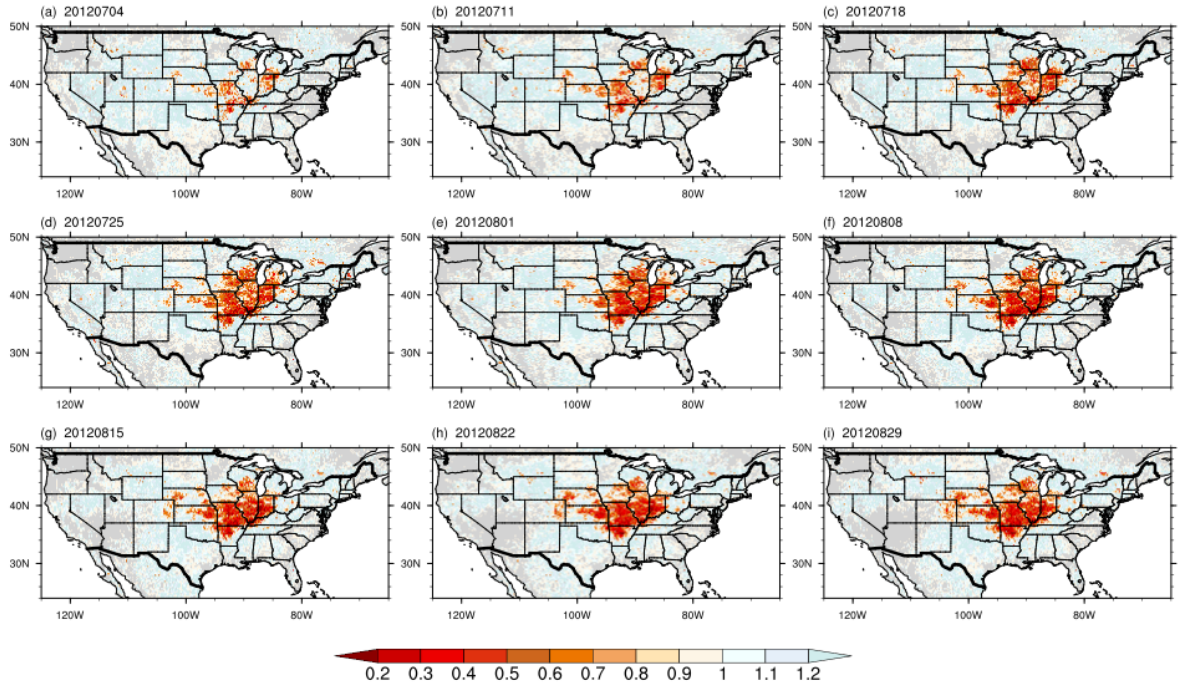

Figure S2.4 The spatial distributions of γ_{sm} calculated by the offline Parameterized Drought Stress (PDS) algorithm in July-August 2012 using the satellite Evapotranspiration Stress Index (ESI) inputs.

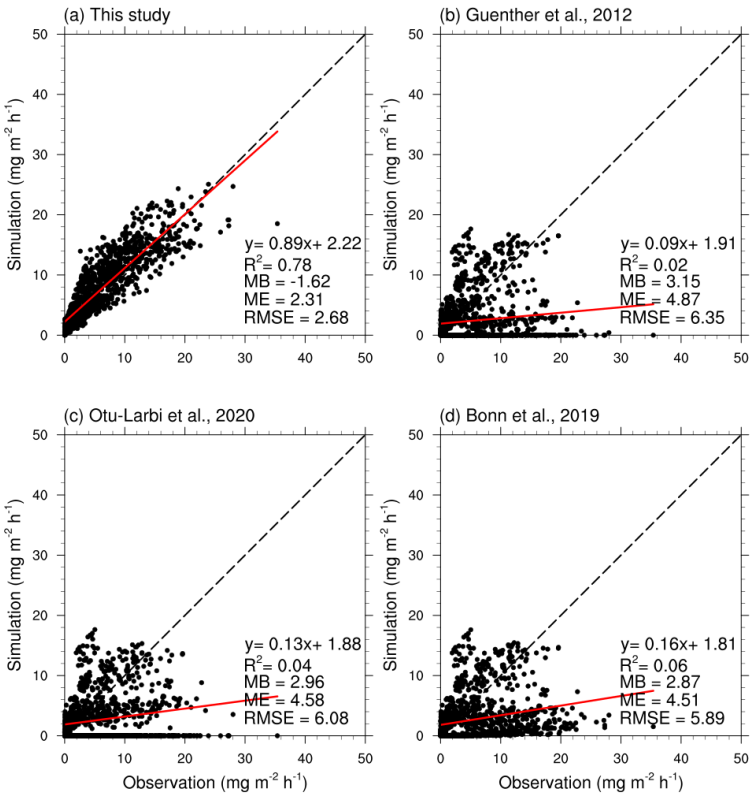

Figure S2.5. Scatter plots of measured diurnal isoprene fluxes and modelled diurnal isoprene fluxes with different drought algorithms (see Table 2.2) and the wilting point of 0.23 m^3 m^{-3}.

CHAPTER 3

ARCTIC HEATWAVES COULD SIGNIFICANTLY INFLUENCE THE ISOPRENE EMISSIONS FROM SHRUBS

The material presented in this chapter is reproduced from:
Wang, H., Welch, A., Nagalingam, S., Leong, C., Kittitananuvong, P., Barsanti, K. C., Sheesley, R. J., Czimczik, C. I., and Guenther, A. B.: Arctic Heatwaves Could Significantly Influence the Isoprene Emissions From Shrubs, Geophysical Research Letters, 51, e2023GL107599, https://doi.org/10.1029/2023GL107599, 2024.

Abstract

Warming climate in the Arctic is leading to an increase in isoprene emission from ecosystems. We assessed the influence of temperature on isoprene emission from Arctic willows with laboratory and field measurements. Our findings indicate that the hourly temperature response curve of Salix spp., the dominant isoprene emitting shrub in the Arctic, aligns with that of temperate plants. In contrast, the isoprene capacity of willows exhibited a more substantial than expected response to the mean ambient temperature of the previous day, which is much stronger than the daily temperature response predicted by the current version of the Model of Emissions of Gases and Aerosols from Nature (MEGAN). With a modified algorithm from this study, MEGAN predicts 66 % higher isoprene emissions for Arctic willows during an Arctic heatwave. However, despite these findings, we are still unable to fully explain the high temperature sensitivity of isoprene emissions from high latitude ecosystems.

3.1 Introduction

Rapid climate change in the Arctic is strongly influencing the local ecosystems (Box et al., 2019; Rantanen et al., 2022; Kim et al., 2020), and the change in both climate and ecosystems can alter the emissions of biogenic volatile organic compounds (BVOCs) and atmospheric chemistry in the Arctic (Rinnan et al., 2020; Faubert et al., 2010; Lindwall et al., 2016a). Isoprene is the most

abundant highly reactive BVOC emitted globally and also in the Arctic (Guenther et al., 2012; Rinnan et al., 2020). The changes in isoprene emissions could affect the formation and characteristics of secondary organic aerosol (SOA), ozone, the lifetime of methane, and thus the climate system in the Arctic (Tunved et al., 2006; Petäjä et al., 2022; Kulmala et al., 2004; Weber et al., 2022; Boy et al., 2022). The emission of isoprene is controlled by environmental conditions including temperature and solar radiation (Guenther et al., 1993; Tingey et al., 1979; Monson et al., 1992), thus a rapidly warming climate in the Arctic is favorable for increasing emission of isoprene (Lindwall et al., 2016b; Kramshøj et al., 2016; Seco et al., 2020; Emmerson et al., 2020; Bauwens et al., 2018). Additionally, climate change is extending the growing season and shifting plant productivity and community composition (Park et al., 2016; Wang et al., 2020; Valolahti et al., 2015), which will also affect BVOC emissions indirectly (Rinnan et al., 2020). Specifically, the expansion of shrubs into graminoid tundra systems ("shrubification") (Mekonnen et al., 2021) is a potential driver of isoprene emission change.

The shrub willow (Salix spp.) is a prevalent source of isoprene in high latitude ecosystems (Potosnak et al., 2013; Simin et al., 2021; Li et al., 2023). Recent whole-ecosystem measurements suggest that the temperature response of isoprene emissions in high-latitude tundra ecosystems is stronger than what current isoprene emission models predict (Angot et al., 2020; Seco et al., 2020; Seco et al., 2022; Li et al., 2023; Vettikkat et al., 2023; Holst et al., 2010; Selimovic et al., 2022). In contrast, leaf/branch-level studies showed that the hourly temperature response of Arctic willow species (Salix pulchra Cham. and S. myrsinites L.) is similar to that of temperate plants (Potosnak et al., 2013; Li et al., 2023). Besides the current temperature, it is known that basal isoprene emission capacity can also acclimate to the temperature and light of the past day or more (Sharkey et al., 1999; Geron et al., 2000; Hanson and Sharkey, 2001; Wiberley et al., 2008). Ground chamber

experiments have qualitatively demonstrated that long-term warming can increase isoprene emissions from high latitude ecosystems (Tiiva et al., 2008; Valolahti et al., 2015; Lindwall et al., 2016b). However, few data are available for quantifying the acclimation to warming and heatwaves in high latitudes. In this study, we designed laboratory and field experiments to investigate the temperature response, on time scales of minutes to days, of isoprene emissions from Arctic Salix spp. This finding was integrated into the Model of Emissions of Gases and Aerosols from Nature (MEGAN) and used to investigate isoprene emissions from high latitude shrubs under warming conditions.

3.2 Materials and Methods

The measurements were conducted as part of the Biogenic Emissions and Aerosol Response on the North Slope (BEAR-oNS) study during the summers of 2022-2023 on the North Slope, Alaska. The vegetation (*Salix* spp.) and volatile organic compound (VOC) samples were collected around the Toolik Field Station (TFS, 68° 38' N, 149° 36' W). Isoprene emissions from three local *Salix* spp. (*Salix pulchra*, *S. glauca* and *S. reticulata*, see Figure S3.1.) were measured. Two types of experiments were designed to assess the impact of short-term and long-term temperature changes on isoprene emissions from *Salix* spp. For the short-term experiments, plant samples were detached and brought to the lab at TFS. Long-term temperature experiments were conducted in the field on two separate *S. glauca* bushes. VOC samples were collected using sorbent cartridges (Tenax TA and Carbograph 5TD; Markes International, UK). The samples were capped, refrigerated, and then shipped back to the lab at the University of California, Irvine for analysis. The time between sample collection and analysis was about 2 weeks.

3.2.1 Temperature response curve experiments

The short-term temperature response experiment aimed to assess response of isoprene emission to temperature changes on a time scale of minutes to hours. A portable custom-made leaf glass chamber system was used for these experiments. The system details are described by Nagalingam et al. (2023). Branches were cut, placed in water, and exposed to a natural light diurnal cycle 1-2 days before each experiment. The duration of darkness ranged from 1 to 5 hours at TFS during the campaign. One chamber blank VOC sample (from an empty chamber) was collected at the beginning of every experiment before putting the plant into the glass chamber. After placing a leaf into the glass chamber, VOC sampling was initiated only after the photosynthesis rate stabilized. The photosynthetic photon flux density (PPFD) is approximately 1000 μmol m^{-2} s^{-1} in the chamber. In 2022, for *S. glauca* (n=3) and *S. pulchra* (n=4), leaf temperature was increased from 10°C to 45°C in 5°C steps. In 2023, for *S. reticulata* (n=4), the temperature was increased from 20°C to 40°C in 5°C steps. Each step lasted one hour (except 20°C, which was 2 hours). Samples were taken using sorbent cartridges (see next section) during the last 10-15 minutes of the hour with a flow rate of 200 cc min^{-1} for 5 minutes, yielding a 1 L VOC sample.

3.2.2 Acclimation experiments

The acclimation experiments focused on investigating the influence of the temperature of the past several days on isoprene emission capacity. Isoprene emissions from seven mature *S. glauca* leaves were measured over 21 days, from July 16 to August 5, 2023. The mean July temperature at TFS was 10.4°C from 2020 to 2023. During our measurement period, there were five days (July 21-24, and Aug. 5) when the daily temperatures exceeded the 95th percentile of the daily temperature records of 16.5 °C for the same period (2020-2023). VOC measurements were taken using an LI-6400XT portable photosynthesis system (LI-COR Biosciences, USA) with an inlet flow rate of 730 cc min^{-1} (Figure S3.2). All measurements occurred between 13:00 and 17:00 local

time to mitigate potential diurnal effects. A chamber blank VOC sample was collected every measurement day from an empty LI-6400XT chamber before measurements. Leaves were placed in the chamber at a fixed 20°C temperature with a PPFD intensity of 1000 μmol m^{-2} s^{-1}. A 1L VOC sample was collected at a flow rate of 200 cc min^{-1} for 5 minutes after the leaves had been in the chamber for 30 minutes. The meteorology data used in this study were measured at TFS and are available through the MesoWest Database (https://mesowest.utah.edu/).

3.2.3 GC-TOF-MS

The sampled sorbent cartridges were transported to our laboratory at the University of California, Irvine, where they were thermally desorbed using a TD autosampler (Ultra-xr; Markes International). The desorbed VOCs were injected into a gas chromatograph (GC) (7890B; Agilent Technologies, CA, USA) equipped with a 60 m Rxi-624Sil MS capillary column (Restek, PA, USA). The column eluate was channeled to an electron impact ionization time-of-flight mass spectrometer (BenchTOF-Select; Markes International) and a flame ionization detector (FID, Agilent) for compound identification and quantification. Detailed explanation of the GC methodology including the GC oven temperature program, calibration protocols, and measurement uncertainties are described by Nagalingam et al., 2022.

3.2.4 MEGAN model

The isoprene flux in MEGAN version 3 is calculated as:

$$F = \varepsilon \cdot LAI \cdot \gamma_T \cdot \gamma_P \cdot \gamma_A \cdot \gamma_C \cdot \gamma_{SM} \quad [3.1]$$

, where ε and LAI represent the leaf-level standard emission factor (μmol m^{-2} s^{-1}),) and leaf area index (LAI, m^2 m^{-2}), respectively. γ_T, γ_P, γ_A, γ_C and γ_{SM} represent the emission activity factors of isoprene emissions for temperature, light condition, leaf age, CO_2 and water stress, respectively. The emission factor (ε) is defined as the rate of isoprene emission when the leaf temperature is 30

°C under a PPFD of 1000 μmol m^{-2} s^{-1}. We will focus on the γ_T in this study, and the details about other factors can be found in previous publications (Guenther et al., 2012; Guenther et al., 2006; Wang et al., 2022).

MEGAN considers the effects of the current temperature and the long-term (1 to 10 days) temperature on isoprene emission. The default temperature response algorithm for isoprene in MEGAN is:

$$\gamma_{\mathrm{T}} = E_{\mathrm{opt}} \cdot \frac{C_{\mathrm{T2}} \cdot e^{C_{\mathrm{T1}} \cdot x}}{\mathrm{C_{T2}} - C_{\mathrm{T1}} \cdot (1 - e^{C_{\mathrm{T2}} \cdot x})} \quad [3.2]$$

, where x is:

$$x = \frac{1}{0.00831} \cdot \left(\frac{1}{T_{\mathrm{opt}}} - \frac{1}{T} \right) \quad [3.3]$$

. T is the leaf temperature. C_{T1} and C_{T2} are both empirical coefficients. E_{opt} and T_{opt} are:

$$T_{\mathrm{opt}} = 40 + 0.6 \cdot (T_{240} - 24) \quad [3.4]$$

$$E_{\mathrm{opt}} = 2 \cdot e^{0.05 \cdot (T_{24} - 24)} \cdot e^{0.05 \cdot (T_{240} - 24)} \quad [3.5]$$

, where T_{24} (°C) and T_{240} (°C) denote the mean air temperature in previous 24 hours and 240 hours, respectively. T_{opt} (°C) and E_{opt} represent the impact of long-term temperatures on the optimal temperature and the shape of the temperature response curve.

3.3 Results and Discussion

3.3.1 The short-term temperature response of isoprene

Our chamber experiments show that the short-term temperature response of isoprene from Arctic willows (*Salix* spp.) is consistent with the MEGAN model (Figure 3.1), with isoprene emission increasing with temperature, reaching an optimal level (point of peak emission) around 40°C before declining, following typical enzyme behavior of increasing activity followed by denaturation (Guenther et al., 1993). The parameters for the temperature response curve of *Salix*

spp. were fitted using the Arrhenius equation format presented in equations (2) and (3), with a comparison of the empirical parameters for the MEGAN default and *Salix* spp. models provided in Table S3.1. The fitted curves for individual samples are presented in Figure S3.3. The optimal temperature for isoprene emission is known to be influenced by the temperature of the past 1 to 10 days, based on measurements of temperate plants (Guenther et al., 2012; Papiez et al., 2009). Arctic willows that grow in a cold environment are expected to have a lower optimal temperature (36 °C) than those growing in a temperate climate. Therefore, the model fitted for willows (*Salix* spp.) has a different optimal temperature (Figure 3.1) than that represented in the current MEGAN model which was based primarily on observations of woody temperate plants (Guenther et al., 2012).

We also compare the short-term temperature response curve of isoprene emissions with observations in the Arctic ecosystem reported by previous studies. We found our temperature response curve is close to the curve derived from the branch chamber experiment by Li et al. (2023) for *S. myrsinites*, and the difference at high temperatures (> 35 °C) is caused by the equation formats that were used to fit the line. In addition, Potosnak et al. (2013) found that their temperature curve experiments for *S. pulchra* reproduced the temperature curve of the MEGAN model. Therefore, we conclude that the temperature curve of willows in the Arctic is consistent with the temperature response in the current MEGAN model, though with a lower optimal temperature. However, the temperature curve of willows is not consistent with the whole ecosystem measurements of isoprene from the high-latitude regions (e.g., Seco et al. (2022), Vettikkat et al. (2022), and Tang et al. (2016)). The temperature curve derived from the whole ecosystem measurements showed the exponential increase regime and did not exhibit a turning point because it is rare for leaf temperature to reach the optimal level in a high-latitude environment. MEGAN

can capture the variability in isoprene emissions in temperate and tropical ecosystems as measured using eddy-covariance techniques (Potosnak et al., 2014; Sarkar et al., 2020). However, it does not account for measurements from high latitudes (Seco et al., 2022; Vettikkat et al., 2022), indicating that discrepancies are not due to measurement methodologies. We also investigated the impact of acclimation of isoprene emission factors to ambient temperature in Section 3.3, but this alone cannot fully explain the differences.

We also observed significant variation in emission factors among different *Salix* spp. ((b) in Figure 3.1). One dwarf willow species, *S. reticulata*, had a notably higher emission factor (21.1 ± 4.2 nmol m^{-2} s^{-1}) compared to *S. glauca* (7.5 ± 8.5 nmol m^{-2} s^{-1}) and *S. pulchra* (4.4 ± 4.7 nmol m^{-2} s^{-1}). The differences are even greater when the emission factor is normalized by leaf mass indicating that the species with lower emissions have denser leaves. Potosnak et al. (2013) reported an averaged emission factor of 12.4 (± 10.6) nmol m^{-2} s^{-1} for *S. pulchra*, and Simin et al. (2021) reported an averaged emission factor of 10.4 (± 6.1) nmol m^{-2} s^{-1} for *S. myrsinites.* In addition to the significant variation among species, environmental temperature could also affect the emission factors. The difference of emission factors for *S. pulchra* between our measurements and those from Potosnak et al. (2013) could be explained by the acclimation of plants to the previous day temperature, which is presented in the next section.

3.3.2 The acclimation of isoprene emission factors to the temperature

Our field measurements show that isoprene emission factors, made under almost identical light and leaf temperature conditions, change with the daily ambient temperature variations as seen in (a) in Figure 2. The highest isoprene emissions occurred during the warmest period of our measurements. Furthermore, the long-term temperature response experiments show that the emission capacity of *S. glauca* increases exponentially with the mean air temperature averaged

over the past one day ((b) in Figure 2). The emissions were measured at a leaf temperature of ~20 °C and then converted to the corresponding value at 30 °C, the standard temperature in MEGAN, using the temperature curve presented for *Salix* spp. in Figure 3.1. The emission factors were normalized by dividing the mean emission factors for individual leaves. The analysis using the original data at 20°C yields the same conclusion (Figure S3.4). We also tested other factors including the mean of temperature, PPFD, VPD (Vapor Pressure Deficit), and the product of PPFD and temperature for the previous 1 to 240 hours before the measurement (Figure S3.5). The mean air temperature over the preceding 35 hours has the highest Pearson's correlation coefficient of 0.88 ($p<0.001$) with the log of emission factors, which is close to Pearson's correlation coefficient for the mean temperature of the previous day. It is known that past growth temperature affects isoprene emission capacity of plants (Wiberley et al., 2008) through the accumulation of enzymes and substrates (Grote and Niinemets, 2008). Isoprene emission can acclimate to a new temperature and light condition within 5-30 hours (Hanson and Sharkey, 2001), and a previous study found that the basal level isoprene emission of oak trees was highly correlated with the average temperature of the previous two days (Hanson and Sharkey, 2001). Our data shows that for S. glauca the emission factors are more related to the mean temperature of the preceding day.

3.3.3 MEGAN simulations

The acclimation mechanism has been included in the current MEGAN model by using an exponential relationship as presented in equation (5) (Guenther et al., 2012), and the validation of flux measurements shows that the acclimation mechanism can improve model performance (e.g., Potosnak et al. (2014)). However, our results indicate that the emission factors of *S. glauca* have a heightened temperature sensitivity to the mean temperature of the preceding day compared to

the current, referred to here as the default, model ((b) in Figure 2). We updated the equation (5) in MEGAN with the equation derived from this study as:

$$E_{\text{opt}} = 7.9 \cdot e^{0.22 \cdot (T_{24} - 24)} \quad [3.6]$$

, where T_{24} (°C) denotes the mean air temperature of the preceding day. We estimated the isoprene flux from a unit area (1 m^2) of *S. glauca* with LAI of 1.5 m^2 m^{-2} at TFS during the heatwave period (July 16-August 1) in 2023. The higher temperature sensitivity of the updated MEGAN model results in lower emissions during cooler days but higher emissions during warmer days, as shown in (a) in Figure 3.3. Additionally, the diurnal cycle reveals that the updated MEGAN model has higher emissions than the default MEGAN model with higher emission factors ((b) in Figure3) during warm periods, and we found that isoprene flux could increase by 66 % by updating the acclimation mechanism of isoprene (Figure 3.3). Consequently, the existing model is likely to considerably underestimate the isoprene emissions from willows during warm periods and overestimate during cold periods. In addition, the isoprene emissions from Arctic willows could undergo a substantial increase in response to the rapid warming in the Arctic region.

To compare with whole ecosystem flux measurements, we constructed the temperature response curve of *S. glauca* based on results from both default and updated MEGAN models during the heatwave ((c) in Figure 3.3). The temperature curves were fitted using the format of the exponential equation:

$$F = F_0 \cdot e^{\beta \cdot (T - T_{\text{std}})} \quad [3.7]$$

, where T_{std} (=30 °C) is the standard leaf temperature in MEGAN. F_0 and β are the empirical parameters.

The results show that acclimation of emission capacity shifted the averaged emission factor (F_0) from 5.1 to 10.3 nmol m^{-2} s^{-1} and increased the temperature sensitivity of isoprene flux, with

β shifting from 0.13 to 0.15. However, this value is still considerably lower than the values of 0.17-0.23 observed for other studies (Tang et al., 2016; Vettikkat et al., 2022; Seco et al., 2022; Seco et al., 2020; Li et al., 2023). Isoprene emission at some of these sites are not dominated by the contribution (percent cover) of *Salix* spp. (Vettikkat et al., 2022; Seco et al., 2022) and so other isoprene emitters, like sedges (Ekberg et al., 2009), are likely to be responsible for the high temperature sensitivity of isoprene observed in ecosystem studies in the Arctic.

3.4 Conclusions

The isoprene emission response of Arctic shrub willows to temperature change was assessed in this study through field and laboratory measurements. We found the temperature response, on time scales of minutes to days, of Arctic willows is consistent with that represented in the current MEGAN model, which was based primarily on observations with woody temperate plants. In addition, we found that the isoprene emission capacity is acclimated to the averaged temperature of the previous day and that response is stronger than that predicted in MEGAN. However, findings in this study still cannot explain the highly temperature sensitive response curves derived from whole-ecosystem measurements, and other isoprene emitters in the Arctic could be responsible for the high temperature sensitivity of isoprene.

References

Angot, H., McErlean, K., Hu, L., Millet, D. B., Hueber, J., Cui, K., Moss, J., Wielgasz, C., Milligan, T., Ketcherside, D., Bret-Harte, M. S., and Helmig, D.: Biogenic volatile organic compound ambient mixing ratios and emission rates in the Alaskan Arctic tundra, Biogeosciences, 17, 6219-6236, 10.5194/bg-17-6219-2020, 2020.

Bauwens, M., Stavrakou, T., Müller, J. F., Van Schaeybroeck, B., De Cruz, L., De Troch, R., Giot, O., Hamdi, R., Termonia, P., Laffineur, Q., Amelynck, C., Schoon, N., Heinesch, B., Holst, T., Arneth, A., Ceulemans, R., Sanchez-Lorenzo, A., and Guenther, A.: Recent past (1979–2014) and future (2070–2099) isoprene fluxes over Europe simulated with the MEGAN–MOHYCAN model, Biogeosciences, 15, 3673-3690, 10.5194/bg-15-3673-2018, 2018.

Box, J. E., Colgan, W. T., Christensen, T. R., Schmidt, N. M., Lund, M., Parmentier, F.-J. W., Brown, R., Bhatt, U. S., Euskirchen, E. S., Romanovsky, V. E., Walsh, J. E., Overland, J. E., Wang, M., Corell, R. W., Meier, W. N., Wouters, B., Mernild, S., Mård, J., Pawlak, J., and Olsen, M. S.: Key indicators of Arctic climate change: 1971–2017, Environmental Research Letters, 14, 045010, 10.1088/1748-9326/aafc1b, 2019.

Boy, M., Zhou, P., Kurtén, T., Chen, D., Xavier, C., Clusius, P., Roldin, P., Baykara, M., Pichelstorfer, L., Foreback, B., Bäck, J., Petäjä, T., Makkonen, R., Kerminen, V.-M., Pihlatie, M., Aalto, J., and Kulmala, M.: Positive feedback mechanism between biogenic volatile organic compounds and the methane lifetime in future climates, npj Climate and Atmospheric Science, 5, 72, 10.1038/s41612-022-00292-0, 2022.

Ekberg, A., Arneth, A., Hakola, H., Hayward, S., and Holst, T.: Isoprene emission from wetland sedges, Biogeosciences, 6, 601-613, 10.5194/bg-6-601-2009, 2009.

Emmerson, K. M., Possell, M., Aspinwall, M. J., Pfautsch, S., and Tjoelker, M. G.: Temperature response measurements from eucalypts give insight into the impact of Australian isoprene emissions on air quality in 2050, Atmos. Chem. Phys., 20, 6193-6206, 10.5194/acp-20-6193-2020, 2020.

Faubert, P., Tiiva, P., Rinnan, Å., Michelsen, A., Holopainen, J. K., and Rinnan, R.: Doubled volatile organic compound emissions from subarctic tundra under simulated climate warming, New Phytologist, 187, 199-208, https://doi.org/10.1111/j.1469-8137.2010.03270.x, 2010.

Geron, C., Guenther, A., Sharkey, T., and Arnts, R. R.: Temporal variability in basal isoprene emission factor, Tree Physiology, 20, 799-805, 10.1093/treephys/20.12.799, 2000.

Grote, R., and Niinemets, Ü.: Modeling volatile isoprenoid emissions – a story with split ends, Plant Biology, 10, 8-28, https://doi.org/10.1055/s-2007-964975, 2008.

Guenther, A., Karl, T., Harley, P., Wiedinmyer, C., Palmer, P., and Geron, C.: Estimates of global terrestrial isoprene emissions using MEGAN (Model of Emissions of Gases and Aerosols from Nature), Atmos. Chem. Phys, 6, 3181-3210, 2006.

Guenther, A. B., Zimmerman, P. R., Harley, P. C., Monson, R. K., and Fall, R.: Isoprene and monoterpene emission rate variability: Model evaluations and sensitivity analyses, Journal of Geophysical Research: Atmospheres, 98, 12609-12617, doi:10.1029/93JD00527, 1993.

Guenther, A. B., Jiang, X., Heald, C. L., Sakulyanontvittaya, T., Duhl, T., Emmons, L. K., and Wang, X.: The Model of Emissions of Gases and Aerosols from Nature version 2.1 (MEGAN2.1): an extended and updated framework for modeling biogenic emissions, Geoscientific Model Development, 5, 1471-1492, 10.5194/gmd-5-1471-2012, 2012.

Hanson, D. T., and Sharkey, T. D.: Rate of acclimation of the capacity for isoprene emission in response to light and temperature, Plant, Cell & Environment, 24, 937-946, https://doi.org/10.1046/j.1365-3040.2001.00745.x, 2001.

Holst, T., Arneth, A., Hayward, S., Ekberg, A., Mastepanov, M., Jackowicz-Korczynski, M., Friborg, T., Crill, P. M., and Bäckstrand, K.: BVOC ecosystem flux measurements at a high latitude wetland site, Atmos. Chem. Phys., 10, 1617-1634, 10.5194/acp-10-1617-2010, 2010.

Kim, J. E., Laguë, M. M., Pennypacker, S., Dawson, E., and Swann, A. L. S.: Evaporative Resistance is of Equal Importance as Surface Albedo in High-Latitude Surface Temperatures Due to Cloud Feedbacks, Geophysical Research Letters, 47, e2019GL085663, https://doi.org/10.1029/2019GL085663, 2020.

Kramshøj, M., Vedel-Petersen, I., Schollert, M., Rinnan, Å., Nymand, J., Ro-Poulsen, H., and Rinnan, R.: Large increases in Arctic biogenic volatile emissions are a direct effect of warming, Nature Geoscience, 9, 349-352, 10.1038/ngeo2692, 2016.

Kulmala, M., Suni, T., Lehtinen, K. E. J., Dal Maso, M., Boy, M., Reissell, A., Rannik, Ü., Aalto, P., Keronen, P., Hakola, H., Bäck, J., Hoffmann, T., Vesala, T., and Hari, P.: A new feedback mechanism linking forests, aerosols, and climate, Atmos. Chem. Phys., 4, 557-562, 10.5194/acp-4-557-2004, 2004.

Li, T., Baggesen, N., Seco, R., and Rinnan, R.: Seasonal and diel patterns of biogenic volatile organic compound fluxes in a subarctic tundra, Atmospheric Environment, 292, 119430, https://doi.org/10.1016/j.atmosenv.2022.119430, 2023.

Lindwall, F., Schollert, M., Michelsen, A., Blok, D., and Rinnan, R.: Fourfold higher tundra volatile emissions due to arctic summer warming, Journal of Geophysical Research: Biogeosciences, 121, 895-902, https://doi.org/10.1002/2015JG003295, 2016a.

Lindwall, F., Svendsen, S. S., Nielsen, C. S., Michelsen, A., and Rinnan, R.: Warming increases isoprene emissions from an arctic fen, Science of The Total Environment, 553, 297-304, https://doi.org/10.1016/j.scitotenv.2016.02.111, 2016b.

Mekonnen, Z. A., Riley, W. J., Berner, L. T., Bouskill, N. J., Torn, M. S., Iwahana, G., Breen, A. L., Myers-Smith, I. H., Criado, M. G., Liu, Y., Euskirchen, E. S., Goetz, S. J., Mack, M. C., and Grant, R. F.: Arctic tundra shrubification: a review of mechanisms and impacts on ecosystem carbon balance, Environmental Research Letters, 16, 053001, 10.1088/1748-9326/abf28b, 2021.

Monson, R. K., Jaeger, C. H., Adams, W. W., Driggers, E. M., Silver, G. M., and Fall, R.: Relationships among Isoprene Emission Rate, Photosynthesis, and Isoprene Synthase Activity as Influenced by Temperature, Plant Physiology, 98, 1175, 10.1104/pp.98.3.1175, 1992.

Nagalingam, S., Seco, R., Musaev, K., Basu, C., Kim, S., and Guenther, A.: Impact of heat stress on foliar biogenic volatile organic compound emission and gene expression in tomato (Solanum lycopersicum) seedlings, Elementa: Science of the Anthropocene, 10, 10.1525/elementa.2021.00096, 2022.

Nagalingam, S., Seco, R., Kim, S., and Guenther, A.: Heat stress strongly induces monoterpene emissions in some plants with specialized terpenoid storage structures, Agricultural and Forest Meteorology, 333, 109400, https://doi.org/10.1016/j.agrformet.2023.109400, 2023.

Papiez, M. R., Potosnak, M. J., Goliff, W. S., Guenther, A. B., Matsunaga, S. N., and Stockwell, W. R.: The impacts of reactive terpene emissions from plants on air quality in Las Vegas, Nevada, Atmospheric Environment, 43, 4109-4123, https://doi.org/10.1016/j.atmosenv.2009.05.048, 2009.

Park, T., Ganguly, S., Tømmervik, H., Euskirchen, E. S., Høgda, K.-A., Karlsen, S. R., Brovkin, V., Nemani, R. R., and Myneni, R. B.: Changes in growing season duration and productivity of northern vegetation inferred from long-term remote sensing data, Environmental Research Letters, 11, 084001, 10.1088/1748-9326/11/8/084001, 2016.

Petäjä, T., Tabakova, K., Manninen, A., Ezhova, E., O'Connor, E., Moisseev, D., Sinclair, V. A., Backman, J., Levula, J., Luoma, K., Virkkula, A., Paramonov, M., Räty, M., Äijälä, M., Heikkinen, L., Ehn, M., Sipilä, M., Yli-Juuti, T., Virtanen, A., Ritsche, M., Hickmon, N., Pulik, G., Rosenfeld, D., Worsnop, D. R., Bäck, J., Kulmala, M., and Kerminen, V. M.: Influence of biogenic emissions from boreal forests on aerosol–cloud interactions, Nature Geoscience, 15, 42-47, 10.1038/s41561-021-00876-0, 2022.

Potosnak, M. J., Baker, B. M., LeStourgeon, L., Disher, S. M., Griffin, K. L., Bret-Harte, M. S., and Starr, G.: Isoprene emissions from a tundra ecosystem, Biogeosciences, 10, 871-889, 10.5194/bg-10-871-2013, 2013.

Potosnak, M. J., LeStourgeon, L., Pallardy, S. G., Hosman, K. P., Gu, L., Karl, T., Geron, C., and Guenther, A. B.: Observed and modeled ecosystem isoprene fluxes from an oak-dominated temperate forest and the influence of drought stress, Atmospheric Environment, 84, 314-322, https://doi.org/10.1016/j.atmosenv.2013.11.055, 2014.

Rantanen, M., Karpechko, A. Y., Lipponen, A., Nordling, K., Hyvärinen, O., Ruosteenoja, K., Vihma, T., and Laaksonen, A.: The Arctic has warmed nearly four times faster than the

globe since 1979, Communications Earth & Environment, 3, 168, 10.1038/s43247-022-00498-3, 2022.

Rinnan, R., Iversen, L. L., Tang, J., Vedel-Petersen, I., Schollert, M., and Schurgers, G.: Separating direct and indirect effects of rising temperatures on biogenic volatile emissions in the Arctic, Proceedings of the National Academy of Sciences, 117, 32476, 10.1073/pnas.2008901117, 2020.

Sarkar, C., Guenther, A. B., Park, J. H., Seco, R., Alves, E., Batalha, S., Santana, R., Kim, S., Smith, J., Tóta, J., and Vega, O.: PTR-TOF-MS eddy covariance measurements of isoprene and monoterpene fluxes from an eastern Amazonian rainforest, Atmos. Chem. Phys., 20, 7179-7191, 10.5194/acp-20-7179-2020, 2020.

Seco, R., Holst, T., Matzen, M. S., Westergaard-Nielsen, A., Li, T., Simin, T., Jansen, J., Crill, P., Friborg, T., Rinne, J., and Rinnan, R.: Volatile organic compound fluxes in a subarctic peatland and lake, Atmos. Chem. Phys., 20, 13399-13416, 10.5194/acp-20-13399-2020, 2020.

Seco, R., Holst, T., Davie-Martin, C. L., Simin, T., Guenther, A., Pirk, N., Rinne, J., and Rinnan, R.: Strong isoprene emission response to temperature in tundra vegetation, Proceedings of the National Academy of Sciences, 119, e2118014119, 10.1073/pnas.2118014119, 2022.

Selimovic, V., Ketcherside, D., Chaliyakunnel, S., Wielgasz, C., Permar, W., Angot, H., Millet, D. B., Fried, A., Helmig, D., and Hu, L.: Atmospheric biogenic volatile organic compounds in the Alaskan Arctic tundra: constraints from measurements at Toolik Field Station, Atmos. Chem. Phys., 22, 14037-14058, 10.5194/acp-22-14037-2022, 2022.

Sharkey, T. D., Singsaas, E. L., Lerdau, M. T., and Geron, C. D.: WEATHER EFFECTS ON ISOPRENE EMISSION CAPACITY AND APPLICATIONS IN EMISSIONS ALGORITHMS, Ecological Applications, 9, 1132-1137, https://doi.org/10.1890/1051-0761(1999)009[1132:WEOIEC]2.0.CO; 2, 1999.

Simin, T., Tang, J., Holst, T., and Rinnan, R.: Volatile organic compound emission in tundra shrubs – Dependence on species characteristics and the near-surface environment, Environmental and Experimental Botany, 184, 104387, https://doi.org/10.1016/j.envexpbot.2021.104387, 2021.

Tang, J., Schurgers, G., Valolahti, H., Faubert, P., Tiiva, P., Michelsen, A., and Rinnan, R.: Challenges in modelling isoprene and monoterpene emission dynamics of Arctic plants: a case study from a subarctic tundra heath, Biogeosciences, 13, 6651-6667, 10.5194/bg-13-6651-2016, 2016.

Tiiva, P., Faubert, P., Michelsen, A., Holopainen, T., Holopainen, J. K., and Rinnan, R.: Climatic warming increases isoprene emission from a subarctic heath, New Phytologist, 180, 853-863, https://doi.org/10.1111/j.1469-8137.2008.02587.x, 2008.

Tingey, D. T., Manning, M., Grothaus, L. C., and Burns, W. F.: The Influence of Light and Temperature on Isoprene Emission Rates from Live Oak, Physiologia Plantarum, 47, 112-118, https://doi.org/10.1111/j.1399-3054.1979.tb03200.x, 1979.

Tunved, P., Hansson, H. C., Kerminen, V. M., Ström, J., Maso, M. D., Lihavainen, H., Viisanen, Y., Aalto, P. P., Komppula, M., and Kulmala, M.: High Natural Aerosol Loading over Boreal Forests, Science, 312, 261-263, 10.1126/science.1123052, 2006.

Valolahti, H., Kivimäenpää, M., Faubert, P., Michelsen, A., and Rinnan, R.: Climate change-induced vegetation change as a driver of increased subarctic biogenic volatile organic

compound emissions, Global Change Biology, 21, 3478-3488, https://doi.org/10.1111/gcb.12953, 2015.

Vettikkat, L., Miettinen, P., Buchholz, A., Rantala, P., Yu, H., Schallhart, S., Seco, R., Männistö, E., Tuittila, E. S., Guenther, A. B., and Schobesberger, S.: High emission rates and strong temperature response make boreal wetlands a large source of terpenes, Atmos. Chem. Phys. Discuss., 2022, 1-21, 10.5194/acp-2022-588, 2022.

Vettikkat, L., Miettinen, P., Buchholz, A., Rantala, P., Yu, H., Schallhart, S., Petäjä, T., Seco, R., Männistö, E., Kulmala, M., Tuittila, E. S., Guenther, A. B., and Schobesberger, S.: High emission rates and strong temperature response make boreal wetlands a large source of isoprene and terpenes, Atmos. Chem. Phys., 23, 2683-2698, 10.5194/acp-23-2683-2023, 2023.

Wang, J. A., Sulla-Menashe, D., Woodcock, C. E., Sonnentag, O., Keeling, R. F., and Friedl, M. A.: Extensive land cover change across Arctic–Boreal Northwestern North America from disturbance and climate forcing, Global Change Biology, 26, 807-822, https://doi.org/10.1111/gcb.14804, 2020.

Wang, H., Welch, A., Nagalingam, S., Leong, C., Kittitananuvong, P., Barsanti, K., Sheesley, R., Czimczik, C. I., and Guenther, A. (2023). Data and scripts for the article entitled "Arctic heatwaves could significantly influence the isoprene emissions from shrubs" [Dataset]. Zenodo. https://doi.org/10.5281/zenodo.10056276.

Weber, J., Archer-Nicholls, S., Abraham, N. L., Shin, Y. M., Griffiths, P., Grosvenor, D. P., Scott, C. E., and Archibald, A. T.: Chemistry-driven changes strongly influence climate forcing from vegetation emissions, Nature Communications, 13, 7202, 10.1038/s41467-022-34944-9, 2022.

Wiberley, A. E., Donohue, A. R., Meier, M. E., Westphal, M. M., and Sharkey, T. D.: Regulation of isoprene emission in Populus trichocarpa leaves subjected to changing growth temperature, Plant, Cell & Environment, 31, 258-267, https://doi.org/10.1111/j.1365-3040.2007.01758.x, 2008.

Figures

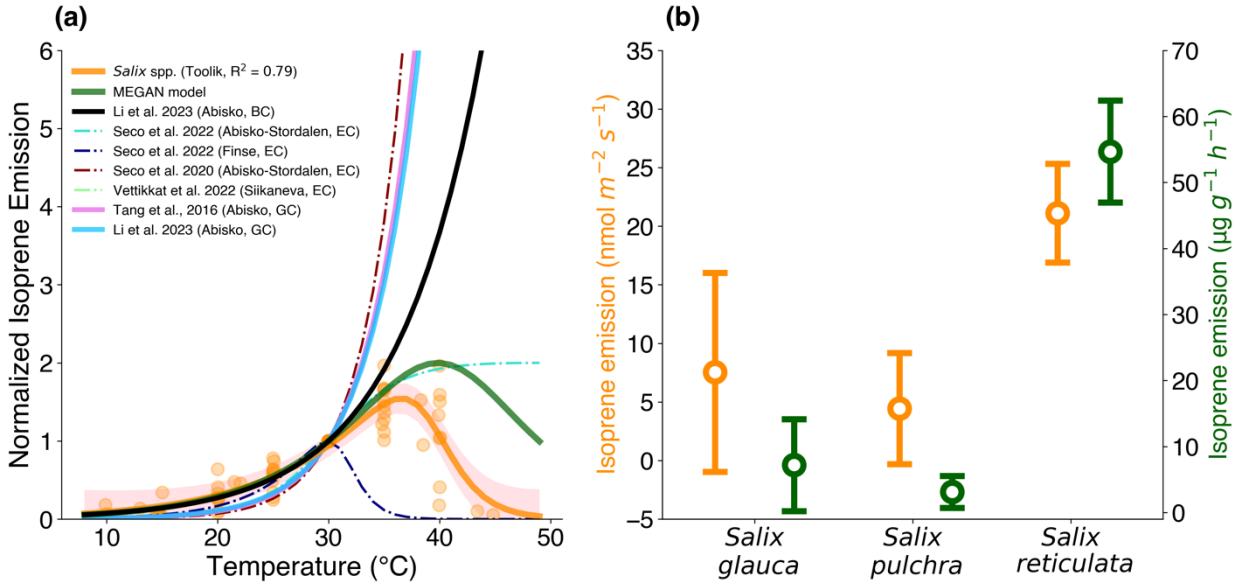

Figure 3.1. (a) Comparing temperature responses of isoprene emissions between this and previous studies. Short-term temperature response curve of willows (orange solid line) derived through leaf chamber experiments in this study, along with tundra whole-ecosystem measurement response curves from previous studies (various colors and patterns). The orange shadow represents the 95% confidence intervals. GC, BC, and EC denote ground chamber, branch chamber, and eddy-covariance measurements. Curves are normalized to emission at a leaf temperature of 30 °C. (b) Emission factors of different *Salix* spp. in the Arctic. Emission factor is defined as isoprene emission capacity at 30 °C and PPFD of 1000 µmol m^{-2} s^{-1}. Averaged emission factors are shown per leaf area (left axis, orange) and per dry leaf mass (right axis, green). Points and error bars represent mean and standard deviation of emission factors.

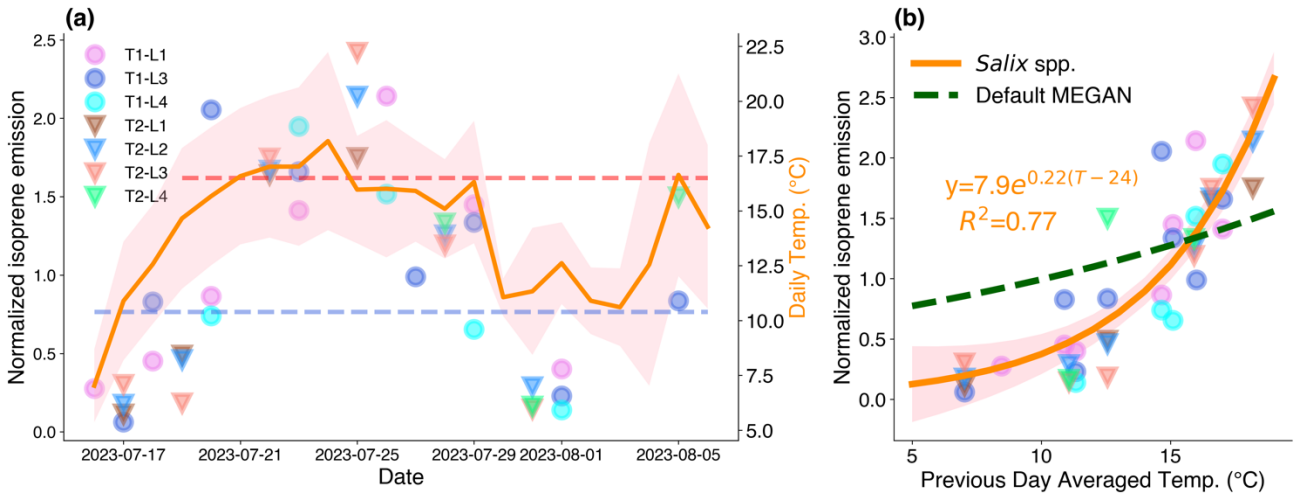

Figure 3.2. (a) The time-series of normalized emission factors from different leaves (various colors and patterns, left axis) and daily temperatures (solid orange line, right axis). The blue and red dashed lines represent the mean daily temperature and 95th percentile of the daily temperature records during 2020-2023, respectively. The orange shadow represents the standard deviation of daily temperature in (a). The emission factors were normalized by dividing the mean emission factors for individual leaves. (b) The correlation between normalized emission factors and the previous-day averaged temperature is shown alongside that in the default MEGAN model (dashed green line). The orange shadow represents the 95% confidence intervals in (b). The equations for the fitted lines in (b) are also presented.

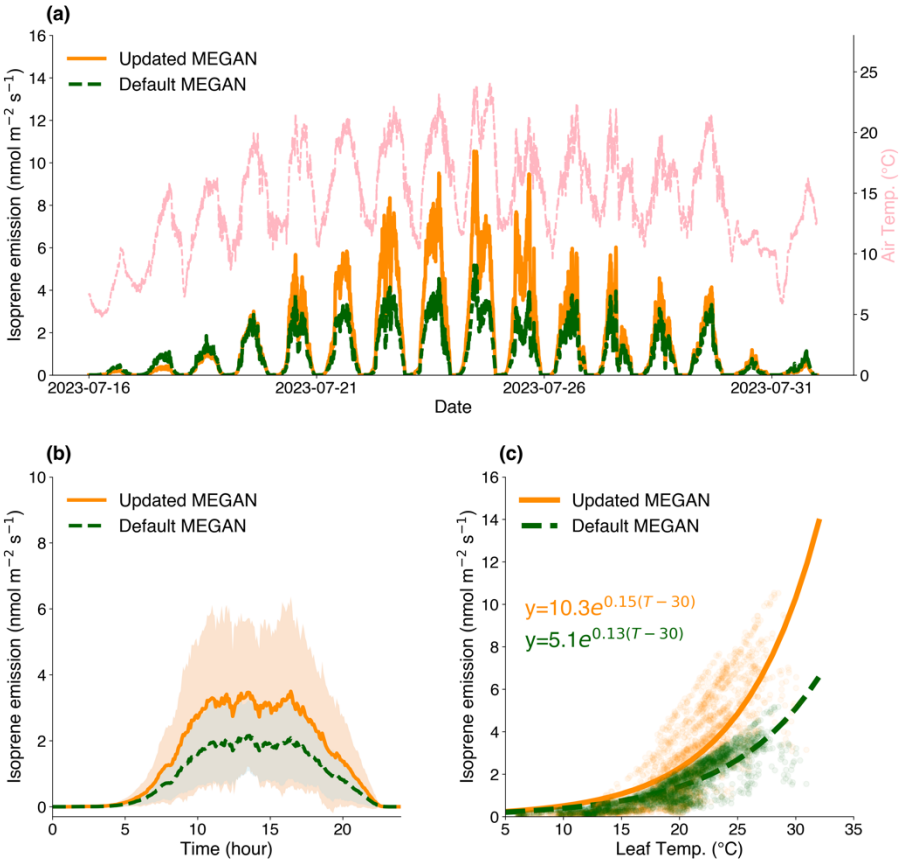

Figure 3.3 The time-series of simulated isoprene emissions from the default (dashed green line, left axis) and updated MEGAN models (solid orange line, left axis), alongside air temperature (dashed pink line, right axis), during the heatwave period (July 16-August 1) in 2023 at the Toolik Field Station (a). The diurnal cycle of simulated isoprene emissions shown in (a) is depicted in (b), and the shadows in (b) represents standard deviations of isoprene emission. (c) presented the short-term temperature response curve of isoprene flux, obtained from flux estimations using both the default and updated MEGAN models. The equations for the fitted lines in (c) are also presented.

Supplementary figures and tables

Figure S3.1. Pictures of *Salix glauca* (a), *S. pulchra* (b), and *S. reticulata* (c).

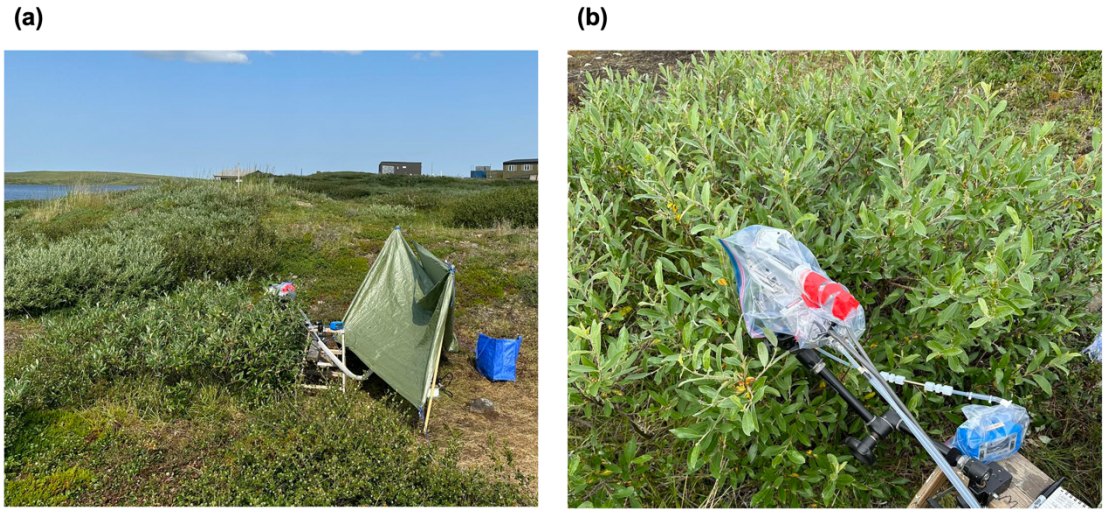

Figure S3.2. Pictures of shrubs and the experimental setup used for acclimating and measuring isoprene emissions from *Salix glauca*. The main control panel for the LI-6400XT is under the tarp (a). (b) shows a leaf chamber with a leaf inside, covered by a plastic bag for waterproofing.

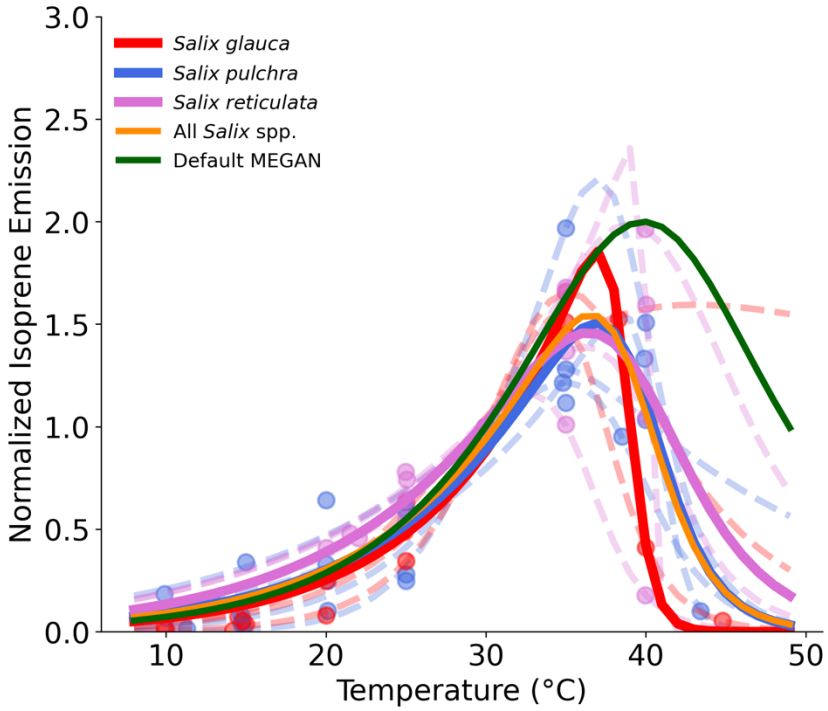

Figure S3.3. Temperature response curves for each *Salix* species are presented. Solid lines with diverse colors illustrate the fitted curves for each individual species. Circles and dashed lines indicate data points and fitted lines corresponding to individual *Salix* samples. The fitted line that incorporates data from all Salix species, along with the default MEGAN model, is represented by the solid orange and green lines, respectively.

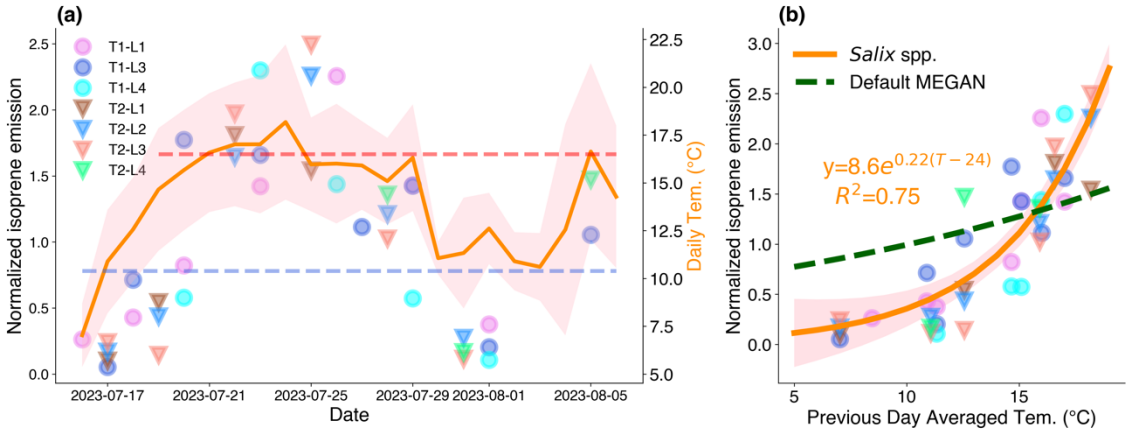

Figure S3.4. The time-series of normalized emission factors from different leaves (various colors and patterns, left axis) and daily temperatures (solid orange line, right axis) are depicted in (a). The blue and red dashed lines represent the mean daily temperature and 95th percentile of the daily temperature records during 2020-2023, respectively. The correlation between normalized emission factors and the previous-day averaged temperature is illustrated in (b), alongside that in the default MEGAN model (dashed green line). The analysis in this figure is the same as in Figure 2 of the manuscript, but it adopted the original measurements taken at a leaf temperature of approximately 20 °C.

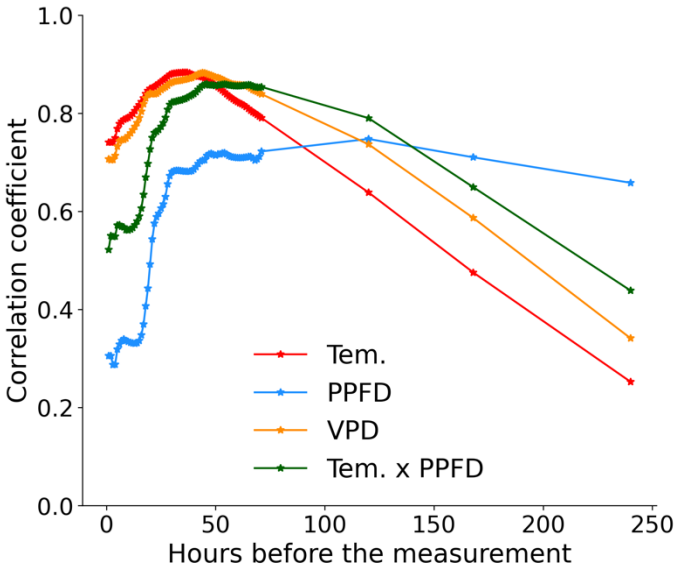

Figure S3.5. Correlation coefficients of the normalized emission factors of *Salix glauca* with the mean temperature, PPFD (Photosynthetic Photon Flux Density), VPD (Vapor Pressure Deficit), and the composite of PPFD and temperature for the previous 1 to 240 hours before the measurement.

Table S3.1. The parameters for the Arrhenius equation for the default MEGAN model and the *Salix* spp.

	E_{opt}	C_{t1}	C_{t2}	T_{opt} (°C)
Default MEGAN	2	95	230	40
Salix spp.	1.5 ± 0.18	83 ± 21	445 ± 237	36 ± 1.1

CHAPTER 4

HIGH TEMPERATURE SENSITIVITY OF ARCTIC ISOPRENE EMISSIONS EXPLAINED BY SEDGES

The material presented in this chapter is reproduced from:
Wang, H., Welch, A. M., Nagalingam, S., Leong, C., Czimczik, C. I., Tang, J., Seco, R., Rinnan, R., Vettikkat, L., Schobesberger, S., Holst, T., Brijesh, S., Sheesley, R. J., Barsanti, K. C., and Guenther, A. B.: High temperature sensitivity of Arctic isoprene emissions explained by sedges, Nature Communications, 15, 6144, 10.1038/s41467-024-49960-0, 2024.

Abstract

Rapid warming in the Arctic can affect biogenic isoprene emissions directly. It has been widely reported that isoprene emissions from the Arctic ecosystem have a strong temperature response. Our study reinforces this through environmental chamber gas exchange experiments, identifying sedges (*Carex* spp. and *Eriophorum* spp.) as key contributors to this sensitivity. We observed that sedges exhibit a markedly stronger temperature response compared to that of other isoprene emitters and predictions by the standard version of the widely accepted isoprene emission model, MEGAN. MEGAN was able to reproduce eddy-covariance flux observations at three high-latitude sites by integrating findings from our chamber experiments. Furthermore, we found that the omission of the strong temperature responses of the Arctic isoprene emitters caused a 20% underestimation of isoprene emissions for the high-latitude regions of the Northern Hemisphere during 2000-2009 in the Community Land Model Version 5 (CLM5), that includes the MEGAN scheme. We also found that the existing model had underestimated the long-term trend of isoprene emissions from 1960 to 2009 by 55% for the high-latitude region. This discrepancy is attributed to both the heightened temperature sensitivity and isoprene emission factors under warming conditions.

4.1 Introduction

Rapid climate change in the Arctic is strongly influencing terrestrial ecosystems (Box et al., 2019; Berner et al., 2020). The change in both climate and ecosystems could alter the atmospheric chemistry and composition in the Arctic atmosphere through biogenic volatile organic compounds (BVOCs) emitted by plants (Rinnan et al., 2020; Faubert et al., 2010; Lindwall et al., 2016a). Since the Arctic has limited anthropogenic VOC sources, BVOCs have a key role in high-latitude atmospheric chemistry (Willis et al., 2018). Because BVOCs are the main precursors of secondary organic aerosol (SOA) (Claeys et al., 2004), changes in BVOC emissions will likely affect the quantity and characteristics of SOA and thus the climate system in the Arctic (Tunved et al., 2006; Petäjä et al., 2022; Kulmala et al., 2004; Weber et al., 2022). Furthermore, the rise in BVOC levels could decrease the atmospheric oxidation capacity and prolong the lifetime of methane, thereby exacerbating global warming (Weber et al., 2022; Boy et al., 2022).

Isoprene is the most abundant reactive BVOC emitted globally and in the Arctic (Guenther et al., 2012; Rinnan et al., 2020; Tang et al., 2023). Isoprene can help vegetations to tolerate abiotic stresses (Sharkey et al., 2008), and isoprene can act as a signaling compound to stimulate plant defense mechanisms during stress periods (Monson et al., 2021). Isoprene is synthesized from dimethylallyl diphosphate (DMADP) derived from the methyl erythritol 4-phosphate (MEP) pathway through IspS (Sharkey and Monson, 2014). Isoprene emission is controlled by environmental conditions, especially temperature and solar radiation (Guenther et al., 1993). Thus, a rapidly warming climate in the Arctic is favorable for increasing the emission of isoprene (Lindwall et al., 2016b; Kramshøj et al., 2016; Seco et al., 2020; Tiiva et al., 2008). The temperature response curves of isoprene emission, used in the current earth system models (ESMs) and the chemistry transport models (CTMs), are based on measurements of a few temperate plants (Guenther et al., 2006; Guenther et al., 2012), and a typical isoprene temperature response curve

has a Q10 of about 3, which is thought to be driven by the influence of temperature on substrate supply and the activity of IspS (Sharkey and Monson, 2014). However, recent whole-ecosystem measurements suggest that the temperature response of isoprene emissions in high-latitude tundra ecosystems has a Q10 over 8, which is also much higher than that predicted by the widely used BVOC emission model, the Model of Emissions of Gases and Aerosols from Nature (MEGAN) (Seco et al., 2020; Seco et al., 2022; Li et al., 2023; Vettikkat et al., 2023; Holst et al., 2010; Selimovic et al., 2022). In contrast, leaf/branch-level studies showed that the Arctic willow species (*Salix pulchra*, *Salix glauca,* and *Salix myrsinites*), which are one of main isoprene emitters in high-latitude tundra ecosystems, have a short-term temperature response that is similar to temperate plants (Potosnak et al., 2013; Li et al., 2023). Our previous study also confirmed that the hourly temperature response curve of *Salix* spp. is consistent with that of temperate plants as well as the MEGAN model (Guenther et al., 2012; Wang et al., 2024). Additionally, we found that the isoprene emission factors of willows show a greater than expected response to the mean ambient temperature of the previous day (Wang et al., 2024). Nonetheless, we concluded that the temperature response of willows in the Arctic is greater than that predicted by current models but still cannot fully explain the high temperature sensitivity of isoprene emissions from high-latitude ecosystems (Wang et al., 2024). Consequently, species-specific investigations are necessary to further explore the strong temperature responses observed at the ecosystem level.

In this study, we identified sedges (*Carex* spp. and *Eriophorum* spp.) as the key contributors to the pronounced temperature sensitivity of isoprene emissions in the Arctic ecosystems. Sedges exhibit a more significant temperature response than both willows and MEGAN. Additionally, we observed that sedges can adjust their temperature sensitivity and emission capacity, which is represented by emission factor in this paper, in response to changes in ambient growth

temperatures. We integrated these findings into the MEGANv2.1 model (Guenther et al., 2012), enhancing its capability to simulate observed ecosystem-scale flux measurements. Moreover, the updated MEGAN model projects a 20% increase in Arctic isoprene emissions and a 55% rise in the long-term isoprene emission trend. Given the ongoing intensification of global warming, the changes in isoprene emissions have the potential to substantially alter atmospheric chemistry in high-latitude regions.

4.2 Materials and methods

4.2.1 BEARS-oNS campaign and Glass Chamber Experiments

The Biogenic Emissions and Aerosol Response on the North Slope (BEAR-oNS) project aimed to explore the impact of climate change on the interactions among BVOC, aerosol and climate in high latitude regions. The first stage of the BEAR-oNS campaign was conducted during July and early August 2022, to characterize the BVOC emission and investigate the source of aerosols in the high-latitude tundra ecosystem near the Toolik Field Station (TFS) in Alaska (USA, 68.65N,149.58W). July mean air temperatures at TFS were 9.6 °C in 2022 and 13.1 °C in 2023, with accumulated precipitation at 220 mm and 105 mm for each year respectively.

The temperature response curve experiments investigated the impact of temperature on isoprene emission. The vegetation specimens analyzed in this study are listed in Table S4.3 and Table S4.4. The vegetation samples were collected from the tussock tundra near the Toolik Field Station. The plant samples were detached from soil with the main root system or cut from the main branch and submerged into water in glass bottles. We chose plants that were in good condition without galls or visible damage.

The temperature curve experiments were conducted with a leaf chamber system (see details in the next section). One chamber blank (background) VOC sample from an empty chamber was

collected at the beginning of every experiment before putting the plant into the glass chamber. After placing a leaf, branch or glass dish with moss into the glass chamber, VOC sampling was initiated after the photosynthesis rate stabilized. For *Carex1* and *Eriophorum1* samples, there were only two temperature steps of 20 °C and 30 °C, collected after the photosynthesis rate was relatively stable. For other sedge samples, the leaf temperature was ramped up from 15 or 20 °C to 35 or 40 °C in steps of 5 °C. Each temperature step lasted 1 hour, and samples were collected with sorbent cartridges (see next section) during the last 10 to 15 minutes of the hour with a flow rate of 200 cc/min for 5 min resulting in a 1 L VOC sample.

4.2.2 Flux measurements

The leaf-level BVOC measurements were conducted using a custom-made, field-portable glass chamber with environmental controls. The chamber has an internal volume of 0.62 L and is mounted on a thermoelectric cooler assembly (Custom Thermoelectric, MD, USA), which allows for precise control of the leaf temperature. A miniature fan was installed to stir the air inside the chamber. A white LED source provided artificial illumination with a photosynthetically active radiation output of approximately 1000 μmol m^{-2} s^{-1}. The ambient air was pushed into the chamber using a diaphragm pump at rates of 0.9–1.0 L min^{-1}, and the VOCs in the inlet air flow were removed by an activated carbon filter. Part of the effluent air from the chamber was sampled onto sorbent cartridges (Tenax TA and Carbograph 5TD; Markes International, UK) for BVOC analysis. Additionally, an infrared gas analyzer (LI-850; LI-COR Biosciences, NE, USA) was used to measure the CO_2 and H_2O mixing ratios in the influent (background) and effluent airflows; the analyzer was switched between the chamber's inlet and outlet every 30 s.

The sampled sorbent cartridges were transported to our laboratory at the University of California, Irvine, where they were thermally desorbed using a TD autosampler (Ultra-xr; Markes

International). The desorbed VOCs were injected into a gas chromatograph (GC) (7890B; Agilent Technologies, CA, USA) equipped with a 60 m Rxi-624Sil MS capillary column (Restek, PA, USA). The column eluate was channeled to an electron impact ionization time-of-flight mass spectrometer (BenchTOF-Select; Markes International) and a flame ionization detector (FID, Agilent) for compound identification and quantification. A detailed explanation of the GC methodology including the GC oven temperature program, calibration protocols, and measurement uncertainties is provided elsewhere (Nagalingam et al., 2022).

Isoprene flux measurements from three high latitude sites were used to validate the models. The flux data used in this study were measured in Abisko (Sweden, 68.36° N, 19.05° E) in 2018, Finse (Norway, 60.60° N, 7.53 ° E) in 2019 and Siikaneva (Finland, 61.83° N, 24.19° E) [20,21] in 2021. The campaign times and major vegetation types at the three sites are listed in Table S4.1, and more details about the flux measurements can be found in Seco et al. (2022) and Vettikkat et al. (2023).

4.2.3 MEGAN model and temperature response curve

MEGAN is a flexible model framework for calculating biogenic volatile organic compound emissions from terrestrial ecosystems (Guenther et al., 2006; Guenther et al., 2012). The isoprene flux in MEGANv2.1 is calculated as:

$$F = \varepsilon \cdot LAI \cdot Cce \cdot \gamma_T \cdot \gamma_P \cdot \gamma_A \cdot \gamma_C \cdot \gamma_{SM} \quad [4.1]$$

, where ε, Cce, and LAI represent the canopy-level standard emission factor (μmol m^{-2} s^{-1}), canopy factor (=0.3), leaf area index (LAI, m^2 m^{-2}). γ_T, γ_P, γ_A, γ_C and γ_{SM} denote the emission activity factors of isoprene emissions including temperature, solar radiation, leaf age, CO_2 inhibition and water stress, respectively. MEGAN considers the BVOC responses to the long-term temperature, defined as the temperature of the past one day or longer, and the current temperature, reflecting

changes on a minute-to-hour scale. The default short-term temperature response curve, γ_T, for isoprene in MEGAN is:

$$\gamma_{\mathrm{T}} = E_{\mathrm{opt}} \cdot \frac{C_{\mathrm{T2}} \cdot e^{\frac{C_{T1}}{R}\left(\frac{1}{T_{\mathrm{opt}}} - \frac{1}{T}\right)}}{\mathrm{C_{T2}} - C_{\mathrm{T1}} \cdot \left(1 - e^{\frac{C_{T2}}{R}\left(\frac{1}{T_{\mathrm{opt}}} - \frac{1}{T}\right)}\right)} \quad [4.2]$$

. *T (K)* is the leaf temperature. R (=0.008314 KJ/mol), C_{T1} (=95 KJ/mol) and C_{T2} (=230 KJ/mol) are the gas constant, and the activation and deactivation energies, respectively. E_{opt} and T_{opt} are:

$$T_{\mathrm{opt}} = 313 + 0.6 \cdot (T_{240} - 297.15) \quad [4.3]$$

$$E_{\mathrm{opt}} = 2 \cdot e^{0.05 \cdot (T_{24} - 297.15)} \cdot e^{0.05 \cdot (T_{240} - 297.15)} \quad [4.4]$$

, where T_{24} (K) and T_{240} (K) denote the mean air temperature of the previous 24 hours and 240 hours, respectively. *Equations (3) and (4) for* T_{opt} (K) and E_{opt} represent the long-term impact of temperature on the optimal temperature and the shape of the temperature response curve.

The updated short-term temperature response curve for sedges in MEGANv2.1 is expressed as:

$$\gamma_{\mathrm{T_{sg}}} = E_{\mathrm{opt\_sg}} \cdot e^{\frac{C_{sg}}{R}\left(\frac{1}{303.15} - \frac{1}{T}\right)} \quad [4.5]$$

. C_{sg} is the activation energy for the isoprene temperature response of sedges and changes with T_{240} as:

$$C_{\mathrm{sg}} = 95 + 9.5 \cdot e^{0.53 \cdot (288.15 - T_{240})} \quad [4.6]$$

. The impact of T_{240} on isoprene emission factor of sedge is as:

$$E_{\mathrm{opt\_sg}} = e^{0.12 \cdot (T_{240} - 288.15)} \quad [4.7]$$

. The PFT of boreal broadleaf deciduous shrub in the updated model adopted the temperature response curve described in the eq. (2)-(4) with the parameters in Wang et al. (2023), and the long-term temperature response for boreal broadleaf deciduous shrub in MEGANv2.1 is updated as:

$$E_{\mathrm{opt\_willow}} = 7.9 \cdot e^{0.22 \cdot (T_{24} - 297.15)} \quad [4.8]$$

. To investigate the capacity of different temperature response curves to explain eddy covariance measurements, we rewrote eq. (1) as:

$$F_{flux} = \sum_{i=1}^{n} E_i \cdot \frac{LAI}{LAI_{max}} \cdot \gamma_{T\_i} \cdot \gamma_{others} \quad [4.9]$$

, where γ_{others} represents the product of C_{ce}, γ_P, γ_A, γ_C and γ_{SM}. The impact of water stress is neglected in this study ($\gamma_{SM} = 1$). γ_{T_i} and E_i denote the temperature response and the total emission capacity of the vegetation type *i*, respectively. In this study, γ_{T_i} represented the temperature response curves of two types of vegetations, Arctic grass and boreal deciduous shrub, as described in equations (2)-(8). The *LAI* is normalized by the maximum value of *LAI* to eliminate the uncertainties of the absolute values of *LAI*, and the ratio between *LAI* and LAI_{max} depicts the relative change of leaf biomass. The E_i represents the total emission capacity of the vegetation *i* in the canopy and is as:

$$E_i = \varepsilon_i^* \cdot CF_i \quad [4.10]$$

. ε_i^* and CF_i represent the canopy-level emission factors and the cover fraction of vegetation *i*, respectively. Canopy-level emission factors were scaled up from the leaf-level emission factors to the scenario with LAI=5 in MEGANv2.1(Vettikkat et al., 2023;Guenther et al., 2012). The leaf-level emission factor for sedges is from the observations for *Eriophorum* spp. in this study at TFS. The leaf-level emission factor for willows is based on the measurements by Wang et al. (2024). We fitted the model to get the optimal E_i for the default model and CF_i for the updated model using the least-squares method to get rid of the uncertainties associated with vegetation fraction input.

4.2.4 Community Land Model 5 and numerical experiments

CLM5(Lawrence et al., 2019) is the land component of the Community Earth System Model (CESM) and can simulate the land surface and terrestrial ecosystem response and feedback to the weather system and climate change. MEGANv2.1 is coupled to CLM5 as the BVOC emission module. We used CLM5 to test the influence of updating the isoprene temperature response curve

on a regional-global scale. We conducted two CLM5 runs: one with the default MEGAN isoprene temperature response and the other with the updated MEGAN using the strong Arctic isoprene temperature responses reported in this study. The emission factors are based on the MEGANv2.1. The model components set is I1850Clm50BgcCrop (https://www.cesm.ucar.edu/models/cesm2/config/compsets.html), and CLM5 is driven by the Global Soil Wetness Project Phase 3 (GSWP3) reanalysis climate forcing dataset with a 3-hour intervals. The spatial resolution of the CLM5 runs is 0.9° x 1.25°, and the numerical experiments cover the period from 1950 to 2009 with the monthly outputs. We adopted the default initial condition of CLM5 that comes from the steady state of the model and treated the first 10 years as the spin-up time. Our analysis is based on the model outputs for the years from 1960 to 2009

4.3 Results and discussion

4.3.1 Isoprene emission from Arctic sedges is sensitive to temperature changes

Our species-level gas exchange chamber experiments showed that the main isoprene emitters among the species measured at Toolik Field Station (TFS), Alaska, USA, are sedges, a major component of Arctic graminoid plants, and willows, a major component of Arctic woody plants (Figure S4.1). Other studies have also indicated that the *Salix* spp., *Carex* spp. and *Eriophorum* spp. exhibit significantly higher isoprene emission levels compared to other tundra species, e.g., *Betula* spp. and *Cassiope* spp.(Simin et al., 2021;Potosnak et al., 2013;Hellén et al., 2021;Männistö et al., 2023;Li et al., 2023) and *Sphagnum* spp. (Ryde et al., 2022;Ekberg et al., 2011;Tiiva et al., 2009). The temperature response of willows in the Arctic cannot explain the high temperature sensitivity of isoprene emissions from high-latitude ecosystems (Wang et al., 2024).

Arctic sedges studied here show a more pronounced temperature response than other plant species, including Arctic woody willow shrubs and any of the plant responses used to develop the MEGAN

model. Our data confirm that the sedges are responsible for the heightened temperature responses of isoprene emissions from high-latitude ecosystems (Figure 4.1a and 1b). We calculated the Q_{10} coefficient for isoprene emissions from sedges (*Carex* spp. and *Eriophorum* spp.) and willows between 25 and 35 °C. The Q_{10} coefficient represents the isoprene emission rate change with a 10 °C rise of the leaf temperature. The Q_{10} values of *Carex* spp. (15.6 ± 8.8) and *Eriophorum* spp. (9.1 ± 7.0) are much higher than the Q_{10} of the Arctic willows (3.2 ± 1.8), which is close to the Q10 of the MEGAN model (2.91) (Figure S4.2). We applied the Arrhenius equation to model the exponential temperature response curves of *Carex* spp. and *Eriophorum* spp. (refer to the Methods section), where the activation energy (Eq. 5) denotes the temperature sensitivity of isoprene emission. Our findings indicate that the temperature response curves of both *Carex* spp. and *Eriophorum* spp. exhibit high temperature sensitivity (or high activation energy) up to 35 °C (Figure S4.3). However, the activation energy and R^2 decrease beyond 40 °C, suggesting a slower increase rate of isoprene emissions from both species (Figure S4.3).

Moreover, there is an inverse relationship between the temperature sensitivity and emission capacity (or emission factor) of isoprene in sedges, both of which are acclimated to the temperature history of the previous days (Figure 4.1c). We used the 10-day average temperature as an indicator of the recent growing environment. This choice is based on the Pearson correlation coefficient for the temperature sensitivities (activation energy in Eq. 5) and emission factors in relation to the mean temperature of the preceding 1 to 15 days for *Eriophorum* spp. (Figure S4.4). The use of a 10-day average temperature also follows the current framework of the MEGAN model but the actual time period influencing isoprene emission is uncertain. With higher 10-day average temperatures, *Carex* spp. and *Eriophorum* spp. exhibit lower temperature sensitivity of isoprene emissions, as indicated by a decrease in activation energy, and higher emission capacity, or

emission factors, compared to those in colder environments. Isoprene emissions are controlled by the enzyme activity and supply of substrates(Sharkey and Monson, 2014). In addition to these two factors, we speculate that the pronounced response of sedges to high temperatures could be also related to enzyme accumulation. The mRNA levels and IspS protein concentrations are likely low in sedges in a cold environment until a warm environment or a specific temperature threshold initiates the gene expression necessary for IspS synthesis. The IspS protein has a half-life time of 5.3 days in a 20 °C environment(Wiberley et al., 2009). Its accumulation, following the onset of gene expression for IspS synthesis, would result in increased isoprene emissions as conditions transition from cold to warm. When the basal level IspS reaches the maximum, isoprene emission would become primarily dependent on enzyme activity and substrate availability(Sharkey and Monson, 2014;Rasulov et al., 2010). One potential piece of evidence is that the isoprene activation energy of *Eriophorum* spp. after a warming period is comparable to that of aspen (*Populus* spp.) at 72.1 kJ/mol(Rasulov et al., 2010) and that of MEGAN at 95 kJ/mol(Guenther et al., 2012), suggesting that IspS levels are no longer limiting factors, and the emission patterns resemble those of temperate isoprene emitters (Figure 4.1c). It has been reported that the isoprene emission of the Arctic sedges varies with the air temperature(Ekberg et al., 2009;Tiiva et al., 2007), and our results provide evidence that the sedges are sensitive to both minutes-hour scale temperature change as well as day-weeks change.

4.3.2 Updated MEGAN model can better explain the whole-ecosystem measurements.

The MEGANv2.1 model, which has 16 plant functional types (PFTs) each with a uniform temperature response curve, cannot fully capture the observed variability in isoprene emissions in Arctic regions. To address this, we updated the temperature response curves in MEGAN version 2.1(Bonan Gordon et al., 2002;Guenther et al., 2012) and evaluated the model using eddy-

covariance flux measurements from three high-latitude sites. Table S4.1 shows that sedges are the dominant isoprene emitters at the Abisko-Stordalen and Siikaneva sites, while the Finse site is dominated by both sedges and willows. In this study, the PFT categories of Arctic grass and boreal broadleaf deciduous shrubs are updated based on our measurements.

The Arctic grass adopted the temperature curve of sedges (Eq. 5 in the Methods) with a dynamic activation energy (Eq. 6 in the Methods) and emission factor (Eq. 7 in the Methods) derived from *Eriophorum* spp. measurements in this study (Figure S4.5). The boreal broadleaf deciduous shrub used the temperature response curve of MEGANv2.1 (Eq. 2, 3 and 4 in the Methods) but included the response of emission factors to previous 1-day average temperature for *Salix* spp. (Eq. 8 in the Methods)(Wang et al., 2024). The leaf-level emission factor was 12.0 nmol m^{-2} s^{-1} for the Arctic grass and 6.5 nmol m^{-2} s^{-1} for the boreal shrub (including willows), respectively, which was based on our glass chamber measurements in this study and Wang et al. (2024). Besides temperature response curves, isoprene emissions at the field sites were also affected by the abundance of sedge and willow. To eliminate uncertainties associated with vegetation fraction input, we used the least squares fitting method to adjust vegetation proportions, thereby optimizing the performance of model in comparison with flux measurements.

The updated model demonstrates an enhanced ability to capture the variability of isoprene flux compared to the default temperature response curve of the MEGANv2.1 model (see Figure 2 and Table S4.2). Across the three sites, the updated model consistently shows an increase in R^2 and a decrease in Root Mean Square Error (RMSE). The updated model can capture both the low values during cold periods and the high values in warm periods more accurately than the default model. In addition, for the Siikaneva site, the model accurately captures the elevated values following heatwaves, after accounting for the effects of warming on temperature response and emission

factors. We also compared the fitted fractions for Arctic grass and boreal shrub from the updated model with the observed land cover/vegetation fractions at the Finse and Siikaneva sites (see Table 4.1). Our findings indicate that the fitted fractions for Arctic grass and boreal shrub closely match the observations or estimates at Finse and Siikaneva sites.

4.3.3 Estimation of high-latitude isoprene emission

We reported a pronounced temperature response curve for sedges in this study. In addition, our previous research indicated that Arctic willows (*Salix* spp.) can significantly increase their isoprene emission capacity in response to an increase in the average temperature of the preceding day(Wang et al., 2024). The different isoprene emission patterns of the two types of high-latitude plants (Arctic grass and boreal shrub) both point to an increase in isoprene emissions due to Arctic warming. To estimate isoprene emissions in the high latitude regions (north of 60°N), we updated MEGANv2.1 in the Community Land Model version 5 (CLM5) (Lawrence et al., 2019) with the temperature curves from this study for the Arctic grass and boreal broadleaf deciduous shrub PFTs. We used the emission factors reported by Guenther et al. (2012) for the CLM simulations. The averaged isoprene emissions estimated by the new model are 20% higher than the original MEGAN estimate for 2000-2009, increasing from 2.71 to 3.25 Tg yr^{-1}, which suggests that the isoprene emissions from the high-latitude regions in the Northern Hemisphere are underestimated in current ESMs. By updating the temperature response, the CLM simulation shows a decrease in isoprene emissions from Arctic grass-dominated tundra, while observing an increase from high-latitude deciduous shrubs (Figure 3 and Figure S4.6). In the updated model, Arctic grass isoprene emissions respond less to low temperatures typical of Arctic climates but increase significantly with rising temperatures compared to the default model (Figure1 and Figure 3). The simulations predict a notable increase in isoprene emissions in the Russian Siberian regions dominated by

boreal deciduous shrubs. The model results presented by Stavrakou et al. (2018) suggested that the interannual variability of Ozone Monitoring Instrument (OMI) formaldehyde (HCHO) measurements in Siberia could be explained by biogenic isoprene emissions. However, more in-situ measurements are crucial to validate the model and understand the biogenic isoprene emissions in Siberia.

Additionally, we calculated the long-term trend of isoprene emissions and found that the updated temperature response results in a 55% increase in the trend of isoprene emissions from 1960 to 2009 in the high-latitude region compared to the default model (Figure 4.4). The default model framework could not capture the rapid change in high-latitude isoprene emissions and their feedback on atmospheric chemistry and the climate system. Furthermore, the results showed that an Arctic heatwave could create a significant isoprene burst event. For example, abnormally warm Arctic weather in 1991 and 2001 were predicted to have an approximately 40% increase in isoprene emissions in high-latitude regions in the Northern Hemisphere (Figure S4.7).

Reference

Berner, L. T., Massey, R., Jantz, P., Forbes, B. C., Macias-Fauria, M., Myers-Smith, I., Kumpula, T., Gauthier, G., Andreu-Hayles, L., Gaglioti, B. V., Burns, P., Zetterberg, P., D'Arrigo, R., and Goetz, S. J.: Summer warming explains widespread but not uniform greening in the Arctic tundra biome, Nature Communications, 11, 4621, 10.1038/s41467-020-18479-5, 2020.

Bonan Gordon, B., Levis, S., Kergoat, L., and Oleson Keith, W.: Landscapes as patches of plant functional types: An integrating concept for climate and ecosystem models, Global Biogeochemical Cycles, 16, 5-1-5-23, 10.1029/2000GB001360, 2002.

Box, J. E., Colgan, W. T., Christensen, T. R., Schmidt, N. M., Lund, M., Parmentier, F.-J. W., Brown, R., Bhatt, U. S., Euskirchen, E. S., Romanovsky, V. E., Walsh, J. E., Overland, J. E., Wang, M., Corell, R. W., Meier, W. N., Wouters, B., Mernild, S., Mård, J., Pawlak, J., and Olsen, M. S.: Key indicators of Arctic climate change: 1971–2017, Environmental Research Letters, 14, 045010, 10.1088/1748-9326/aafc1b, 2019.

Boy, M., Zhou, P., Kurtén, T., Chen, D., Xavier, C., Clusius, P., Roldin, P., Baykara, M., Pichelstorfer, L., Foreback, B., Bäck, J., Petäjä, T., Makkonen, R., Kerminen, V.-M., Pihlatie, M., Aalto, J., and Kulmala, M.: Positive feedback mechanism between biogenic volatile organic compounds and the methane lifetime in future climates, npj Climate and Atmospheric Science, 5, 72, 10.1038/s41612-022-00292-0, 2022.

Claeys, M., Graham, B., Vas, G., Wang, W., Vermeylen, R., Pashynska, V., Cafmeyer, J., Guyon, P., Andreae, M. O., and Artaxo, P.: Formation of secondary organic aerosols through photooxidation of isoprene, Science, 303, 1173-1176, 2004.

Dobricic, S., Russo, S., Pozzoli, L., Wilson, J., and Vignati, E.: Increasing occurrence of heat waves in the terrestrial Arctic, Environmental Research Letters, 15, 024022, 10.1088/1748-9326/ab6398, 2020.

Ekberg, A., Arneth, A., Hakola, H., Hayward, S., and Holst, T.: Isoprene emission from wetland sedges, Biogeosciences, 6, 601-613, 10.5194/bg-6-601-2009, 2009.

Ekberg, A., Arneth, A., and Holst, T.: Isoprene emission from Sphagnum species occupying different growth positions above the water table, Boreal Environment Research, 16, 47-59, 2011.

Faubert, P., Tiiva, P., Rinnan, Å., Michelsen, A., Holopainen, J. K., and Rinnan, R.: Doubled volatile organic compound emissions from subarctic tundra under simulated climate warming, New Phytologist, 187, 199-208, https://doi.org/10.1111/j.1469-8137.2010.03270.x, 2010.

Guenther, A., Karl, T., Harley, P., Wiedinmyer, C., Palmer, P., and Geron, C.: Estimates of global terrestrial isoprene emissions using MEGAN (Model of Emissions of Gases and Aerosols from Nature), Atmos. Chem. Phys, 6, 3181-3210, 2006.

Guenther, A. B., Zimmerman, P. R., Harley, P. C., Monson, R. K., and Fall, R.: Isoprene and monoterpene emission rate variability: Model evaluations and sensitivity analyses, Journal of Geophysical Research: Atmospheres, 98, 12609-12617, doi:10.1029/93JD00527, 1993.

Guenther, A. B., Jiang, X., Heald, C. L., Sakulyanontvittaya, T., Duhl, T., Emmons, L. K., and Wang, X.: The Model of Emissions of Gases and Aerosols from Nature version 2.1 (MEGAN2.1): an extended and updated framework for modeling biogenic emissions, Geoscientific Model Development, 5, 1471-1492, 10.5194/gmd-5-1471-2012, 2012.

Hellén, H., Praplan, A. P., Tykkä, T., Helin, A., Schallhart, S., Schiestl-Aalto, P. P., Bäck, J., and Hakola, H.: Sesquiterpenes and oxygenated sesquiterpenes dominate the VOC (C5–C20) emissions of downy birches, Atmos. Chem. Phys., 21, 8045-8066, 10.5194/acp-21-8045-2021, 2021.

Holst, T., Arneth, A., Hayward, S., Ekberg, A., Mastepanov, M., Jackowicz-Korczynski, M., Friborg, T., Crill, P. M., and Bäckstrand, K.: BVOC ecosystem flux measurements at a high latitude wetland site, Atmos. Chem. Phys., 10, 1617-1634, 10.5194/acp-10-1617-2010, 2010.

Jones, M. W., Abatzoglou, J. T., Veraverbeke, S., Andela, N., Lasslop, G., Forkel, M., Smith, A. J. P., Burton, C., Betts, R. A., van der Werf, G. R., Sitch, S., Canadell, J. G., Santín, C., Kolden, C., Doerr, S. H., and Le Quéré, C.: Global and Regional Trends and Drivers of Fire Under Climate Change, Reviews of Geophysics, 60, e2020RG000726, https://doi.org/10.1029/2020RG000726, 2022.

Kramshøj, M., Vedel-Petersen, I., Schollert, M., Rinnan, Å., Nymand, J., Ro-Poulsen, H., and Rinnan, R.: Large increases in Arctic biogenic volatile emissions are a direct effect of warming, Nature Geoscience, 9, 349-352, 10.1038/ngeo2692, 2016.

Kulmala, M., Suni, T., Lehtinen, K. E. J., Dal Maso, M., Boy, M., Reissell, A., Rannik, Ü., Aalto, P., Keronen, P., Hakola, H., Bäck, J., Hoffmann, T., Vesala, T., and Hari, P.: A new feedback mechanism linking forests, aerosols, and climate, Atmos. Chem. Phys., 4, 557-562, 10.5194/acp-4-557-2004, 2004.

Lawrence, D. M., Fisher, R. A., Koven, C. D., Oleson, K. W., Swenson, S. C., Bonan, G., Collier, N., Ghimire, B., van Kampenhout, L., Kennedy, D., Kluzek, E., Lawrence, P. J., Li, F., Li, H., Lombardozzi, D., Riley, W. J., Sacks, W. J., Shi, M., Vertenstein, M.,

Wieder, W. R., Xu, C., Ali, A. A., Badger, A. M., Bisht, G., van den Broeke, M., Brunke, M. A., Burns, S. P., Buzan, J., Clark, M., Craig, A., Dahlin, K., Drewniak, B., Fisher, J. B., Flanner, M., Fox, A. M., Gentine, P., Hoffman, F., Keppel-Aleks, G., Knox, R., Kumar, S., Lenaerts, J., Leung, L. R., Lipscomb, W. H., Lu, Y., Pandey, A., Pelletier, J. D., Perket, J., Randerson, J. T., Ricciuto, D. M., Sanderson, B. M., Slater, A., Subin, Z. M., Tang, J., Thomas, R. Q., Val Martin, M., and Zeng, X.: The Community Land Model Version 5: Description of New Features, Benchmarking, and Impact of Forcing Uncertainty, Journal of Advances in Modeling Earth Systems, 11, 4245-4287, https://doi.org/10.1029/2018MS001583, 2019.

Li, T., Baggesen, N., Seco, R., and Rinnan, R.: Seasonal and diel patterns of biogenic volatile organic compound fluxes in a subarctic tundra, Atmospheric Environment, 292, 119430, https://doi.org/10.1016/j.atmosenv.2022.119430, 2023.

Lindwall, F., Schollert, M., Michelsen, A., Blok, D., and Rinnan, R.: Fourfold higher tundra volatile emissions due to arctic summer warming, Journal of Geophysical Research: Biogeosciences, 121, 895-902, https://doi.org/10.1002/2015JG003295, 2016a.

Lindwall, F., Svendsen, S. S., Nielsen, C. S., Michelsen, A., and Rinnan, R.: Warming increases isoprene emissions from an arctic fen, Science of The Total Environment, 553, 297-304, https://doi.org/10.1016/j.scitotenv.2016.02.111, 2016b.

Männistö, E., Ylänne, H., Losoi, M., Keinänen, M., Yli-Pirilä, P., Korrensalo, A., Bäck, J., Hellén, H., Virtanen, A., and Tuittila, E.-S.: Emissions of biogenic volatile organic compounds from adjacent boreal fen and bog as impacted by vegetation composition, Science of The Total Environment, 858, 159809, https://doi.org/10.1016/j.scitotenv.2022.159809, 2023.

McFiggans, G., Mentel, T. F., Wildt, J., Pullinen, I., Kang, S., Kleist, E., Schmitt, S., Springer, M., Tillmann, R., Wu, C., Zhao, D., Hallquist, M., Faxon, C., Le Breton, M., Hallquist, Å. M., Simpson, D., Bergström, R., Jenkin, M. E., Ehn, M., Thornton, J. A., Alfarra, M. R., Bannan, T. J., Percival, C. J., Priestley, M., Topping, D., and Kiendler-Scharr, A.: Secondary organic aerosol reduced by mixture of atmospheric vapours, Nature, 565, 587-593, 10.1038/s41586-018-0871-y, 2019.

Monson, R. K., Weraduwage, S. M., Rosenkranz, M., Schnitzler, J.-P., and Sharkey, T. D.: Leaf isoprene emission as a trait that mediates the growth-defense tradeoff in the face of climate stress, Oecologia, 10.1007/s00442-020-04813-7, 2021.

Nagalingam, S., Seco, R., Musaev, K., Basu, C., Kim, S., and Guenther, A.: Impact of heat stress on foliar biogenic volatile organic compound emission and gene expression in tomato (Solanum lycopersicum) seedlings, Elementa: Science of the Anthropocene, 10, 10.1525/elementa.2021.00096, 2022.

Paxian, A., Eyring, V., Beer, W., Sausen, R., and Wright, C.: Present-Day and Future Global Bottom-Up Ship Emission Inventories Including Polar Routes, Environmental Science & Technology, 44, 1333-1339, 10.1021/es9022859, 2010.

Petäjä, T., Tabakova, K., Manninen, A., Ezhova, E., O'Connor, E., Moisseev, D., Sinclair, V. A., Backman, J., Levula, J., Luoma, K., Virkkula, A., Paramonov, M., Räty, M., Äijälä, M., Heikkinen, L., Ehn, M., Sipilä, M., Yli-Juuti, T., Virtanen, A., Ritsche, M., Hickmon, N., Pulik, G., Rosenfeld, D., Worsnop, D. R., Bäck, J., Kulmala, M., and Kerminen, V. M.: Influence of biogenic emissions from boreal forests on aerosol–cloud interactions, Nature Geoscience, 15, 42-47, 10.1038/s41561-021-00876-0, 2022.

Potosnak, M. J., Baker, B. M., LeStourgeon, L., Disher, S. M., Griffin, K. L., Bret-Harte, M. S., and Starr, G.: Isoprene emissions from a tundra ecosystem, Biogeosciences, 10, 871-889, 10.5194/bg-10-871-2013, 2013.

Ramtvedt, E. N.: Predicting Net surface Radiation for Alpine Surface Types Using Linear Models and Artificial Neural Networks, 2018.

Rasulov, B., Hüve, K., Bichele, I., Laisk, A., and Niinemets, Ü.: Temperature Response of Isoprene Emission in Vivo Reflects a Combined Effect of Substrate Limitations and Isoprene Synthase Activity: A Kinetic Analysis, Plant Physiology, 154, 1558-1570, 10.1104/pp.110.162081, 2010.

Rinnan, R., Iversen, L. L., Tang, J., Vedel-Petersen, I., Schollert, M., and Schurgers, G.: Separating direct and indirect effects of rising temperatures on biogenic volatile emissions in the Arctic, Proceedings of the National Academy of Sciences, 117, 32476, 10.1073/pnas.2008901117, 2020.

Ryde, I., Davie-Martin, C. L., Li, T., Naursgaard, M. P., and Rinnan, R.: Volatile organic compound emissions from subarctic mosses and lichens, Atmospheric Environment, 290, 119357, https://doi.org/10.1016/j.atmosenv.2022.119357, 2022.

Seco, R., Holst, T., Matzen, M. S., Westergaard-Nielsen, A., Li, T., Simin, T., Jansen, J., Crill, P., Friborg, T., Rinne, J., and Rinnan, R.: Volatile organic compound fluxes in a subarctic peatland and lake, Atmos. Chem. Phys., 20, 13399-13416, 10.5194/acp-20-13399-2020, 2020.

Seco, R., Holst, T., Davie-Martin, C. L., Simin, T., Guenther, A., Pirk, N., Rinne, J., and Rinnan, R.: Strong isoprene emission response to temperature in tundra vegetation, Proceedings

of the National Academy of Sciences, 119, e2118014119, 10.1073/pnas.2118014119, 2022.

Selimovic, V., Ketcherside, D., Chaliyakunnel, S., Wielgasz, C., Permar, W., Angot, H., Millet, D. B., Fried, A., Helmig, D., and Hu, L.: Atmospheric biogenic volatile organic compounds in the Alaskan Arctic tundra: constraints from measurements at Toolik Field Station, Atmos. Chem. Phys., 22, 14037-14058, 10.5194/acp-22-14037-2022, 2022.

Sharkey, T. D., Wiberley, A. E., and Donohue, A. R.: Isoprene Emission from Plants: Why and How, Annals of Botany, 101, 5-18, 10.1093/aob/mcm240, 2008.

Sharkey, T. D., and Monson, R. K.: The future of isoprene emission from leaves, canopies and landscapes, Plant, Cell & Environment, 37, 1727-1740, https://doi.org/10.1111/pce.12289, 2014.

Simin, T., Tang, J., Holst, T., and Rinnan, R.: Volatile organic compound emission in tundra shrubs – Dependence on species characteristics and the near-surface environment, Environmental and Experimental Botany, 184, 104387, https://doi.org/10.1016/j.envexpbot.2021.104387, 2021.

Stavrakou, T., Müller, J. F., Bauwens, M., Smedt, I., Roozendael, M., and Guenther, A.: Impact of Short-term Climate Variability on Volatile Organic Compounds Emissions Assessed Using OMI Satellite Formaldehyde Observations, Geophysical Research Letters, 0, 10.1029/2018GL078676, 2018.

Tang, J., Schurgers, G., Valolahti, H., Faubert, P., Tiiva, P., Michelsen, A., and Rinnan, R.: Challenges in modelling isoprene and monoterpene emission dynamics of Arctic plants: a case study from a subarctic tundra heath, Biogeosciences, 13, 6651-6667, 10.5194/bg-13-6651-2016, 2016.

Tang, J., Zhou, P., Miller, P. A., Schurgers, G., Gustafson, A., Makkonen, R., Fu, Y. H., and Rinnan, R.: High-latitude vegetation changes will determine future plant volatile impacts on atmospheric organic aerosols, npj Climate and Atmospheric Science, 6, 147, 10.1038/s41612-023-00463-7, 2023.

Tiiva, P., Rinnan, R., Faubert, P., Räsänen, J., Holopainen, T., Kyrö, E., and Holopainen, J. K.: Isoprene emission from a subarctic peatland under enhanced UV-B radiation, New Phytologist, 176, 346-355, https://doi.org/10.1111/j.1469-8137.2007.02164.x, 2007.

Tiiva, P., Faubert, P., Michelsen, A., Holopainen, T., Holopainen, J. K., and Rinnan, R.: Climatic warming increases isoprene emission from a subarctic heath, New Phytologist, 180, 853-863, https://doi.org/10.1111/j.1469-8137.2008.02587.x, 2008.

Tiiva, P., Faubert, P., Räty, S., Holopainen, J. K., Holopainen, T., and Rinnan, R.: Contribution of vegetation and water table on isoprene emission from boreal peatland microcosms, Atmospheric Environment, 43, 5469-5475, https://doi.org/10.1016/j.atmosenv.2009.07.026, 2009.

Tunved, P., Hansson, H. C., Kerminen, V. M., Ström, J., Maso, M. D., Lihavainen, H., Viisanen, Y., Aalto, P. P., Komppula, M., and Kulmala, M.: High Natural Aerosol Loading over Boreal Forests, Science, 312, 261-263, 10.1126/science.1123052, 2006.

Vettikkat, L., Miettinen, P., Buchholz, A., Rantala, P., Yu, H., Schallhart, S., Seco, R., Männistö, E., Tuittila, E. S., Guenther, A. B., and Schobesberger, S.: High emission rates and strong temperature response make boreal wetlands a large source of terpenes, Atmos. Chem. Phys. Discuss., 2022, 1-21, 10.5194/acp-2022-588, 2022.

Vettikkat, L., Miettinen, P., Buchholz, A., Rantala, P., Yu, H., Schallhart, S., Petäjä, T., Seco, R., Männistö, E., Kulmala, M., Tuittila, E. S., Guenther, A. B., and Schobesberger, S.: High

emission rates and strong temperature response make boreal wetlands a large source of isoprene and terpenes, Atmos. Chem. Phys., 23, 2683-2698, 10.5194/acp-23-2683-2023, 2023.

Wang, H., Welch, A., Nagalingam, S., Leong, C., Kittitananuvong, P., Barsanti, K. C., Sheesley, R. J., Czimczik, C. I., and Guenther, A. B.: Arctic Heatwaves Could Significantly Influence the Isoprene Emissions From Shrubs, Geophysical Research Letters, 51, e2023GL107599, https://doi.org/10.1029/2023GL107599, 2024.

Weber, J., Archer-Nicholls, S., Abraham, N. L., Shin, Y. M., Griffiths, P., Grosvenor, D. P., Scott, C. E., and Archibald, A. T.: Chemistry-driven changes strongly influence climate forcing from vegetation emissions, Nature Communications, 13, 7202, 10.1038/s41467-022-34944-9, 2022.

Whaley, C. H., Law, K. S., Hjorth, J. L., Skov, H., Arnold, S. R., Langner, J., Pernov, J. B., Bergeron, G., Bourgeois, I., Christensen, J. H., Chien, R. Y., Deushi, M., Dong, X., Effertz, P., Faluvegi, G., Flanner, M., Fu, J. S., Gauss, M., Huey, G., Im, U., Kivi, R., Marelle, L., Onishi, T., Oshima, N., Petropavlovskikh, I., Peischl, J., Plummer, D. A., Pozzoli, L., Raut, J. C., Ryerson, T., Skeie, R., Solberg, S., Thomas, M. A., Thompson, C., Tsigaridis, K., Tsyro, S., Turnock, S. T., von Salzen, K., and Tarasick, D. W.: Arctic tropospheric ozone: assessment of current knowledge and model performance, Atmos. Chem. Phys., 23, 637-661, 10.5194/acp-23-637-2023, 2023.

Wiberley, A. E., Donohue, A. R., Westphal, M. M., and Sharkey, T. D.: Regulation of isoprene emission from poplar leaves throughout a day, Plant, Cell & Environment, 32, 939-947, https://doi.org/10.1111/j.1365-3040.2009.01980.x, 2009.

Willis, M. D., Leaitch, W. R., and Abbatt, J. P. D.: Processes Controlling the Composition and Abundance of Arctic Aerosol, Reviews of Geophysics, 56, 621-671, https://doi.org/10.1029/2018RG000602, 2018.

Zheng, B., Ciais, P., Chevallier, F., Yang, H., Canadell, J. G., Chen, Y., van der Velde, I. R., Aben, I., Chuvieco, E., Davis, S. J., Deeter, M., Hong, C., Kong, Y., Li, H., Li, H., Lin, X., He, K., and Zhang, Q.: Record-high CO2 emissions from boreal fires in 2021, Science, 379, 912-917, 10.1126/science.ade0805, 2023.

Figures and tables

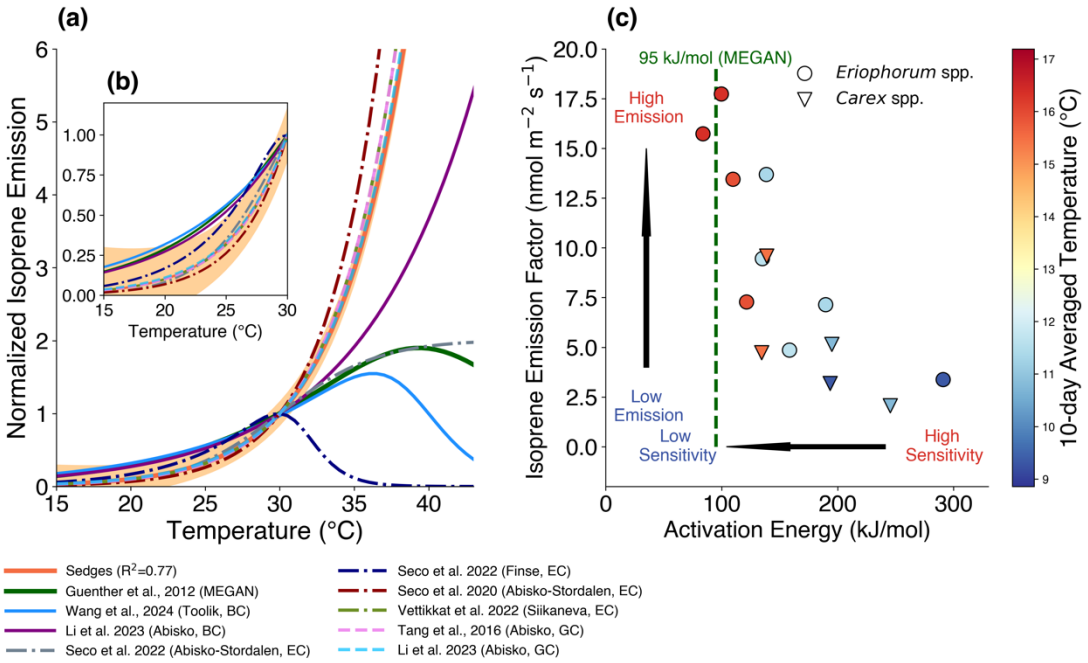

Figure. 4.1. (a) presents the temperature responses of isoprene emissions from this and previous studies in the northern high-latitude regions. (b) is the same plot as (a), but only for temperatures under 30°C; (c) shows the relationship between the isoprene temperature sensitivities and emission capacities of sedges. The short-term temperature response curves of sedges up to 35 °C from this study is showed by the orange solid line, and the orange shading represents the 95% confidence intervals. The short-term temperature response curves of tundra ecosystem from previous studies are also presented by lines with different colors and patterns. GC, BC and EC represent ground chamber experiments, branch chamber experiments and eddy-covariance measurements. The temperature response curves are normalized to the emission level when the leaf temperature equals 30 °C. The temperature curves in Tang et al. (2016) and Li et al. (2023) came from the ground chamber observations of mixed local vegetation at the Abisko site. Li et al. (2023) also did the branch chamber experiments for *Salix myrsinites* L. (purple solid line). The site in Seco et al. (2020) is located in a sedge-dominated fen near the Abisko-Stordalen site.

The Abisko measurements in Seco et al. (2022) (2022) happened at a different location within the same Abisko-Stordalen area on an ombrotrophic permafrost plateau. The Finse site in Seco et al. (2022) (2022) is a tundra with mixture of fen and heath vegetation with shrubs and lichens. The Siikaneva site is in a fen dominated by moss, sedges and dwarf shrubs, and surrounded by Scots pine forest. (Vettikkat et al., 2023) (c) presents an inverse relationship between the activation energies of the isoprene temperature response and the isoprene emission factors for *Eriophorum* spp. (circle) and *Carex* spp. (triangle). The green dashed line in (c) shows the activation energy in the Model of Emissions of Gases and Aerosols from Nature (MEGAN) (Guenther et al., 2012). The colors of markers denote the average temperatures over the previous 10 days, and emission factor is defined as the level of isoprene emission at a leaf temperature of 30 °C and a photosynthetic photon flux density (PPFD) of 1,000 μmol m^{-2} s^{-1}.

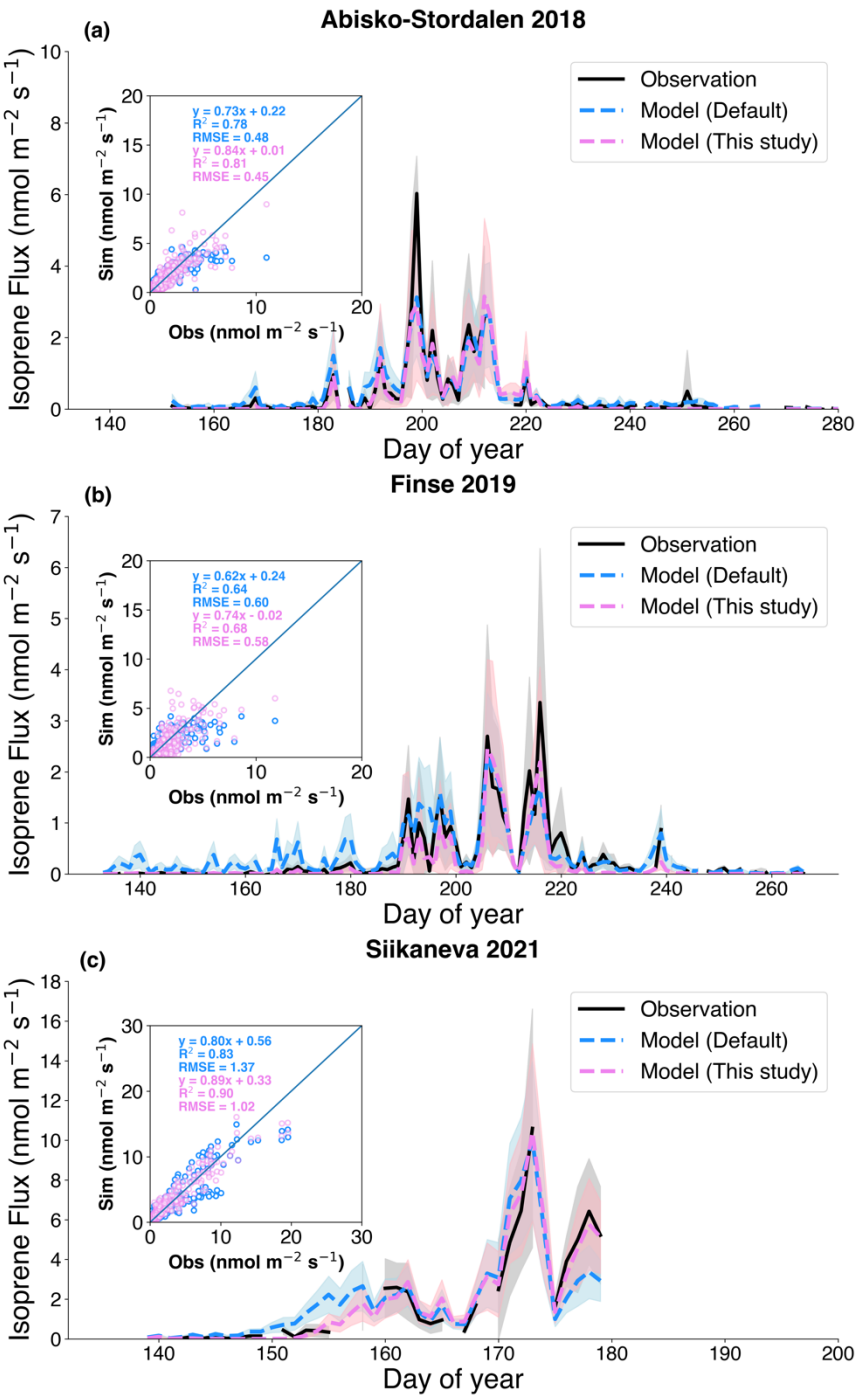

Figure 4.2. Time series of the daily observed and simulated isoprene flux by MEGAN with the default (blue) and updated (pink) temperature responses. The eddy-covariance flux measurements (black line) from three high-latitude sites, Abisko-Stordalen site in 2018(Seco et al., 2022) (a), Finse site in 2019(Seco et al., 2022) (b) and the Siikaneva site in 2021(Vettikkat et

al., 2022) (c), were evaluated. The shaded areas in different colors represent the standard deviation of the daily fluxes from observations (grey), the default MEGAN (blue), and the updated MEGAN (pink), respectively. The scatter plots illustrate the performance of the models compared to half-hourly isoprene flux measurements. Isoprene measurements with a photosynthetic photon flux density exceeding 300 μmol m^{-2} s^{-1} were taken for comparison. The updated model incorporates Arctic grass and boreal shrub temperature response curves, while the default model uses the temperature curves in MEGAN v2.1(Guenther et al., 2012).

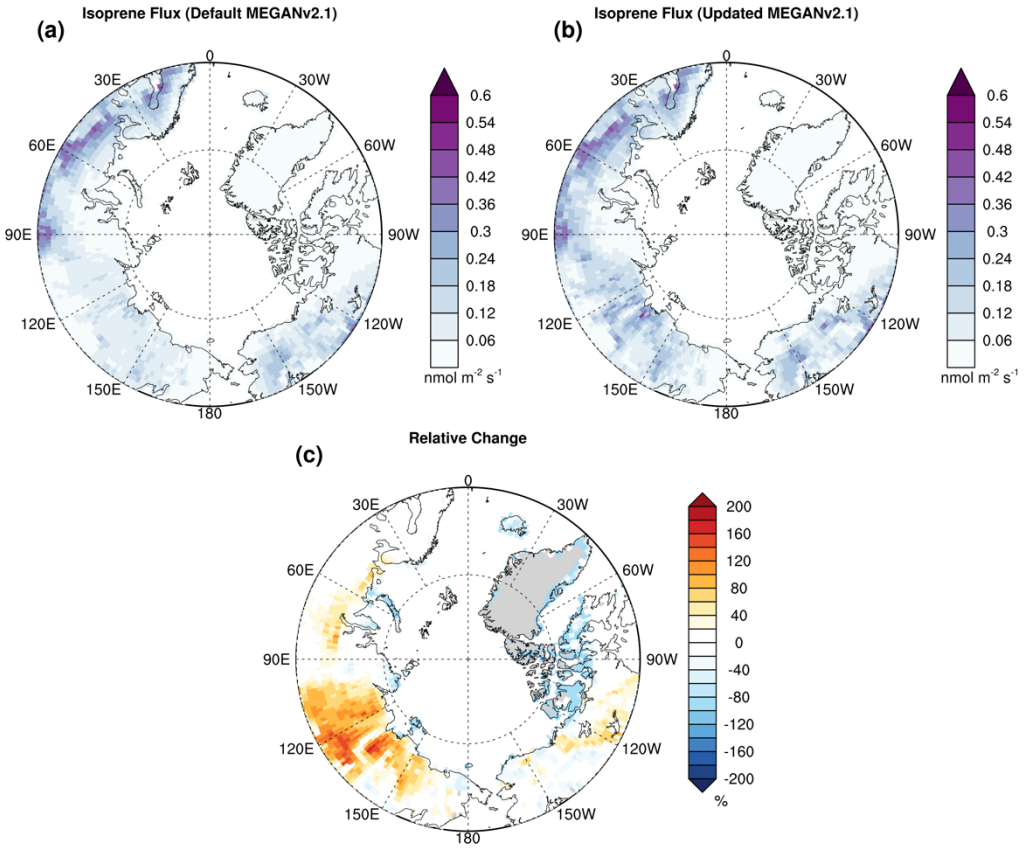

Figure 4.3. The averaged isoprene emissions in high-latitude regions (north of 60°N) during 2000-2009 estimated by MEGAN. The default MEGAN (a) and the updated MEGAN (b) were driven by the CLM5 model. The relative change caused by the new temperature response curves is presented in (c). The averaged isoprene emissions estimated by the new model are 3.25 Tg yr^{-1}, around 20 % higher than the original MEGAN estimate of 2.71 Tg yr^{-1}.

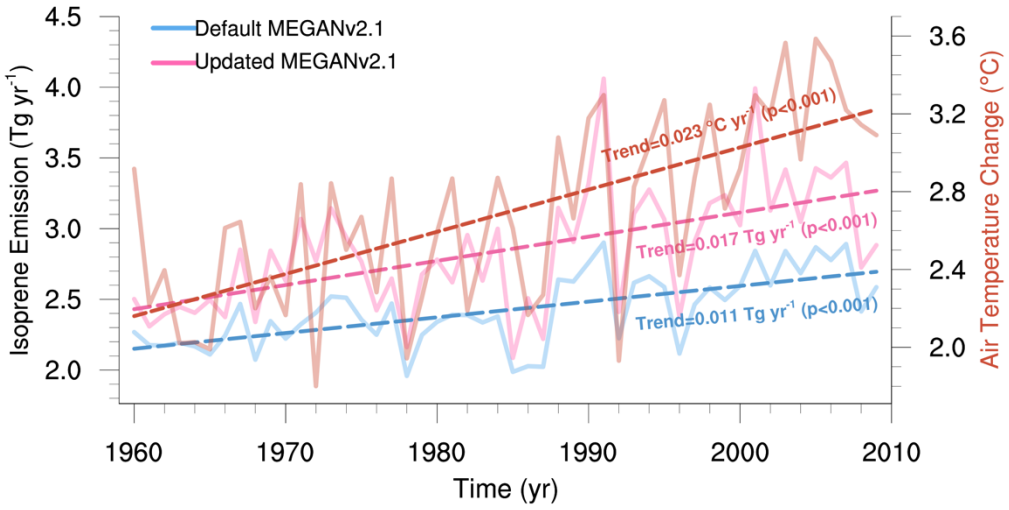

Figure 4.4. Long-term trend of isoprene emission in high-latitude regions (north of 60°N) estimated by MEGAN during 1960-2009. Time series of isoprene emissions, as estimated by the default MEGAN and the updated MEGAN, are depicted by the pink and blue solid lines, respectively. Changes in air temperature over land are shown by the orange solid line. The linear trends of isoprene emissions, as estimated by the default MEGAN and the updated MEGANv2.1, are indicated by the pink and blue dashed lines, respectively. The linear trend of air temperature over land is represented by the orange dashed line. The significance of the linear trends for isoprene emissions and air temperature was tested using the Mann-Kendall test. For high latitude regions (north of 60°N), the linear trends in isoprene emissions are estimated to be 0.017 Tg yr^{-1} ($p < 0.001$) for the updated MEGANv2.1 and 0.011 Tg yr^{-1} ($p < 0.001$) for the default MEGANv2.1.

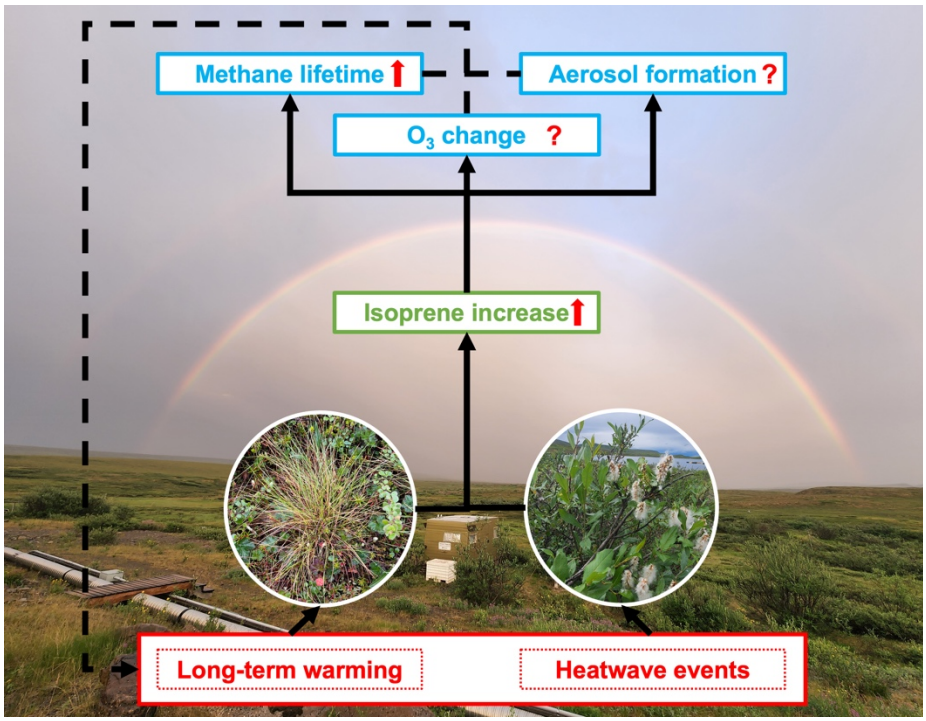

Figure 4.5. Schematic representation of isoprene emission increase and atmospheric chemical changes induced by the response of sedges and willows to Arctic warming. Warming will increase isoprene emission from Arctic ecosystems. This change in isoprene emissions due to warming can alter tropospheric chemistry, resulting in extended methane lifetime, altered tropospheric ozone concentration, and changed aerosol formation. These changes can influence the local radiation energy balance and exacerbate climate fluctuations.

Table 4.1. The cover fractions of plant functional types that were estimated by the model and land survey at the Finse, Abisko-Stordalen and Siikaneva sites. The cover fractions of sedges and isoprene-emitting shrubs in the model are fitted using the least square methods.

	Fitted sedge fraction (%)	Observed/Estimated sedge fraction (%)	Fitted shrub fraction (%)	Observed/Estimated shrub fraction (%)	Reference
Abisko-Stordalen	11.1	-	-	-	-
Finse	13.3	17.2	7.4	6.3	Ramtvedt (2018)
Siikaneva	26.8	24.0	-	-	Vettikkat et al. (2023)

Supplementary figures and tables

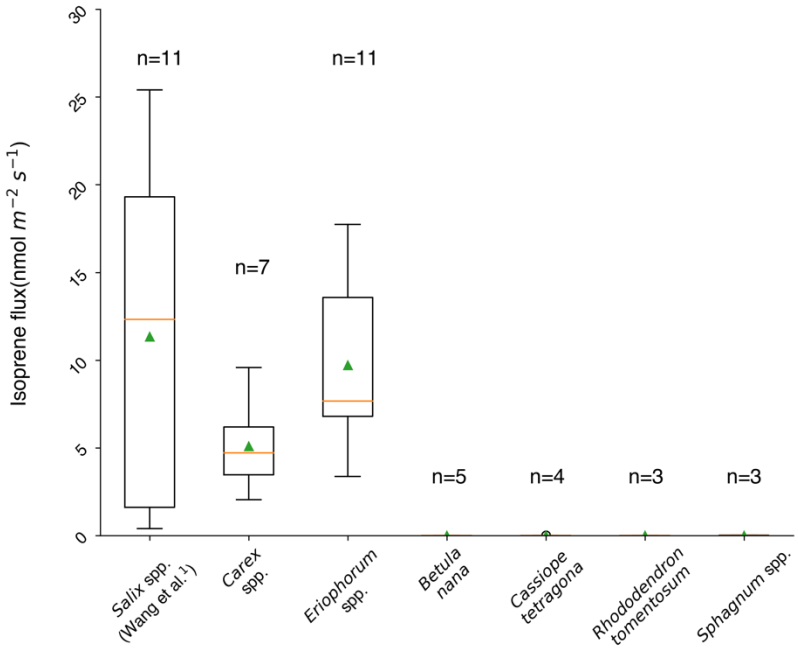

Figure S4.1. Comparison of leaf-level isoprene emissions from vegetation species at the Toolik Field Station. The measurements were conducted when the leaf temperature was about 30°C under a PPFD of 1000 μmol m^{-2} s^{-1}. The green triangle represents the mean, while the orange line represents the median. The upper and lower boundaries of the box represent the first and third quartiles, respectively. The whiskers extend from the box by 1.5 times the inter-quartile range.

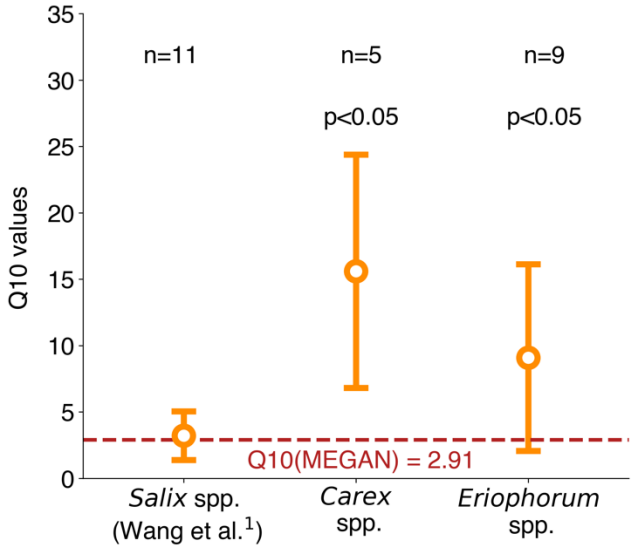

Figure S4.2. The Q_{10} values between 25 and 35 °C from *Salix* spp. (willows), *Carex* spp., and *Eriophorum* spp. The Q_{10} values between 25 and 35 °C from Arctic sedges are significantly ($p<0.05$) higher than those of willows measured at the Toolik Field Station. The Q_{10} value of MEGAN (=2.91) is presented by a red dashed line. Points and error bars represent mean and standard deviation of Q10.

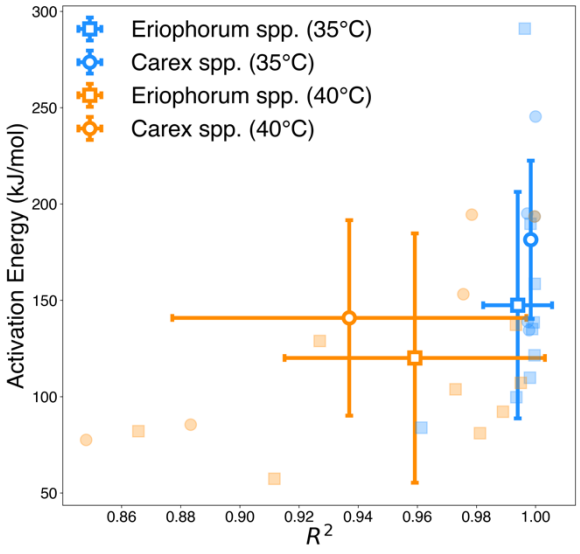

Figure S4.3. Comparison of temperature sensitivities and R^2 for the fitted curves of sedges from measurements with the highest temperature of 35 °C and 40 °C. Temperature sensitivities are represented by the activation energy in Equation (5). *Eriophorum* spp. and *Carex* spp. are represented by squares and circles, respectively. The colors blue and orange denote the temperature curves fitted with the highest temperatures of 35 °C and 40 °C, respectively. Solid marks indicate the mean values of activation energy and R^2, with error bars representing the standard deviation. Transparent marks represent the values for individual sedges.

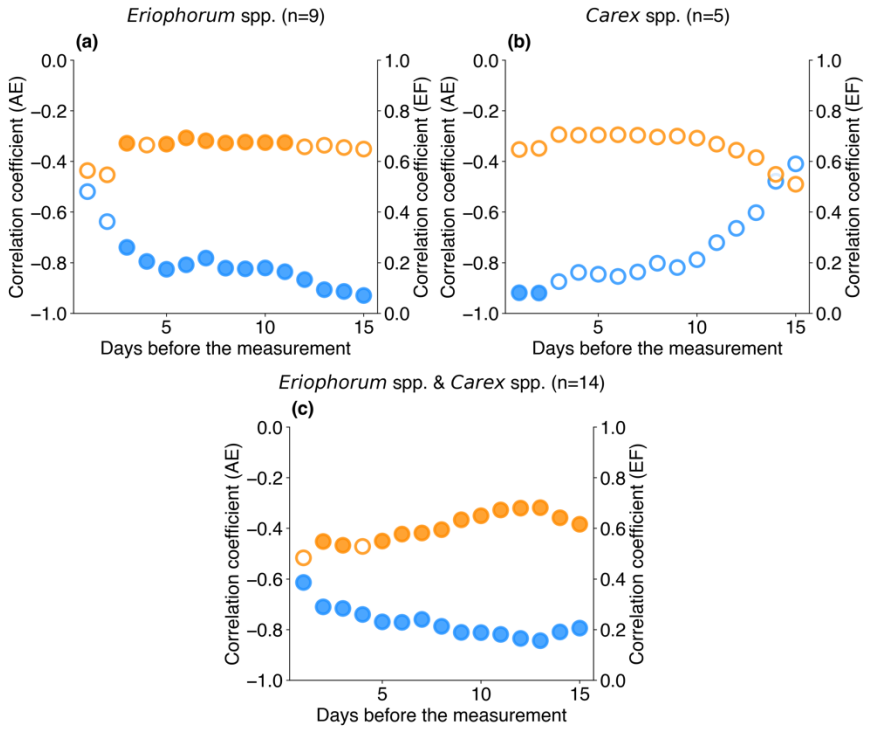

Figure S4.4. Correlation coefficients of the activation energy (left axis, in blue) and the emission factors (right axis, in orange) of sedges with the mean temperature during the 1 to 15 days preceding the measurement. (a), (b), and (c) display the Pearson correlation coefficients for the activation energy (AE) and emission factors (EF) in relation to the mean temperature of the preceding 1 to 15 days for *Eriophorum* spp., *Carex* spp., and a combined analysis of both species, respectively. Statistically significant correlation coefficients ($p < 0.05$) are indicated by solid filled points.

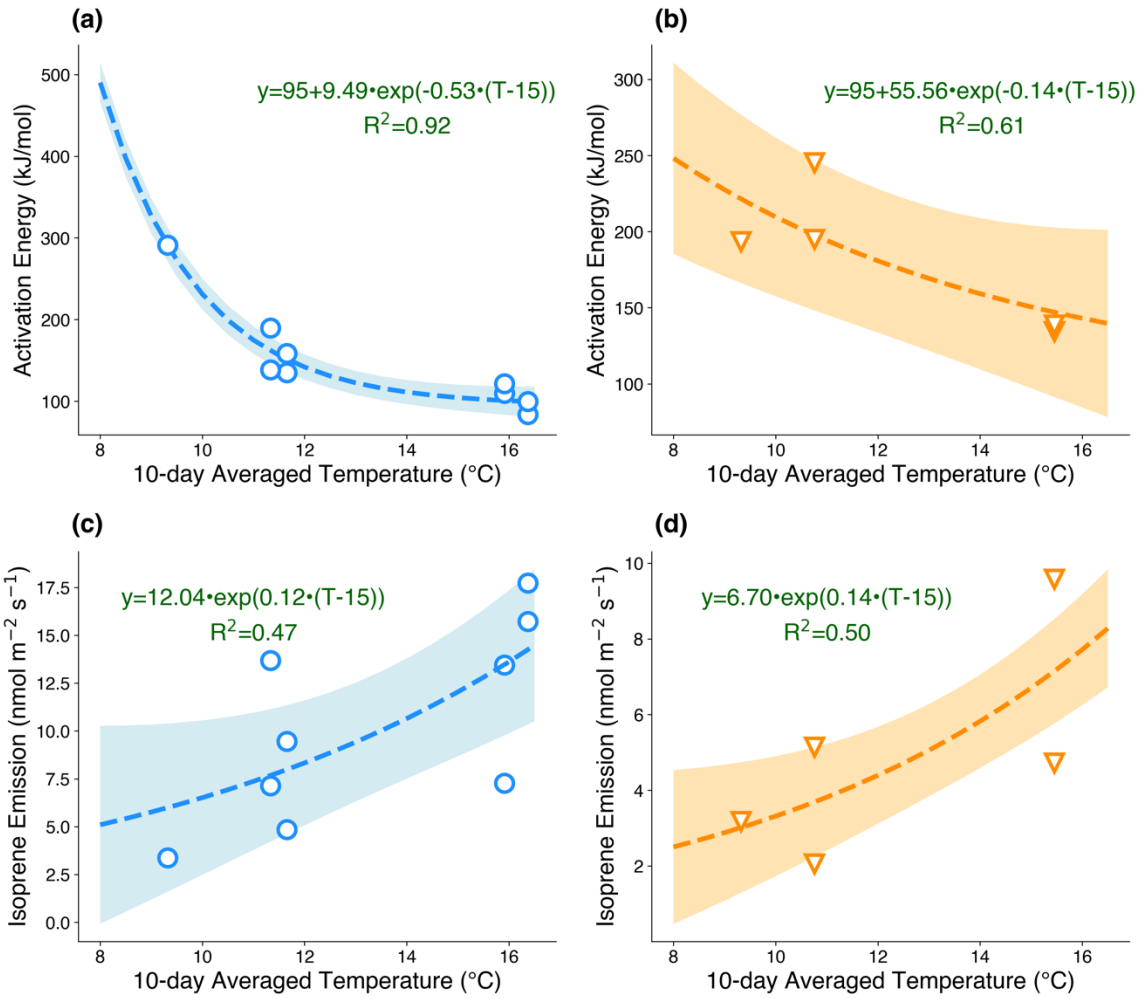

Figure S4.5. The response curves of the temperature sensitivity and emission factor to the past 10-day average air temperature. (a) and (b) present the relationship between the activation energy or temperature sensitivity to the past 10-day average temperature for *Eriophorum* spp. (blue) and *Carex* spp. (orange). (c) and (d) depict emission factors versus the past 10-day average temperature for *Eriophorum* spp. (blue) and *Carex* spp. (orange). The fitted equation and R^2 are both presented.

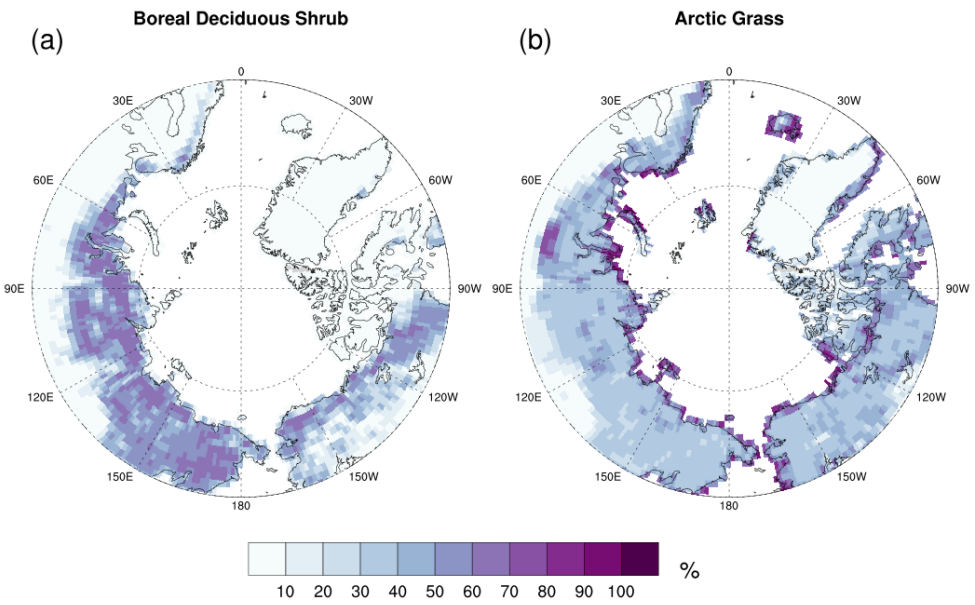

Figure S4.6. The spatial distribution of cover fraction for the boreal deciduous shrub and Arctic grass in the Community Land Model version 5.

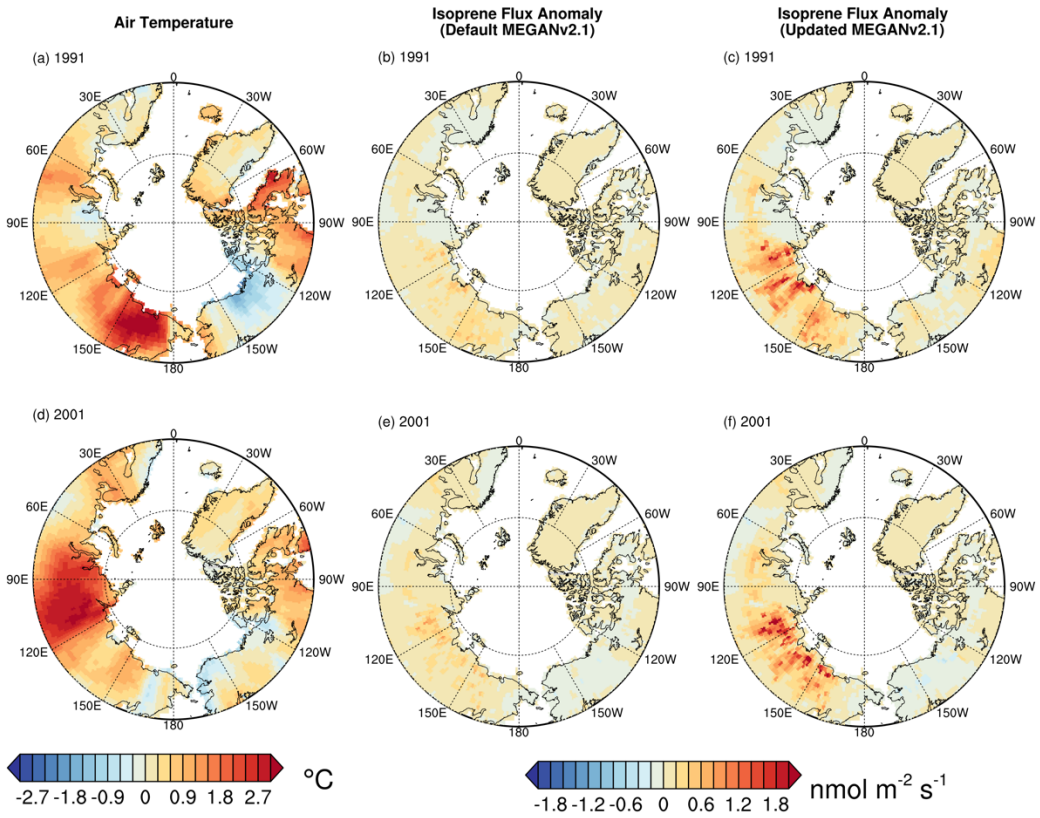

Figure S4.7. Air temperature and isoprene emission anomalies in the high-latitude regions (north of 60°N) in 1991 and 2001. Air temperature ((a) and (d)) and isoprene emission anomalies in summer estimated by the default and updated MEGANv2.1 in 1991 ((b) and (c)) and 2001 ((e) and (f)).

Table S4.1. Details about the flux measurements used in this study.

Site Name	Position	Sample period	Major vegetation species	Reference
Abisko-Stordalen	68.36° N, 19.05° E	Jun. 01 – Oct. 19, 2018	*Empetrum hermaphroditum, Carex rotundata, Betula nana, Rubus chamaemorus, Eriophorum vaginatum, Dicranum elongatum, Sphagnum fuscum, Sphagnum balticum, Drepanucladus schulzei, and Politrichum jensenii*	Seco, et al. [2]
Finse	60.60° N, 7.53 ° E	May 13 – Sep. 26, 2019	*E. hermaphroditum, Salix herbacea and other Salix* spp.*, Eriophorum angustifolium, and Carex spp, Ptilidium ciliare and Polytrichum juniperinum, Alectoria ochroleuca, Nephromopsis nivalis, and Cetraria islandica.*	Seco, et al. [2]
Siikaneva	61.83° N, 24.19° E	May 19, - Jun. 28, 2021	*Sphagnum balticum, S. papillosum, S. magellanicum, S. majus, Carex rostrata, C. limosa, C. lasiocarpa, and Eriophorum vaginatum, Andromeda polifolia, Betula nana, Rubus chamaemorus, and Vaccinium oxycoccus.*	Vettikkat, et al. [3]

Table S4.2. The performances of models. The statistics of the different temperature response curve models at the Abisko-Stordalen, Finse, and Siikaneva sites with the least square fitting. RMSE and MAE are short for the root mean square error and mean absolute error in the unit of nmol m^{-2} s^{-1}, respectively. T-tests were applied to test the significance between the differences of MAE.

Site	Abisko-Stordalen				Finse				Siikaneva			
-	R^2	Slope	RMSE	*MAE* *(p<0.05)*	R^2	Slope	RMSE	*MAE* *(p=0.22)*	R^2	Slope	RMSE	MAE (p<0.01)
Updated MEGAN v2.1	0.81	0.84	0.45	0.24	0.68	0.74	0.58	0.28	0.90	0.89	1.02	0.87
Default MEGAN v2.1	0.78	0.73	0.48	0.21	0.64	0.62	0.60	0.27	0.83	0.80	1.37	0.64

Table S4.3. Emission factors of sedges grown near Toolik, AK, USA. Specimens were collected near Imnavait Creek or at Toolik from the local tundra (Toolik). The isoprene emission factor is defined as the isoprene emission rate when the leaf temperature equals 30°C at a photosynthetic photon flux density of 1000 μmol m^{-2} s^{-1}.

Plant ID	Species or Genus	Collection Date	Sample type	Collection Location	Emission Factor (nmol m^{-2} s^{-1})	Experiment
Carex1	*Carex* sp.	Jul. 9, 2022	Leaf	Toolik	3.75	20°C, 30°C
Carex2	*Carex* sp.	Jul. 27, 2022	Leaves	Toolik	3.18	15°C-35°C
Carex3	*Carex* sp.	Jul. 27, 2022	Leaves	Toolik	7.26	15°C-35°C*
Carex4	*Carex* sp.	Jul. 17, 2023	Leaves	Toolik	5.14	20°C-40°C
Carex5	*Carex* sp.	Jul. 17, 2023	Leaves	Toolik	2.06	20°C-40°C
Carex6	*Carex* sp.	Jul. 27, 2023	Leaves	Toolik	4.73	20°C-40°C
Carex7	*Carex* sp.	Jul. 27, 2023	Leaves	Toolik	9.58	20°C-40°C
Eriophorum1	*Eriophorum* sp.	Jul. 16, 2022	Leaves	Imnavait	7.67	20°C, 30°C
Eriophorum2	*Eriophorum* sp.	Jul. 27, 2022	Leaves	Toolik	3.37	15°C-35°C

Eriophorum3	*Eriophorum* sp.	Jul. 27, 2022	Leaves	Toolik	6.48	15°C-35°C*
Eriophorum4	*Eriophorum vaginatum*	Jul. 15, 2023	Leaves	Toolik	4.86	20°C-40°C
Eriophorum5	*Eriophorum vaginatum*	Jul. 15, 2023	Leaves	Toolik	9.46	20°C-40°C
Eriophorum6	*Eriophorum vaginatum*	Jul. 16, 2023	Leaves	Toolik	13.69	20°C-40°C
Eriophorum7	*Eriophorum vaginatum*	Jul. 16, 2023	Leaves	Toolik	7.14	20°C-40°C
Eriophorum8	*Eriophorum vaginatum*	Jul. 30, 2023	Leaves	Toolik	15.73	20°C-40°C
Eriophorum9	*Eriophorum vaginatum*	Jul. 30, 2023	Leaves	Toolik	17.73	20°C-40°C
Eriophorum10	*Eriophorum vaginatum*	Jul. 31, 2023	Leaves	Toolik	13.44	20°C-40°C
Eriophorum11	*Eriophorum vaginatum*	Jul. 31, 2023	Leaves	Toolik	7.28	20°C-40°C

*The VOC samples were only taken at 20 and 30°C.

Table S4.4. Emission factors of plants other than sedges at Toolik Field Station. The isoprene emission factor is defined as the isoprene emission rate when the leaf temperature equals 30°C at a photosynthetic photon flux density of 1000 μmol m^{-2} s^{-1}.

Plant ID	Species or Genus	Collection Date	Sample type	Collection Location	Emission Factor (nmol m^{-2} s^{-1})
Willow1	*Salix glauca*	Jul. 13, 2022	Leaf	Toolik	19.53
Willow2	*Salix pulchra*	Jul. 14, 2022	Branch	Toolik	3.84
Willow3	*Salix pulchra*	Jul.16, 2022	Leaf	Toolik	12.33
Willow4	*Salix glauca*	Jul. 25, 2022	Leaf	Toolik	2.07
Willow5	*Salix pulchra*	Aug. 1, 2022	Leaf	Toolik	0.41
Willow6	*Salix glauca*	Aug. 1, 2022	Leaf	Toolik	1.02
Willow7	*Salix pulchra*	Aug. 4, 2022	Leaf	Toolik	1.18
Willow8	*Salix reticulata*	Jul. 25, 2023	Leaf	Toolik	24.8
Willow9	*Salix reticulata*	Jul. 25, 2023	Leaf	Toolik	19.07
Willow10	*Salix reticulata*	Jul. 31, 2023	Leaf	Toolik	15.19
Willow11	*Salix reticulata*	Jul. 31, 2023	Leaf	Toolik	25.39
Birch1	*Betula nana*	Jul. 14, 2022	Branch	Toolik	0.011

Birch2	*Betula nana*	Jul. 16, 2022	Branch	Toolik	0.003
Birch3	*Betula nana*	Jul. 25, 2022	Branch	Toolik	0.008
Birch4	*Betula nana*	Aug. 4, 2022	Branch	Toolik	0*
Birch5	*Betula nana*	Aug. 4, 2022	Branch	Toolik	0.016
Cassiope1	*Cassiope tetragona*	Jul. 17, 2022	Branch	Toolik	0.024
Cassiope2	*Cassiope tetragona*	Jul. 28, 2022	Branch	Toolik	0*
Cassiope3	*Cassiope tetragona*	Aug. 2, 2022	Branch	Toolik	0*
Cassiope4	*Cassiope tetragona*	Aug. 6, 2022	Branch	Toolik	0*
Rhododendron1	*Rhododendron tomentosum*	Jul. 17, 2022	Branch	Toolik	0*
Rhododendron2	*Rhododendron tomentosum*	Jul. 28, 2022	Branch	Toolik	0*
Rhododendron3	*Rhododendron tomentosum*	Aug. 2, 2022	Branch	Toolik	0*
Sphagnum1	*Sphagnum sp.*	Jul. 14, 2022	Leaves	Toolik	0.001
Sphagnum2	*Sphagnum sp.*	Jul. 21, 2022	Leaves	Toolik	0.03
Sphagnum3	*Sphagnum sp.*	Jul. 21, 2022	Leaves	Toolik	0.011

* The measurements are lower than the blank tube concentration.

CHAPTER 5

CONCLUSIONS AND FUTURE DIRECTIONS

In my dissertation, I integrated lab experiments and in-situ measurements to establish model frameworks for estimating the impact of drought and heatwaves on isoprene emissions in the MEGAN model.

In the first chapter, I developed an empirical algorithm based on whole-canopy flux measurements to simulate the impact of drought, ranging from mild to severe stages. I applied the algorithm in the CLM-CAM-chem model to simulate the impact of drought on isoprene emissions and found that drought can decrease global isoprene emissions by 11%. Since satellite-observed HCHO vertical column density is often used as a proxy for isoprene emissions, I compared the vertical column density simulated by CAM-chem to satellite HCHO observations to assess the impact of drought on isoprene. The results indicate that the proposed drought algorithm improves the alignment of simulated HCHO with observations under drought conditions, although its performance is limited by the ability of CLM to accurately represent drought severity.

In the second and third chapters, I investigated the isoprene emissions from Arctic ecosystems, where temperatures are increasing rapidly due to the "Arctic Amplification" phenomenon. I was able to characterize two representative types of isoprene emitters in Arctic tundra: willows (*Salix* spp.) and sedges (*Carex* spp. and *Eriophorum* spp.).

I investigated the impact of temperature and heatwave on isoprene emissions in the Arctic willows in the second chapter. I found that the hourly temperature response curve of willows, the dominant isoprene emitting shrubs in the Arctic, aligns with that of temperate plants. In contrast, the isoprene capacity of willows exhibited a more substantial than expected response to the mean ambient temperature of the previous day, which is much stronger than the daily temperature

response predicted by the current version of MEGAN. With a modified algorithm from this study, MEGAN predicts 70% higher isoprene emissions for Arctic willows during an Arctic heatwave.

I also explored the impact of temperature on isoprene from sedges, another major isoprene emitter in the Arctic in the third chapter. I found that sedges exhibit a markedly stronger temperature response compared to that of other isoprene emitters and predictions by MEGAN. MEGAN was able to reproduce eddy-covariance flux observations at three high-latitude sites by integrating findings from our chamber experiments.

I found that the omission of the strong temperature responses of the Arctic isoprene emitters from both willows and sedges caused a 20% underestimation of isoprene emissions for the high-latitude regions of the Northern Hemisphere during 2000-2009 in the Community Land Model Version 5 (CLM5), that includes the MEGAN scheme. We also found that the existing model had underestimated the long-term trend of isoprene emissions from 1960 to 2009 by 55% for the high-latitude region. This discrepancy is attributed to both the heightened temperature sensitivity and isoprene emission factors under warming conditions.

Increased heatwave frequency (Dobricic et al., 2020) and general warming could intensify isoprene impacts, with significant shifts in isoprene emissions potentially altering local atmospheric chemistry and climate dynamics. The isoprene emitters, including sedges and willows, would respond to both short-term, intense heatwaves and long-term warming by increasing their isoprene emissions. The lower atmospheric oxidative capacity caused by rising isoprene emissions could further increase the lifetime of methane and then exacerbate warming. Boy et al. (2022) suggest that a 6°C warming could increase the lifetime of methane by 11% at a boreal site dominated by monoterpene emissions. The pronounced response of isoprene to warming suggested by this study will exacerbate the BVOC-OH-CH_4 feedback. Additionally, the

increased isoprene emissions could also disturb aerosol (McFiggans et al., 2019) and ozone formation, as well as aerosol-cloud interactions (Weber et al., 2022; Kulmala et al., 2004). BVOCs, including isoprene, act as sinks for tropospheric ozone in the Arctic (Whaley et al., 2023), and the increase of isoprene could further diminish tropospheric ozone. However, the increased frequency and intensity of wildfire and anthropogenic emissions from more human activities (Paxian et al., 2010; Zheng et al., 2023; Jones et al., 2022), the atmospheric transport of NOx ($NO+NO_2$) and peroxyacetyl nitrate could alter the chemical regime and change the tropospheric ozone and aerosol formation. This research could contribute to predicting isoprene emissions under rapid climate change and, more importantly, provide a foundation for evaluating the impact of these changing emissions on climate and air quality.

Therefore, a major future research direction is to understand the role of isoprene in future climate scenarios. Under the different Shared Socioeconomic Pathways (SSP) scenarios (O'Neill et al., 2016), we could evaluate the impact of warming and extreme events on isoprene emissions and the corresponding changes induced by chemical reactions. In addition, I recognize that another important driver of BVOCs is vegetation change. Rapid climate change, along with human activities such as deforestation and reforestation, will undoubtedly disturb isoprene and other BVOCs emissions through vegetation changes. Jing et al. (2023) found that vegetation changes in high latitudes can disturb local chemistry and alter the local climate. Similarly, Wang et al. (2022) found that reforestation is the major driver of BVOCs changes in China. Therefore, understanding BVOCs, including isoprene changes and their impact on atmospheric chemistry and climate, requires considering both direct climatic changes and the indirect effects of vegetation type and biomass changes.

Reference

Boy, M., Zhou, P., Kurtén, T., Chen, D., Xavier, C., Clusius, P., Roldin, P., Baykara, M., Pichelstorfer, L., Foreback, B., Bäck, J., Petäjä, T., Makkonen, R., Kerminen, V.-M., Pihlatie, M., Aalto, J., and Kulmala, M.: Positive feedback mechanism between biogenic volatile organic compounds and the methane lifetime in future climates, npj Climate and Atmospheric Science, 5, 72, 10.1038/s41612-022-00292-0, 2022.

Dobricic, S., Russo, S., Pozzoli, L., Wilson, J., and Vignati, E.: Increasing occurrence of heat waves in the terrestrial Arctic, Environmental Research Letters, 15, 024022, 10.1088/1748-9326/ab6398, 2020.

Jones, M. W., Abatzoglou, J. T., Veraverbeke, S., Andela, N., Lasslop, G., Forkel, M., Smith, A. J. P., Burton, C., Betts, R. A., van der Werf, G. R., Sitch, S., Canadell, J. G., Santín, C., Kolden, C., Doerr, S. H., and Le Quéré, C.: Global and Regional Trends and Drivers of Fire Under Climate Change, Reviews of Geophysics, 60, e2020RG000726, https://doi.org/10.1029/2020RG000726, 2022.

Kulmala, M., Suni, T., Lehtinen, K. E. J., Dal Maso, M., Boy, M., Reissell, A., Rannik, Ü., Aalto, P., Keronen, P., Hakola, H., Bäck, J., Hoffmann, T., Vesala, T., and Hari, P.: A new feedback mechanism linking forests, aerosols, and climate, Atmos. Chem. Phys., 4, 557-562, 10.5194/acp-4-557-2004, 2004.

McFiggans, G., Mentel, T. F., Wildt, J., Pullinen, I., Kang, S., Kleist, E., Schmitt, S., Springer, M., Tillmann, R., Wu, C., Zhao, D., Hallquist, M., Faxon, C., Le Breton, M., Hallquist, Å. M., Simpson, D., Bergström, R., Jenkin, M. E., Ehn, M., Thornton, J. A., Alfarra, M. R., Bannan, T. J., Percival, C. J., Priestley, M., Topping, D., and Kiendler-Scharr, A.:

Secondary organic aerosol reduced by mixture of atmospheric vapours, Nature, 565, 587-593, 10.1038/s41586-018-0871-y, 2019.

O'Neill, B. C., Kriegler, E., Riahi, K., Ebi, K. L., Hallegatte, S., Carter, T. R., Mathur, R., and van Vuuren, D. P.: A new scenario framework for climate change research: the concept of shared socioeconomic pathways, Climatic Change, 122, 387-400, 10.1007/s10584-013-0905-2, 2014.

Paxian, A., Eyring, V., Beer, W., Sausen, R., and Wright, C.: Present-Day and Future Global Bottom-Up Ship Emission Inventories Including Polar Routes, Environmental Science & Technology, 44, 1333-1339, 10.1021/es9022859, 2010.

Tang, J., Zhou, P., Miller, P. A., Schurgers, G., Gustafson, A., Makkonen, R., Fu, Y. H., and Rinnan, R.: High-latitude vegetation changes will determine future plant volatile impacts on atmospheric organic aerosols, npj Climate and Atmospheric Science, 6, 147, 10.1038/s41612-023-00463-7, 2023.

Wang, H., Wu, Q., Guenther, A. B., Yang, X., Wang, L., Xiao, T., Li, J., Feng, J., Xu, Q., and Cheng, H.: A long-term estimation of biogenic volatile organic compound (BVOC) emission in China from 2001–2016: the roles of land cover change and climate variability, Atmos. Chem. Phys., 21, 4825-4848, 10.5194/acp-21-4825-2021, 2021.

Wang, H., Welch, A., Nagalingam, S., Leong, C., Kittitananuvong, P., Barsanti, K. C., Sheesley, R. J., Czimczik, C. I., and Guenther, A. B.: Arctic Heatwaves Could Significantly Influence the Isoprene Emissions From Shrubs, Geophysical Research Letters, 51, e2023GL107599, https://doi.org/10.1029/2023GL107599, 2024.

Weber, J., Archer-Nicholls, S., Abraham, N. L., Shin, Y. M., Griffiths, P., Grosvenor, D. P., Scott, C. E., and Archibald, A. T.: Chemistry-driven changes strongly influence climate

forcing from vegetation emissions, Nature Communications, 13, 7202, 10.1038/s41467-022-34944-9, 2022.

Whaley, C. H., Law, K. S., Hjorth, J. L., Skov, H., Arnold, S. R., Langner, J., Pernov, J. B., Bergeron, G., Bourgeois, I., Christensen, J. H., Chien, R. Y., Deushi, M., Dong, X., Effertz, P., Faluvegi, G., Flanner, M., Fu, J. S., Gauss, M., Huey, G., Im, U., Kivi, R., Marelle, L., Onishi, T., Oshima, N., Petropavlovskikh, I., Peischl, J., Plummer, D. A., Pozzoli, L., Raut, J. C., Ryerson, T., Skeie, R., Solberg, S., Thomas, M. A., Thompson, C., Tsigaridis, K., Tsyro, S., Turnock, S. T., von Salzen, K., and Tarasick, D. W.: Arctic tropospheric ozone: assessment of current knowledge and model performance, Atmos. Chem. Phys., 23, 637-661, 10.5194/acp-23-637-2023, 2023.

Zheng, B., Ciais, P., Chevallier, F., Yang, H., Canadell, J. G., Chen, Y., van der Velde, I. R., Aben, I., Chuvieco, E., Davis, S. J., Deeter, M., Hong, C., Kong, Y., Li, H., Li, H., Lin, X., He, K., and Zhang, Q.: Record-high CO2 emissions from boreal fires in 2021, Science, 379, 912-917, 10.1126/science.ade0805, 2023.